Measurements of particle loading on bubbles in froth flotation

Clayton Bhondayi

A dissertation submitted to the Faculty of Engineering and the Built Environment, University of the Witwatersrand, in fulfilment of the requirements for the degree of Master of Science in Engineering

Johannesburg, 2010

Statement of Originality

I hereby certify that the work embodied in this thesis is the result of original research and has not been submitted for another degree at any other university or institution.

Signed: **…….**
Clayton Bhondayi

Date **.....** the day of …**…… 2010**

Abstract

This work explores the measurement of particle loading on bubbles in the collection zone during flotation. Existing methods and instruments are critically reviewed to form a basis for developing a new bubble load meter. The new bubble load measuring device which is based on the Dyer (1995) and Seaman et al., (2004) concept is presented.

It was noted that the Dyer (1995) concept as improved by Moys et al. (2010) had advantages that with refinement could yield a more robust working instrument. The device had to meet the following objectives: It must measure bubble loads accurately without particle losses as a result of bubble coalescence, or break up. Secondly the instrument should also be capable of collecting a solid sample in excess of 200 grams which is the minimum mass required for PGM analysis as function of particle size.

Results of applying this newly designed bubble load meter in the laboratory and industrial plant are presented. It was shown at laboratory level through salt tracer experiments that the 20mm and 30mm riser worked well for the bubble load meter without sampling unattached particles. The intensity of the axial mixing in the 50mm riser resulted in some salt transport up the riser, to an extent that would compromise the bubble load quality.

An axial mixing model with 16 tanks in series was developed for the bubble load meter riser and parameters were estimated using Matlab's Simulink toolbox. A satisfactory fit was obtained after the inclusion of an additional parameter that accounts for salt transport as a result of mechanical push by bubble swarms and the salt adsorbed on the bubble lamella.

Industrial work at Lonmin's EPC plant yielded a maximum sample mass of 35.5grams with the 20mm ID riser instead of the target mass of 200grams. This was attributed to a number of factors which include that the sample was taken using small diameter riser (20mm ID) which meant that fewer bubbles were collected per unit cross sectional area and also the occasional breakage of the

filter paper due to blinding which reduced sampling times. A froth recovery parameter R_f of 0.68 was obtained on the primary cleaner cells while a froth flow number (R_{fn}) of 1.55 was obtained on the primary rougher cell, this value of froth flow number in the primary rougher cell indicated high entrainment. A froth flow number was calculated for the primary rougher cell data instead of a froth recovery parameter because of the unavailability assays due to low sample masses. While the froth recovery parameter was defined as the fraction of particles that are recovered by true flotation that reports to the concentrate, the froth flow number was defined as the ratio between the total mass of solids recovered in concentrate (by true flotation +entrainment) and the mass of solids entering the froth by true flotation, i.e. collected mineral (particle-bubble aggregates). A froth flow number can assume any value less than, equal to or greater than one depending on the contribution of entrainment and true flotation. It was also demonstrated that bubble load values in conjunction with certain assumptions can be used to estimate entrainment. Results of applying bubble load data revealed that chromite recovery in the concentrate is a contribution of both true flotation and entrainment. The results also indicated that 2.4% of the total concentrate flow in this primary cleaner was chromite and was mainly constituted of -25μm particles. It was also discovered that 3.1% of the bubble load was Chromite. Comparison of the bubble load assays per size class with concentrate assays and mass balances showed that most of the floatable chromite drains back into the pulp phase.

Acknowledgements

It is by standing on the shoulders of others that I have been able to see far, Sir Isaac Newton said. I would also want to recorded my profound gratitude to all those who made the completion of this research possible. These include:

- My supervisor, Prof. M.H. Moys for his immense interest in this project and the invaluable time he spend introducing me to the time honoured skills of research and data analysis. His assistance and expertise in mineral processing and froth flotation in particular will forever be valued. The communition group under his supervision is also greatly honoured for its assistance in carrying out some of the experiments.

- Dr. M. Bwalya for the numerous suggestions and corrections he made.

- Lonmin for allowing me to carry out tests on their EPC concentrator. Particularly Dr. Victor Ross, Lebo and Aaron for their great assistance in carrying out industrial tests.

- My parents, brothers and sisters for being there for me all the time, their enthusiasm made the day.

- To Stella for being an all weather friend. Thank you very much.

- Finally to my friends, Pheneas, Gwiranayi and Tirivaviri, I say to them you made the going easier. Thank you.

TABLE OF CONTENTS

Chapter 4

Chapter 5

List of Figures

List of Tables

Chapter 1

Introduction

1.1 Project motivation

Flotation is a separation process used in many mining operations to concentrate the desired mineral before further downstream processing. The operation of the flotation process is a complex one which is not entirely understood. Froth flotation utilises the differences in physico-chemical surface properties of particles of various minerals. After treating milled mineral ore with chemicals, the hydrophobic particles will attach to the rising air bubbles forming particle-bubble aggregates which then rise to the froth phase where a portion of the particles are recovered as concentrate.

One major issue that has been identified as critical to explaining the flotation mechanism is particle loading on bubbles or true flotation. It is the main mechanism by which floatable particles are transferred from the pulp phase to the froth phase (Savassi *et al.,* 1997). Other mechanisms suggested (Thorne, 1975 as reported by Savassi *et al., op cit)* include: entrainment in the water which passes through the froth and physical entrapment between particles in the froth attached to the air bubbles (often referred to as aggregation). Knowledge of particle loading on bubbles in the pulp phase is very important in understanding the collection zone phase sub-processes (Bradshaw and O'Connor, 1996). A method of directly measuring bubble loading in industrial flotation cells is important in evaluating froth recovery parameters of existing flotation cells. Bubble load data is also important in modelling flotation process, especially where the froth phase is separated from the pulp phase. Several researchers have developed methods of measuring bubble loads but most of the methods have the following limitations.

i. Applicable to ideal conditions that can only exist in the lab (Bradshaw and O'Connor, 1996).
ii. Applicable to certain sections of the plant i.e. rougher cells (Savassi, 1997).

iii. Low mass of samples taken which may have high sampling errors.
iv. Loss of attached particles in some methods or devices which leads to incorrect results.
v. No attention is paid to the kind of flow regime that exists in riser (Seaman et al., 2004; Dyer, 1995; Falatsu and Dobby, 1992) and the effect of sampling column/riser size (diameter) on bubble load quality.
vi. Possibility of particles flowing back into flotation cell with the wash water.

1.2 Thesis objectives

This research project explores the measurement of particle loading on bubbles in the collection zone during flotation. It assesses the applicability and limitations of the existing methods and instruments with the ultimate objective of developing a new bubble load measuring device. Ways of coming up with proper dimensions that ensure that particles are not lost through coalescence and churn turbulence in the instrument are explored. Thorough laboratory and industrial testing of the instrument to validate its applicability and accuracy in evaluating flotation kinetics is carried out. The research endeavours to fulfil the following objectives.

1. Develop an instrument or device to measure bubble loading in industrial flotation machines based on the Dyer (1995) concept as improved by Moys et al. (2010).
   - The device should measure bubble loads accurately without particle loses as a result of bubble coalescence, or break up. The instrument should also be capable of collecting a solid sample in excess of 200 grams in a reasonable time for PGM analysis as function of particle size.
2. Quantify effect of riser/sampling column diameter on axial mixing. The intensity of axial mixing and its subsequent effect to the bubble load quality will also be investigated.
3. Verify the applicability of the device in industrial flotation machines. Bubble loads from the device will be used in evaluating flotation kinetic data.
4. Develop hydrodynamic theory that predicts flow rates in various channels in the device based on standard chemical engineering equations.

1.3 Thesis Layout

In this chapter, the reader is introduced to the importance of bubble load measurements in evaluating froth flotation kinetics. Bubble load is defined and its importance to the flotation process is highlighted. Limitations of the existing bubble load measuring methods that prompted this research are outlined.

Chapter 2 provides a detailed review of previous research on particle loading on bubbles in froth flotation. The methods and approaches used by various researchers are critically analyzed; highlighting specific areas which need further attention and then the set of objectives for this thesis based on these limitations is presented.

Chapter 3 presents the details of the experimental work carried out in this thesis; it begins with a general description of the bubble load meter. Experiments carried out to test/validate the meter and subsequent improvements made on the device are highlighted. Industrial validation equipment set up is also described.

Chapter 4 describes the commissioning of the initial the bubble load meter; it highlights the developmental stages that resulted in the final bubble load meter. Changes in design, conclusions which lead to modifications on each design are presented. The actual description of experiments is in chapter 3. Results of tests done to validate the hydrodynamics, particle drop off, axial mixing are presented. The final design and its operating procedure are also included in this chapter.

Chapter 5 initially presents the basic theory that predicts pressure drop in the riser based on standard chemical engineering principles. It goes on to discuss the axial mixing model. The model describes the mixing taking place in the riser section of the bubble load meter. It aims to predict the salt concentration and hence inter-bubble particle concentration as a function of height above the bubble entry point. The model assumes that the mixing taking place in the riser can be approximated by a large number of mixers in series.

In addition to presenting the bubble load results obtained in the laboratory and industrial measurements at Lonmin Platinum, chapter 6 also summarises the important aspects of the

bubble load meter design. It discusses how the bubble loads can be used to interpret flotation kinetic data, estimation of froth recovery parameter and estimation of entrainment.

In chapter 7 the work is concluded and some recommendations are suggested. Bubble load meter aspects that critically affect bubble load measurement are highlighted. Limitations on the number of industrial results are also presented. Modifications to improve the bubble load meter are also given.

Chapter 2

Literature review

The chapter begins with a brief overview of the flotation process. Next it describes how particle loading on bubbles can be used to understand and improve the flotation kinetics. A detailed review of the different methods and devices that have been developed by various researchers for measuring bubble loading are presented. Key areas of interest include sampling methodologies, sampling column dimensions, bubble coalescence and break up, control of the hydrodynamics in the envisaged bubble loading device, maximizing the mass of sample that can be taken per unit time and the effectiveness of bubble load information in describing flotation kinetics. Based on the limitations of the current research into bubble load measurement in flotation, a number of objectives for this thesis are presented.

2.1 Froth flotation

Due to the low head grades of ore being mined (typically 3 to 10g/t PGM for platinum ores), it is necessary to upgrade the concentration of the desired mineral prior to further processing such as smelting. Froth flotation is a physico-chemical separation process that is often used in the mining industry to remove unwanted waste (gangue) material from the desirable mineral(s).

2.1.1 Grinding Circuit

Mineral extraction process begins with the grinding circuit, where the ore is first crushed, and then milled to obtain a particle size distribution that is typically between 10 and 100μm (Wills, 1992). The desired particle size distribution differs from mine to mine, and is usually a function of the mineralogy of the ore. The reason for grinding is to liberate the grains of the desired mineral(s). Water is added to the mills to transport the ore through the mill and onwards to the classification section. Closed loop control of the milling is achieved by using a classification circuit. The coarse particles are fed back to the mill for re-grinding. The fine particles are passed on to the flotation section. It is not uncommon to have multiple mills, screens and hydro-

cyclones in the grinding circuit. Figure 2.1 shows a typical schematic flow diagram of a single stage grinding circuit.

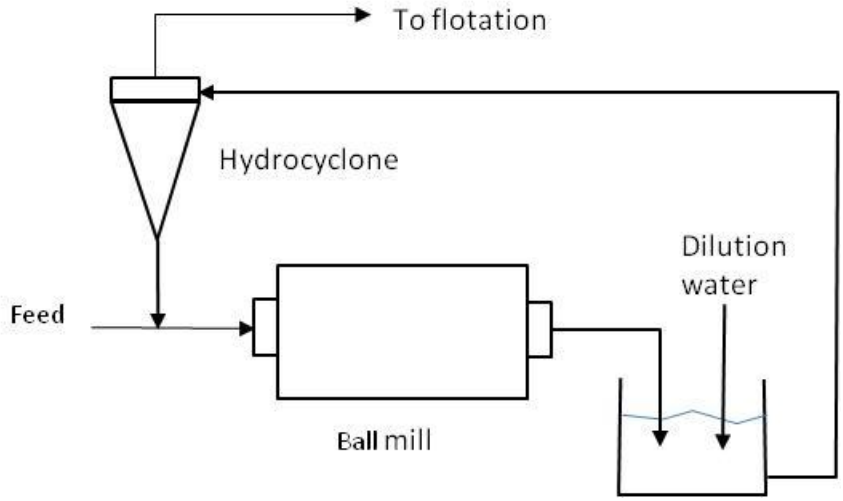

Figure 2.1 Typical single stage grinding circuit

2.1.2 Flotation Circuit

Prior to flotation, the pulp or slurry is pumped into conditioning tanks were flotation reagents are added. The conditioning tanks are sized to give enough time to allow the reagents to react with the slurry before flotation. The slurry is pumped from the conditioning tank to the first flotation cell.

A flotation cell is essentially a large tank that contains an impeller to agitate the slurry/air mix, and by so doing promote contacting between air bubbles and particles in the slurry. In certain flotation cells, the air rate is fixed while in others it is possible to set it to a desired value. In mechanical flotation cells an impeller is used to break the air into bubbles of a desired mean diameter and to keep the mineral particles in suspension. In flotation columns spargers are used to introduce air bubbles of desired mean diameter into the column.

Industrial scale flotation is a continuous process. Cells are arranged in series forming a bank. The pulp enters the first cell of the bank and gives up some of its valuable minerals as froth. Underflow from this cell passes to the second cell, where more mineralized froth is removed, and

so on until barren tailings flows out of the last cell in the bank. The first cells in a flotation circuit are known as *roughers* and the remaining cells as *scavengers*. Preferably, the concentrate from the *rougher cells* is refloated in *cleaner* cells to produce high grade concentrate. The use of *recleaners* is also not uncommon in commercial flotation. Figure 2.2 shows a typical schematic of a flotation circuit.

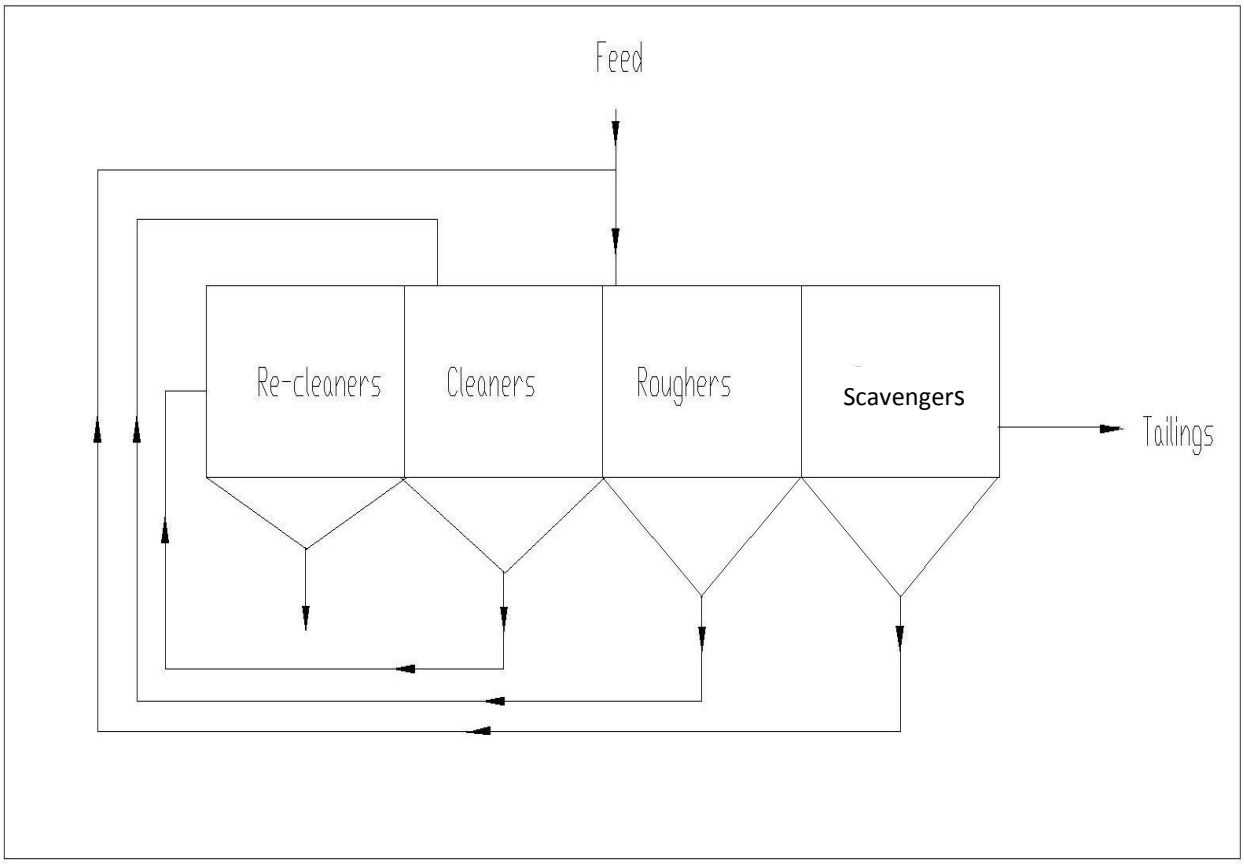

Figure 2.2 Typical Flotation Circuit

2.1.3 Flotation reagents

The chemical state of the pulp in the flotation cell is of utmost importance to ensure that optimal performance is achieved. Various reagents (collectors, frothers, and regulators) are added to the pulp for a variety of reasons:

1) Collectors

   These are chemicals which when adsorbed onto the surface of minerals renders them hydrophobic and so enable bubble-particle bonding. It is important for flotation collectors to be selective to avoid recovery of undesired minerals.

2) Frothers

   These are surface active reagents that interact with the water content of the slurry, reducing its surface tension. This allows for the formation of thin liquid films that make up the froth layer. A good frother produces a froth which is just stable enough to facilitate the transfer of floated mineral from the cell surface to the collecting launder (Wills, 1992)

3) Regulators

   These are chemicals that are added to modify the action of collectors. They are classed as activators, depressants, or pH modifiers. *Activators* are added to modify the surface of minerals so that it becomes hydrophobic by the action of collectors. *Depressants* render certain minerals hydrophilic when adsorbed to the mineral surface. The action of depressants increases the selectivity of the flotation process as it allows the collector to act on the desired mineral. Pulp alkalinity is also a very important control variable in flotation, It regulates the function of collectors which adsorb on to the surfaces of minerals at certain pH values. Chemicals used to control alkalinity are called *pH modifiers.*

2.3 Importance of bubble loading

Particles can leave the pulp phase through one of the two following routes: by collision with and attachment to a bubble or direct to the froth phase by entrainment at the pulp-froth interface. This process by which hydrophobic particles progressively attach themselves to the rising air bubble is called bubble loading. It includes bubble particle collision, attachment and possible detachment and is dependent on the hydrodynamic and kinetic criteria existing in the pulp phase of the flotation cell. The importance of bubble loading as a criterion for evaluating flotation kinetics has long been recognized. King et al. (1974), performed single bubble experiments showing how bubble-load increases as the bubble rises through the pulp phase. Seaman et al.

(2004) developed a device to measure bubble loading and used the bubble load result to estimate froth recovery parameter and froth selectivity. This device is further discussed in section 2.6.4 below.

2.3.1 Flotation Performance analysis

Metallurgical performance in flotation-related processes has been typically evaluated by two key indexes: mineral recovery and concentrate grade. Three approaches are commonly used to characterize the overall recovery in flotation equipment and these are: Single Stage process and overall flotation rate model, two stage processes and overall flotation rate model and two stage process and mass balance model (Yianatos et al., 2008)

Single stage process

In single stage process, the influence of the froth phase is not separated from the pulp phase. The overall recovery of minerals is determined by the combined recovery of minerals in the pulp and froth phase. Flotation response is described as a first order process with respect to floatable mineral concentration as in equation [2.1]

$$\frac{dC_i(t)}{dt} = -k_i C_i(t) \qquad [2.1]$$

where $C_i(t)$ concentration of floatable mineral at time t

k_i is the first order rate constant for size class i

From equation [2.1], overall Recovery is given by $R = 1 - \exp(-kt)$. [2.2]

Mathe et al. (2000) noted that there is no parameter which can be explicitly associated with the froth phase and overall recovery does not always fit equation [2.1] well. The two stage process was introduced.

Two stage process (Pulp and froth) and overall flotation rate model

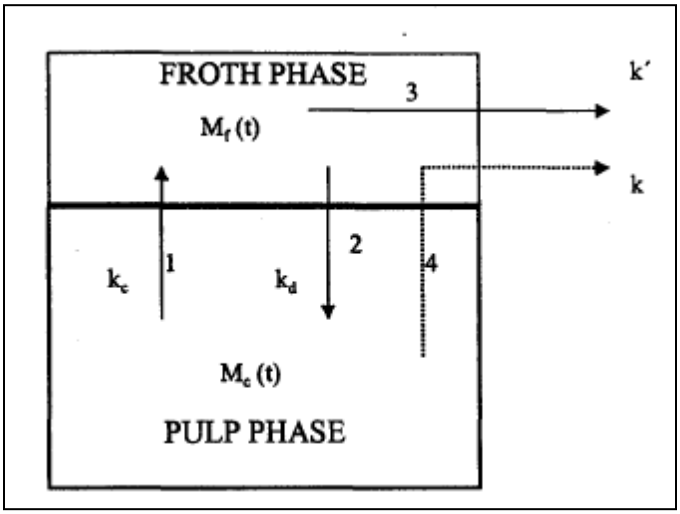

Figure 2.3 Two phase flotation (after Arbiter and Harris, 1962).

1 = transfer of material (selective and non-selective) from pulp to froth;

2 = dropback of particles from froth to pulp (detached and entrained particles);

3 = transfer of material out of the cell;

4 = overall transfer of material from the cell (pulp + froth) to the launder.

Arbiter and Harris (1962) introduced the two stage process (pulp and froth) and overall flotation rate model, illustrated in Figure 2.3. This approach recognizes the fact of flotation that the overall flotation rate is a contribution of the processes taking place in the pulp phase and as well as the froth phase. In this approach the apparent rate constant is related to pulp zone processes and froth characteristics. To calculate the overall rate constant, Finch and Dobby (1990) introduced the froth recovery parameter to account for the froth effect in flotation columns; froth recovery parameter R_f was defined mathematically as follows

$$R_f = \frac{k}{k_c} \qquad [2.3]$$

where k and k_c as defined in Figure 2.3.

The overall or apparent rate constant k' is then defined as

$$k' = k_c R_f \qquad [2.4]$$

Savassi et al. (1997) also defined froth recovery parameter as the fraction of particles entering the froth phase attached to the air bubbles that reports to the concentrate launder i.e.

$$R_f = \frac{\text{Flowrate of particles to the concentrate via the particle-bubble attachment process}}{\text{Flowrate of particles attached to bubbles entering the froth phase}}$$

Harris (1978) using the two stage process and the overall rate constant derived the following relationship to calculate the overall rate constant k'

$$k' = \frac{k_c}{(1 + k_d \tau_f)} \qquad [2.4b]$$

where constants are as described in Figure 2.3 and τ_f is froth residence time.

Two stage process (pulp and froth) and mass balance model

This approach (Finch and Dobby, 1990 and Yianatos et al., 2008) is depicted in Figure 2.4, the overall recovery is related to the collection and froth zones recoveries from mass balances according to Figure 2.4. The overall flotation recovery is defined mathematically by equation [2.5]

$$R_G = \frac{R_c R_f}{1 - R_c(1 - R_f)} \qquad [2.5]$$

where is R_G the overall flotation recovery

R_C is the collection zone recovery

R_f is the froth zone recovery

These recoveries are as defined in figure 2.4.

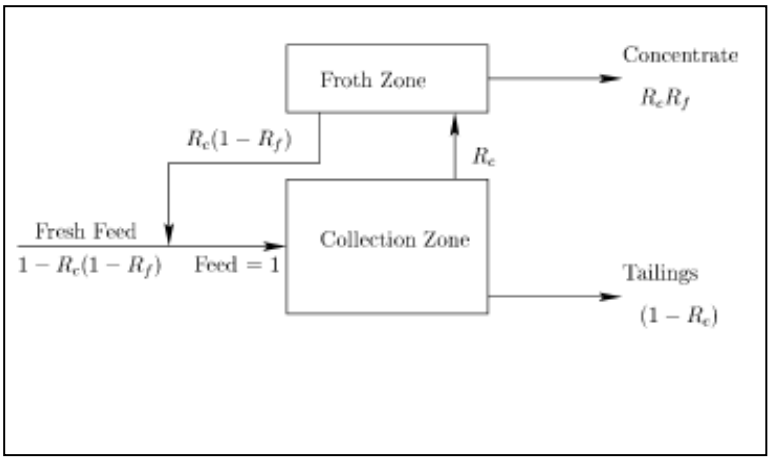

Figure 2.4 Pulp and froth recovery model

Froth recovery is central to the evaluation of the overall flotation performance. The project focus on the direct method of estimating froth recovery i.e. the use of bubble loads. Equation [2.7] was derived by Yianatos et al. (2008) to estimate froth recovery using bubble load information.

$$R_f = \frac{M_C}{M_B} \qquad [2.7]$$

where M_C (tph) is the mass flowrate of floatable minerals recovered into the concentrate by true flotation,
M_B (tph) is the mass flowrate of minerals entering the froth, as particle-bubble aggregate (true flotation), across the pulp/froth interface.

$$R_f = \frac{C.X_C}{\lambda_B.J_G.A_C.X_B} \qquad [2.8]$$

By defining C (tph) as the overall concentrate mass flowrate; X_C as the mineral (or valuable species) grade in the concentrate; λ_B as the bubble load(kg/m^3); X_B as bubble load grade; J_G as superficial gas velocity and A_C as cell cross sectional area at the interface level, Yianatos et al. (2008), developed equation [2.8] above to estimate froth recovery of minerals collected by true flotation using bubble load data.

2.4 Entrainment

Entrainment is the process by which particles that are not attached to bubbles are transferred from the pulp phase to the froth phase and out of the flotation cell with concentrate. Two mechanisms are used to explain entrainment, viz. unattached particles carried upwards in bubble lamella (Moys, 1978) and particles being carried in the wake of ascending air bubbles (Yianatos et al., 1986). Smith and Warren (1989), using the bubble swarm theory suggested that water in the pulp phase is mechanically pushed into the froth phase by a rising swarm of bubbles. Entrainment always occurs in parallel with true flotation and is responsible for most gangue recovery especially fines. Entrainment recovery has a significant effect on concentrate grade. Several models have been developed to estimate entrainment in flotation. A large number of researchers have shown consistently that there is a strong correlation between the water recovery and gangue recoveries (Zheng et al., 2006; Savassi et al., 1998; Neethling and Cilliers, 2002)

Entrainment recovery of particles of ith size class $R_{ent,i}$ is related to Water recovery R_w through the degree of entrainment ENT_i as proposed by Zheng et al, (2005) and is stated as follows

$$R_{ent,i} = ENT_i \times R_w \qquad [2.9]$$

where the degree of entrainment is defined as a classification function and is expressed as follows:

$$ENT_i = \frac{mass\ of\ free\ gangue\ particles\ of\ the\ ith\ size\ class\ per\ unit\ of\ water\ in\ the\ concentrate}{mass\ of\ free\ gangue\ of\ the\ ith\ size\ class\ per\ unit\ of\ water\ in\ the\ pulp}$$

[2.10]

In order to estimate gangue recovery in terms of water recovery, then it is important to know the degree of entrainment.

2.4.1 Modelling of degree of entrainment

Once the correlation between the entrainment recovery and the water recovery is confirmed, modelling of entrainment is transformed into the task of modelling the degree of entrainment and the recovery by entrainment can be determined if the water recovery is known (Zheng et al,2006)

To facilitate the calculation of froth recovery by true flotation in an industrial flotation cell the entrainment recovery needs to be estimated. Since water recovery can be measured directly, correlations/models to estimate the degree of entrainment are needed. Several models to estimate the degree of entrainment have been developed.

Ross and Van Deventer (1988) proposed equation [2.11] after conducting laboratory batch tests.

$$X_i = 1 - 0.429\log(d_i - 1).(\rho_s - 1) \quad [2.11]$$

where: $X_i = \frac{E_i.C_w}{W_i C_m}$ =degree of entrainment [2.12]

E_i = cumulative mass of entrained solids recovered (g)

W_i = cumulative mass of water recovered (g)

C_w = concentration of water in the pulp (g/l)

C_m =concentration of solids in pulp (g/l)

d_i = particle size

Maachar and Dobby (1992) as reported by Savassi et al. (1998) conducted tests in a laboratory column presented equation [2.13]

$$\frac{E_s}{R_{FW}} = \exp(-0.0325^* - \Delta\rho).\exp(-0.0063.d_i) \quad [2.13]$$

where: E_s = recovery of entrained solids

$\Delta\rho$ = difference in specific gravity of the mineral and that of the water

R_{FW} = recovery of water which is calculated from:

$$R_{FW} = 2.58\frac{\exp(-13.1.J_b)}{J_f} \quad [2.14]$$

J_b = water bias in the froth

J_f = superficial feed rate (volumetric flowrate/cell area)

d_i = particle size

Kirjavainen (1996) conducted flotation tests in laboratory and suggested that

$$P = \frac{W^{0.7}}{W^{0.7} + b.s.v^{-0.5}.m^{0.5s^{0.4}}} \quad [2.15]$$

where: P = entrainment factor = ratio of the recoveries of gangue and water.

W = water recovery rate (kg/m^2/s)

m = particle recovery (pg)

v = slurry viscosity (mPa s)

s =dynamic shape factor

b = constant = 0.00694

All these empirical models were developed from laboratory experiments where conditions were highly controlled. Savassi (1998) presented an empirical partition curve that describes the degree of entrainment within a conventional flotation cell as:

$$ENT_i = \frac{2}{\exp\left(2.292\left(\frac{d_i}{\xi}\right)^{adj}\right) + \exp\left(-2.292\left(\frac{d_i}{\xi}\right)^{adj}\right)} \quad [2.16]$$

$$adj = 1 - \frac{\ln(1/\delta)}{\exp\left(d_i/\xi\right)} \quad [2.17]$$

where: d_i = particle size

ξ = entrainment parameter, or the particle size for which the degree of entrainment is 20%.

δ = drainage parameter, related to the preferential drainage of coarse particles.

2.4.2. Use of chromite as non floatable tracer in UG2 PGM flotation

Estimation of entrainment is essential when calculating froth recovery by true flotation. Ekmekci et al. (2003) presented a method of estimating entrainment in a paper in which he investigated the effects of frother type and froth height on the flotation behaviour of chromite in UG2 ore. In situations where chromite is not activated, it can be taken as none or partially floatable and can be used to estimate parameters for the calculation of degree of entrainment. Chromite is activated, when it adsorbs copper in the form of $Cu(OH)^+$ at pH 9 (Wesseldijk et al., 1999). In

the absence of activation, chromite should report to flotation concentrate by entrainment or as locked to the floatable minerals. The approach of using chromite as non floatable gangue is tested in this work. Where a part of the chromite is activated, the degree of its floatability will be estimated from the bubble load analysis.

2.5 Froth recovery measurement

Several methods to measure froth recovery have been generated during the last few years. Moys et al. (2010) summarised them as follows.

1) The use of specially designed laboratory apparatus which effectively separates the collection zone from the froth zone and allows the collection of particles dropping out from the froth zone (Falutsu and Dobby, 1989).

2) Measurement of a wide range of variables and development of a model based on certain assumptions leading to the ability to solve for flowrates into the froth phase. Van Deventer et al. (2001) fitted a comprehensive model for column hydrodynamics to experimental data involving measurements of gas holdup and pulp concentrations in the column in addition to the usual measurements required to establish the overall mass balance.

3) Measurement of the effect of froth depth h_f on overall flotation recovery; the assumption that R_f tends to 1 as h_f tends to 0 allows the estimation of froth zone recovery (Vera et al., 1999).

4) Direct measurement of loading on bubbles:

Falutsu and Dobby (1992) measured loading on bubbles using a pipe passing downwards to below the froth phase with counter-current addition of water to ensure slurry does not get sampled. Dyer (1995) and Seaman et al. (2004), developed methods to measure bubble loading for calculating froth recovery parameter.

2.6 Bubble load measuring methods

Bubble load measuring methods presents a big step forward in attempts to quantify the recovery across the froth phase. Bubble load measuring devices developed thus far measures the desired parameter directly using relatively simple methods and do not depend on questionable

assumptions or complex models. No changes to plant operation are required, nor do the methods interfere with plant operation. The reproducibility of the instruments i.e. (Seaman et al., 2004) is remarkable and it has been used with good effect to analyze the behaviour of several flotation operations. After recognizing the importance of bubble loading information in flotation kinetics evaluation, several researchers developed methods and devices to accurately measure it. Some of the research progress made so far is discussed in the following section.

2.6.1 Bradshaw and O'Connor (1996)

Bradshaw and O'Connor (1996) developed a method to measure bubble loading in a micro-flotation column for the purpose of measuring the sub-processes of bubble loading. The method involved introducing air into the cell using a syringe. The loaded bubbles then rose through the cell and were deflected by a cone at the top of the cell and would report to the launder where the product is collected and weighed. Bubble size is measured first using a method developed by Randall *et al.* (1989). Though reproducible bubble loads have been reported by the authors, it cannot be used in an industrial setting. Furthermore the technique requires careful and meticulous control of bubble size, which (as acknowledged by the authors) became overloaded when the bubbles size goes below a certain bubble size and could not rise until particles became detached. The equipment setup used by the authors is shown in Figure 2.5.

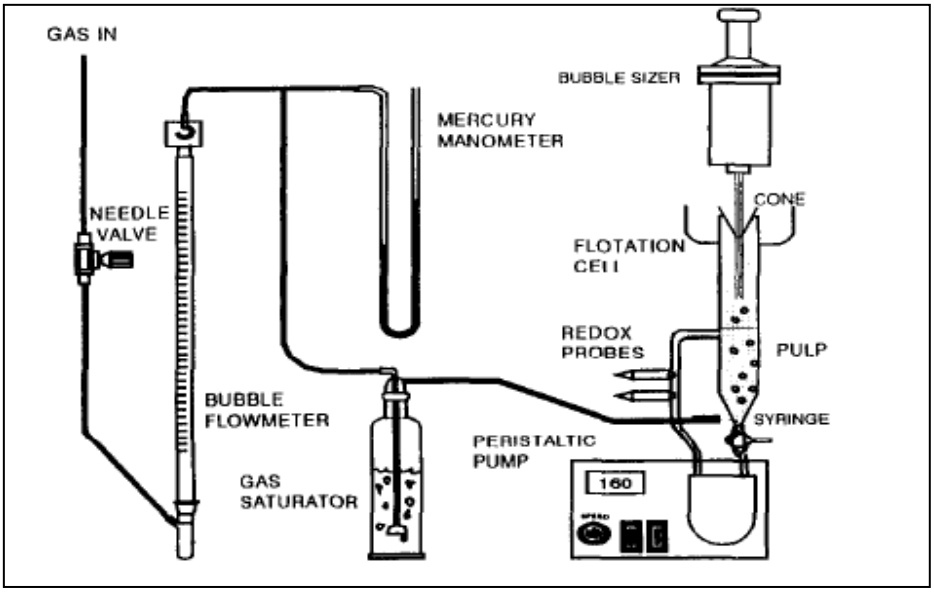

Figure 2.5: Experimental setup (Bradshaw and O'Connor, 1996))

2.6.2 Falutsu and Dobby (1992)

Falutsu and Dobby (1992) in their work to measure froth performance in commercial sized flotation columns, presented a technique to measure bubble loading, shown in Figure 2.6. The method involved dipping a 2.5 cm in diameter probe into the flotation column. Using a peristaltic pump, wash water was added to prevent sampling of the slurry (unattached particles). Liquid bias velocities ranging between 8cm/s to 15cm/s were used. Another peristaltic pump at the top of the riser was used to suck the loaded bubbles. Using the dry weight of the sample, sampling times and the gas rate, bubble load was calculated. However as mentioned by Seaman *et al.* (2004), no attention is paid in these methods to the possibility of collision of aggregates, the possible coalescence of bubbles, detachment of particles at high shear rates or rejection of fine bubbles or heavily loaded bubbles. It also is worth mentioning that the effects of column dimensions on flow dynamics in the column were not mentioned. Furthermore these tests were carried out in flotation columns alone and not mechanical cells.

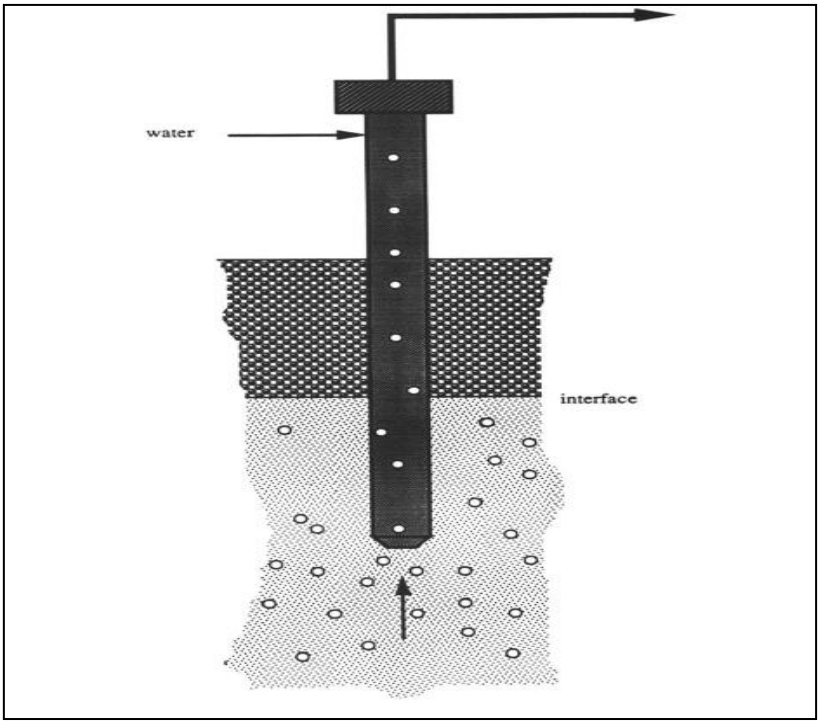

Figure 2.6: Experimental setup (Falutsu and Dobby, 1992)

2.6.3 Seaman *et al.* (2004)

Using the positive displacement principle, Seaman *et al.* (2004) developed a device to measure bubble loading in flotation machines, see Figure 2.7. This device is similar in concept to that designed by Dyer (1995). In this device loaded bubbles are trapped in a collection chamber, where the bubbles burst losing their load which is then collected weighed and assayed after the experiment. The air released by the bubbles displaces the water from the device causing it to travel down the riser at water bias velocity equal to the superficial gas velocity J_g. This is important to avoid sampling of particles suspended in the slurry. Superficial gas velocity being equal to the downward bias velocity ensures that no classification of bubbles at the bottom end of the riser takes place. Good reproducible bubble load measurements have been reported using this technique. The technique has also been used to determine froth zone recovery R_f and other flotation parameters with accuracy. One of the limitations of this method is the possibility of fine particles following streamlines down the riser to the flotation cell with the displaced water.

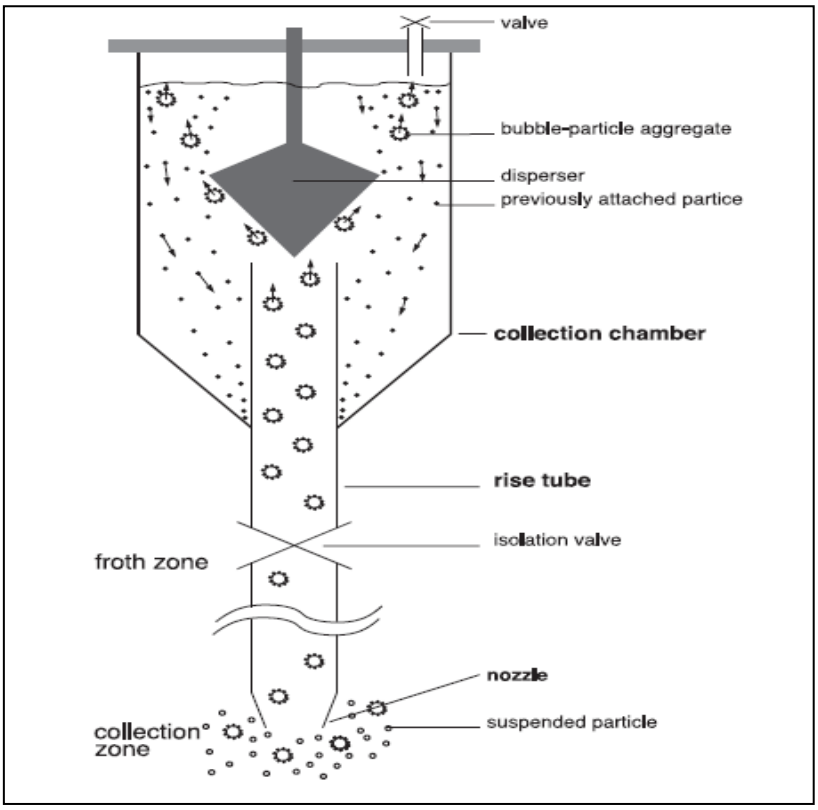

Figure 2.7: Experimental setup (Seaman *et al.*, 2004))

2.6.4 Dyer (1995)

The devices developed by Dyer (1995) also use the positive displacement principle, as shown in Figure 2.8. Bubble-particle aggregates are trapped in a collection chamber, within which the bubbles burst releasing their particles and the air. The air then displaces the plant water that was initially in the instrument. The displaced water flows down the riser ensuring that suspended particles in the pulp phase are not sampled. To eliminate the effect of bubble classification at the sampling point, a side drain which encouraged liquid to flow out side-ways was introduced. Regardless of the device's simplicity and its high propensity to be used in industry, it however did not produce satisfactory bubble load results. It is reported that the froth zone recovery R_f calculated using this method was greater than 1, resulting in the speculation that there could have been particle losses in the riser of the device.

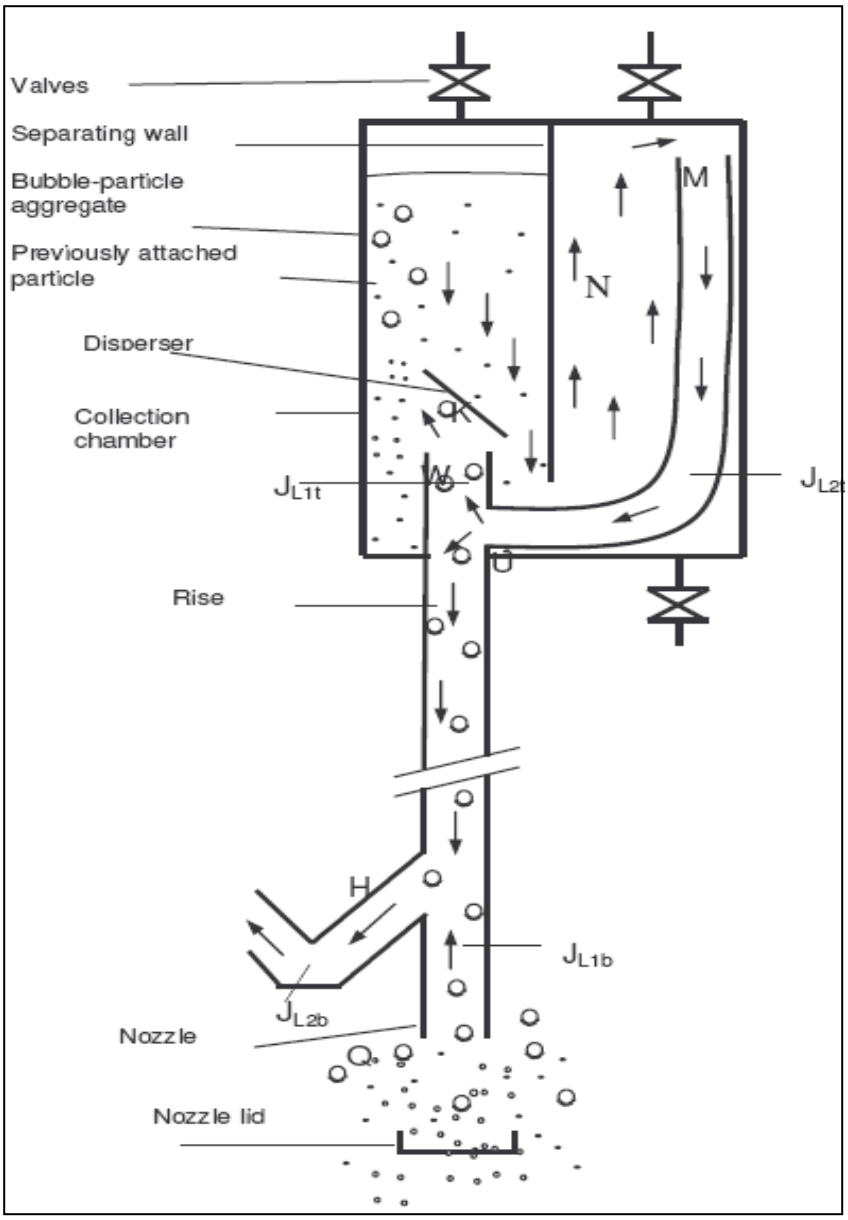

Figure 2.8: Experimental setup (Dyer, 1995)

2.7 Limitations of the existing methods

The limitations of the existing bubble load measuring methods are summarized below. These limitations and the strength of as discussed above will form the basis for the design of the new bubble load measuring device. The limitations include:

i. Applicable to ideal conditions that can only exist in the laboratory (Bradshaw and O'Connor, 1992).

ii. Applicable to certain sections of the plant i.e. rougher cells (Savassi, 1997).
iv. Low mass of samples taken which may have high sampling errors. For PGM analyses a large sample mass is required, at least 200grams.
v. Loss of attached particles in some methods or devices which leads to incorrect results.
vi. No attention is paid to the kind of flow regime that exists in riser (Seaman et al., 2004; Dyer, 1995; Falatsu and Dobby, 1992) and the effect of sampling/riser diameter on flow regime and axial mixing.

It important to note that to design bubble load measuring device based on the positive displacement theory used by Dyer (1995) and Seaman et al. (2004), three phase hydrodynamics of the fluids inside the column must be understood. The following section gives an overview of flow regimes that may arise in two phase systems and their contribution to the accuracy of the envisaged bubble load measuring device.

2.8 Flow regime in bubble columns

The hydrodynamic flow regime in the column/riser of the devices is important in ensuring that no particles are lost due to turbulence or bubble coalescence. So an understanding of the flow hydrodynamics in bubble columns becomes crucial in development of this device. Four types of flow patterns have been observed in two phase bubble columns (Shaikh and Al-Dahhan, 2007), viz. homogeneous (bubbly), heterogeneous (churn turbulent), slug and annular. Homogeneous flow regime generally happens at low to moderate superficial gas velocities. It is characterised by uniformly sized bubbles travelling upwards with minor transverse and axial oscillations, there is practically no coalescence and bubble break up. Heterogeneous flow occurs at high superficial gas velocities. There is intense bubble coalescence and break up, large bubbles churn through the liquid resulting in the name churn turbulent. Transition from one flow regime to the other depends on parameters such as superficial gas velocity, column diameter, and liquid and gas phase properties. Manipulation of these parameters will help size a riser that ensures no loss of particles and that enough sample is collected for analysis.

2.9 Effects of operating parameters on flow transition

Shaikh and Al-Dahhan (2007) summarised the effects of operating parameters on flow transition as given in Table 2.1. Transition velocity is the superficial gas velocity at which change from homogeneous flow to churn flow occurs.

Table 2.1: Generalized effect of operating and Design parameters on flow transition (*adapted from Shaikh and Al-Dahhan, 2007)*

Parameter	Effect on Flow Regime Transition	Reference:
Pressure	In general, an increase in pressure results in an increase in transition velocity	Krishna *et al.* (1991); Wilkinson *et al.* (1992); Reilly *et al.* (1994); Lin et al. (1999); Shaikh and Al-Dahhn (2005)
Temperature	An increase in temperature increases the transition velocity and delays flow regime transition	Bukur et al. (1987); Lin *et al.* (1999)
Viscosity	An increase in viscosity, in general, advances flow regime transition	Wilkinson (1991); Ruzicka *et al.* (2001)
Surface tension	Reduction in surface tension increases transition velocity	Gover *et al.* (1984); Urseanu (2000)
Solids loading	An increase in solids loading, in general, decreases transition velocity	Krishna *et al.* (1999); Vandu (2005); Mena *et al.* (2005), Shaikh and Al-Dahhan (2006)
Liquid height	An increase in liquid height reduces the transition velocity	Sarrafi *et al.* (1999); Ruzicka *et al.* (2001)
Column diameter	Conflicting results. An increase in column diameter increases transition velocity (Group 1) while column diameter advances flow regime transition (Group 2)	**Group 1:** Ohki and Inoue (1970); Sarrafi et al.(1999); Jamialahmadi *et al.* (2000); Urseanu (2000) **Group 2:** Zahradnik *et al.* (1997); Ruzicka *et al.* (2001)

The effect of liquid height (riser height) will determine among other things the length of the sampling section/riser of the bubble load meter.

2.10 Prediction of flow regime transition

The prediction of flow regime has been achieved by development of various models that includes empirical correlations, semi empirical and phenomenological models, stability theory and

Computational Fluid Dynamics. As mentioned by Shaikh and Al-Dahhan (2007), several researchers produced correlations for predicting flow regime in two-phase flow. Some of them are shown in Table 2.2

Table 2.2: Flow regime prediction models and references.

Flow prediction model type	**Reference**
Empirical correlations	(Wilkinson et al.,1992; Reilly et al.,1994)
Semi empirical correlations	For small diameter pipes or tubes (Taitel et al.,1980; Mishima and Ishii,1984) For large diameter bubble columns (Kelkar, 1986; Ranade and Joshi,1987Sarrafi et al., 1999; Ruzicka et al.,2001)
Stability theory	(Bhole and Joshi, 2005; Leon-Becerril and Line, 2001; Joshi et al.,2001; Lister and Flower, 1992; Shnip et al., 1992; Bieseuvel and Gorisson, 1990; Pauchon and Banerjee, 1988)
Computational fluid dynamics	(Wang et al., 2005)

Some of these empirical models were used to predict flow regime during the design of the riser of the device.

2.11 Flow pattern transition models

For prediction of transition in small diameter columns the model developed by Taitel et al. (1980) is discussed below. In order to develop generally applicable transition models for vertical flow, Taitel et al. (1980) attempted to suggest physically based mechanisms and to model the transitions based on these mechanisms. They suggested the following equation which characterizes transition from bubbly flow to slug flow

$$U_L = 3U_G - 1.15\left[\frac{g(\rho_L - \rho_G)\sigma}{\rho_L^2}\right]^{0.25} \quad [2.18]$$

For the existence of bubbly flow he suggested the following criterion

$$\left[\frac{\rho_L^2 g D^2}{(\rho_L - \rho_G)\sigma}\right]^{0.25} \leq 4.36 \quad [2.19]$$

where ρ_L - Liquid density (kg/m^3)

ρ_G – Gas density (kg/m^3

D - Column diameter (m)

U_L -Liquid superficial velocity (m/s)

U_G - Gas superficial velocity (m/s)

σ -Surface tension (N/m)

2.12 Axial mixing

The effects of axial mixing have implications for the final design of the bubble load meter. Axial mixing limits the final riser diameter of the bubble load meter. Transport of unattached particles up the riser is a strong function of the axial mixing in the riser. The mixing in a vessel involves redistribution of material by slippage or eddies and all the contribution of backmixing of fluid in the vertical x direction which is analogous to the Fick law is modelled as

$$\frac{dC}{dt} = D\frac{\partial^2 C}{\partial x^2} \quad [2.20]$$

where

D is called the axial dispersion coefficient

C is concentration of tracer in mols/litre

x is the length in the direction of flow (cm)

The axial dispersion model ADM (Levenspiel, 1972) has been used traditionally to quantify backmixing. The axial dispersion coefficient can be readily extracted from experiments. The most important aspect for this thesis is the implications of the magnitude of the axial dispersion coefficient on an acceptable column/riser diameter

2.13 Research objectives

Measurement of particle loading on bubbles has been used to measure froth zone recovery and to evaluate the performance of flotation machines. Regardless of the reported success of the available measuring methods, they have limitations. This research in addition to addressing some of the limitations of the available methods explores the hydrodynamics of the device. Questions such as the effects of increasing or decreasing the sampling column or riser diameter to the flow regime are explored. The height of the liquid column, which governs the length of the device and its effect to the prevalent flow regime, is explored as well. The simple effect of particle losses as fine particles follow liquid stream lines from the collection devices is also explored. A hydrodynamic model to predict the flow in the various parts of the device is needed. The thesis objectives in addition to those mentioned earlier are to:

1. Develop a hydrodynamic model that predicts flow rates in various channels in the device based on standard chemical engineering equations.
2. Develop an instrument or device to measure bubble loading in industrial flotation machines based on the Dyer (1995) concept. The device should measure bubble loads accurately without particle losses as a result of bubble coalescence, or break up. The instrument should also be capable of collecting a solid sample in excess of 200 grams in a reasonable time.
3. Verify the applicability of the device in industrial machines and evaluate the effectiveness of the bubble loads obtained using the device in evaluating flotation kinetic data.

Chapter 3

Experimental Equipment and Methods

The main aim of this chapter is to present the details of the experimental work done. It begins with a general description of the bubble load meter and its operating principle, followed by a detailed description of the laboratory and industrial tests done. The experiments are divided into two categories, those that are intended to test and verify design aspects and those intended to tests the final design's industrial applicability. The set up, equipment description and experimental designs are all included in this chapter.

3.1 Bubble loading measurement device-Bubble load meter

To measure the particle loading on bubbles needs careful consideration. Several factors have to be critically examined and taken into account, these include that

1) The bubble sample must be a true representative of the bubble population.
2) No particles should detach from the bubbles as they rise in the riser.
3) The hydrodynamics in the collecting device should ensure no loss of particles or carrier gas and should prevent collection of entrained particles.
4) It must be easily used in an industrial environment.

In designing the bubble load measuring meter, the positive displacement principle as articulated by Dyer (1995) and Seaman *et al. (*2004) was adopted.

3.1.1 Initial design

The device designed initially is shown in Figure 3.1. It is constructed out of transparent Perspex to enable clear observation. It is divided in to two basic sections viz. the sampling section and the collection section.

The Sampling section

The sampling section consists of 1500X30mm Perspex column which is attached to 100x300mm horizontal section. The hydrodynamics in this section should be controlled carefully as it determines the accuracy and precision of the measuring device. The riser part of the sampling section is provided with sampling ports as depicted in Figure 3.1 Sampling ports provides samples of the inter-bubble liquid for checking if there is any particle drop off.

The collection section

The collection section is made up of a circulating peristaltic pump, water rotameter, filter, a collection chamber with pressure gauge and surge tank to smooth out pulses from the peristaltic pump. In the collection chamber the volume of the collected air is measured and particles are collected. The filter ensures that no particles are re-circulated back into the sampling section with the water. The technical specifications of the bubble load meter are shown in Table 3.1

Table 3.1: Bubble load meter specifications

Section	**Dimensions**
Riser diameter (cm)	3.00
Length (cm^3)	150.00
Collection chamber volume(cm^3)	8000
Objective sample(grams)	200.00
Assumed bubble load rate(g/l)	26.80
Gas volume (litres)	7.46
Bubble velocity(cm/s)	1.33
$J_L = J_b$	
Volumetric flow rate in the riser(ml/s)	**9.40**
Recirculation flowrate(ml/s)	**18.80**

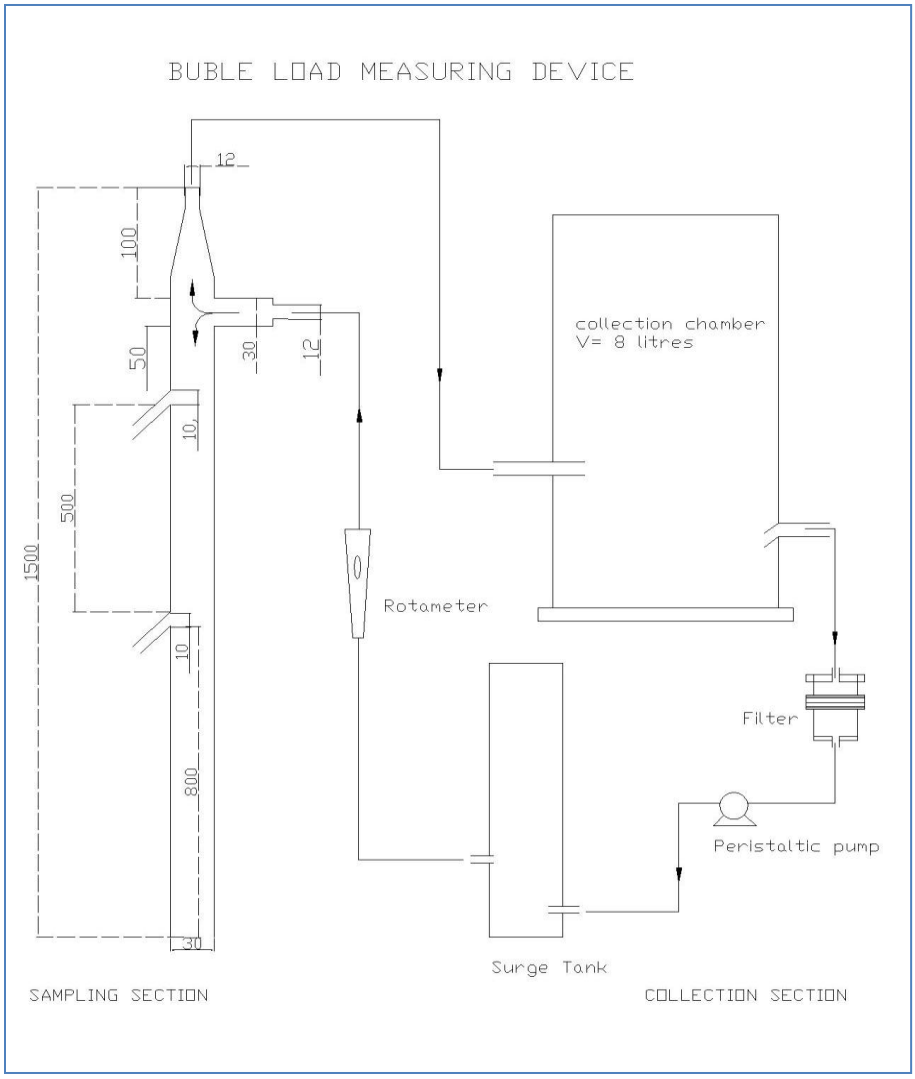

Figure 3.1: Bubble load measuring device

3.2 Bubble load meter operating principle

The bubble load meter works on positive displacement principle, where the volume of gas collected in the collection chamber displaces an equal volume of water. The displaced water is pumped to the riser column and flows down into the flotation cell. In addition to this water, the pump also takes a fraction of the water in the collection chamber and circulates back to the collection chamber as shown in Figure 3.2. This is important in that it provides the liquid media in which bubbles can flow from the sampling section to the collection section. The velocity of

the recirculating water increases at the sudden contraction as the channel of flow is reduced from an ID of 30mm to 12mm. This is important in that it facilitate particles that detach from bubbles at the sudden contraction to be carried over to the collection chamber. It is also important to note that the volume of liquid displaced down the column is equal to the volume of air collected in the collection chamber and thus superficial liquid velocity (J_L) is equal to superficial gas velocity (J_g) at the pressure in the collection chamber. Maintaining J_L equal to J_g reduces bubble segregation at the entry point in the pulp phase and particle detachment in the sampling section/ riser. The displaced liquid also prevents unattached particles from rising up the column with the inter-bubble liquid. At the end of each run, the valve between the sampling section and the collection chamber is closed and time taken, gas volume and mass of particles collected is recorded.

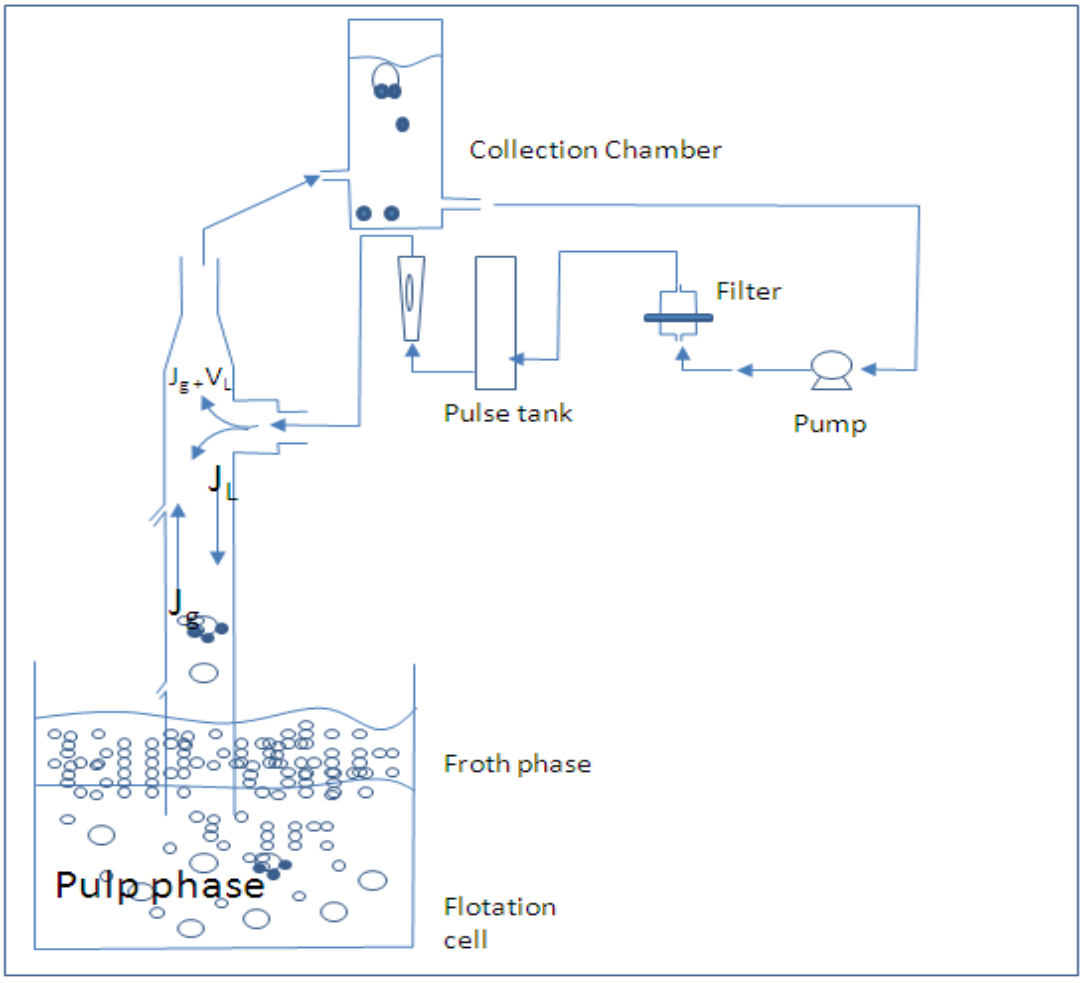

Figure 3.2: Bubble load meter operation

3.2.1 Recirculation measurement and control

Water flow control is very important in the operation of the bubble load meter. The volume of water displaced from the collection chamber is equal to the volume of air collected in the collection chamber, thus the downward flow of water in the sampling section depends on superficial gas velocity (J_g). Consequently the water recirculation rate is also a function of J_g. In the operation of the bubble load meter, water recirculation rate was set to be twice the gas flowrate. This ensured that the water going back to the collection chamber was equal to the water being displaced down the column. A Watson Marlow 514 peristaltic pump was used to meter and circulate water at a desired flowrate. A water rotameter was also used to verify the flowrate. To avoid pumping particles collected in the collection chamber back into the sampling section, a filter was provided at the discharge side of the pump. A photograph of the pump filter surge tank and water rotameter is shown in Figure 3.3.

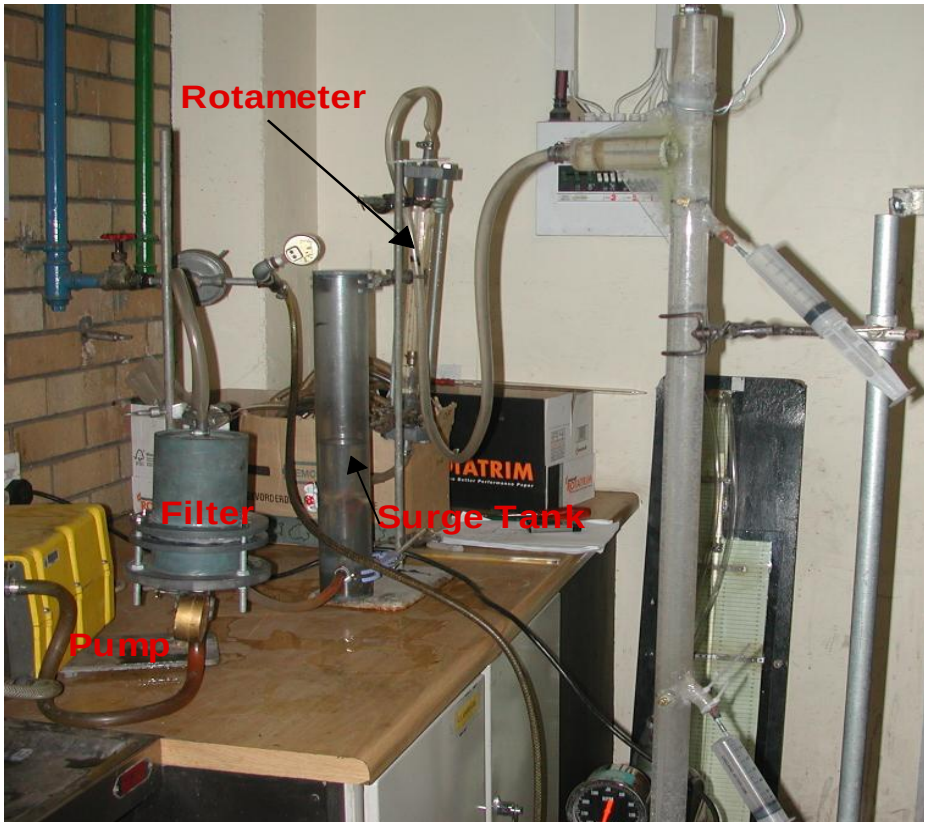

Figure 3.3: Pump, Filter, Surge Tank and Rotameter arrangement

3.3 Laboratory tests of the bubble load meter

After designing the bubble load meter, its operability and conformance to design objectives needed to be tested before doing industrial bubble load measurement. The design objectives stated in section 3.1 needs to be verified. Experiments to test particle drop off, rejection of suspended particles, and flow regime identification were designed.

The experiments were carried out in a Denver D12 laboratory flotation cell. The 8 litre flotation cell is made of stainless steel; Figure 3.4 shows its dimensions. Though the cell is self aerated, to maintain the required air flowrate, air at 1 bar was throttled through a valve and measured by the rotameter. The agitator was maintained at 2000 rpm for the all experiments. To control bubble sizes, MIBC was used as the frother. For easier frother dosage control, MIBC was diluted to 1% v/v solution.

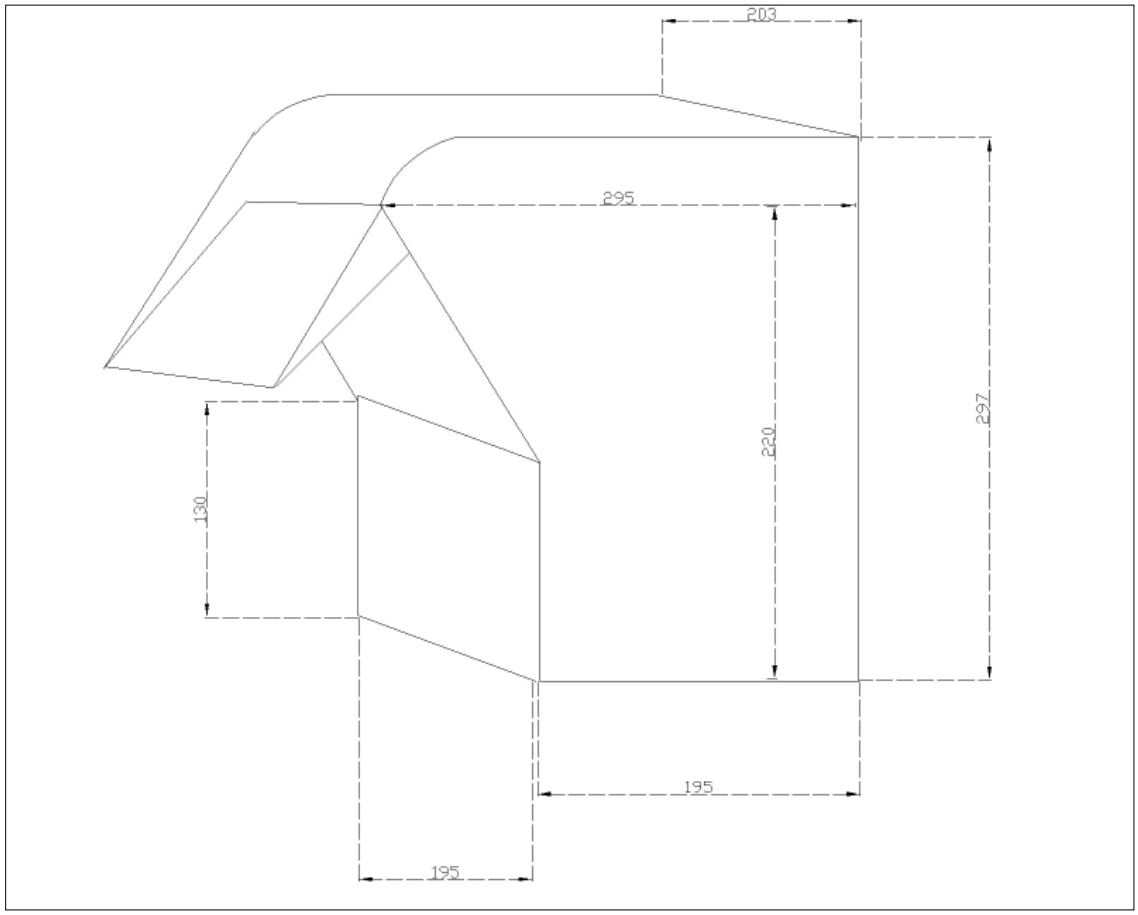

Figure 3.4: Flotation cell dimensions

3.3.1 Rejection of suspended particles experimental set up.

Only particles that are attached to bubbles should report to the collection chamber. This is very important in that only particles collected by true flotation constitute bubble load. Unattached particles can only report to the collection chamber if inter-bubble liquid rises up the riser as a result of axial mixing. Thus axial mixing became very important in the design of the bubble load meter. Stimulus-response experiments have been widely used to characterize flow patterns in reactors (Levenspiel, 1972). These experiments involve introducing a tracer into the inlet and monitoring how the system responds to the stimulus and thus information about the system is acquired.

To quantify the effect of axial mixing to the flow of inter-bubble liquid, conductivity (stimulus-response) experiments were done with NaCl as the tracer. Three 5mm brass conductivity probes were glued at different heights above the entry point of sampling section as shown in Figure 3.5. The brass conductivity probes were glued at 300, 770 and 1380mm above the entry point to the riser. They were glued in such a way that their end was flush with the internal surface of the riser. This was done to make sure that the distance between the probes is equal to the ID of that particular riser

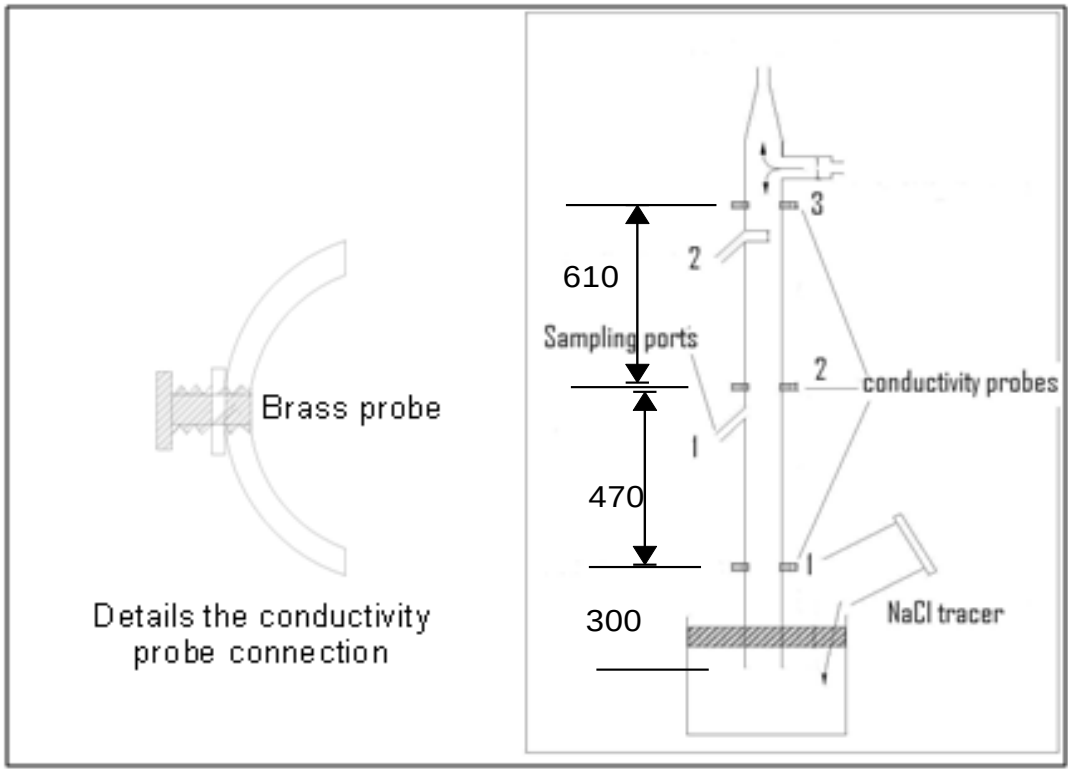

Figure 3.5: Conductivity probe positions and connections

Conductivity experiments procedure

The schematic of the experimental set up for the conductivity experiments is shown in Figure 3.6. The experiments were carried out in the Denver flotation cell. The bubble load meter was filled with frother water first and conductivity probes were connected to the PC through a conductivity circuit and pci703 data board. It was then dipped into the flotation cell to about 30mm below the pulp froth interface. After connections, the experimental run was started with water alone, air (bubbles) were introduced into the flotation cell after 30 seconds. To cater for the effect of bubbles to the output voltage 30seconds were allowed with the water-air system, after which an impulse change was introduced by adding 500ml of 1mole solution NaCl into the flotation cell. The experiment was run for further 480 seconds before stopping. It is important to note that these experiments were done with air-water system alone without floating any particles. The oscilloscope on the Waveview for windows was used to record and store the output data from the conductivity experiments.

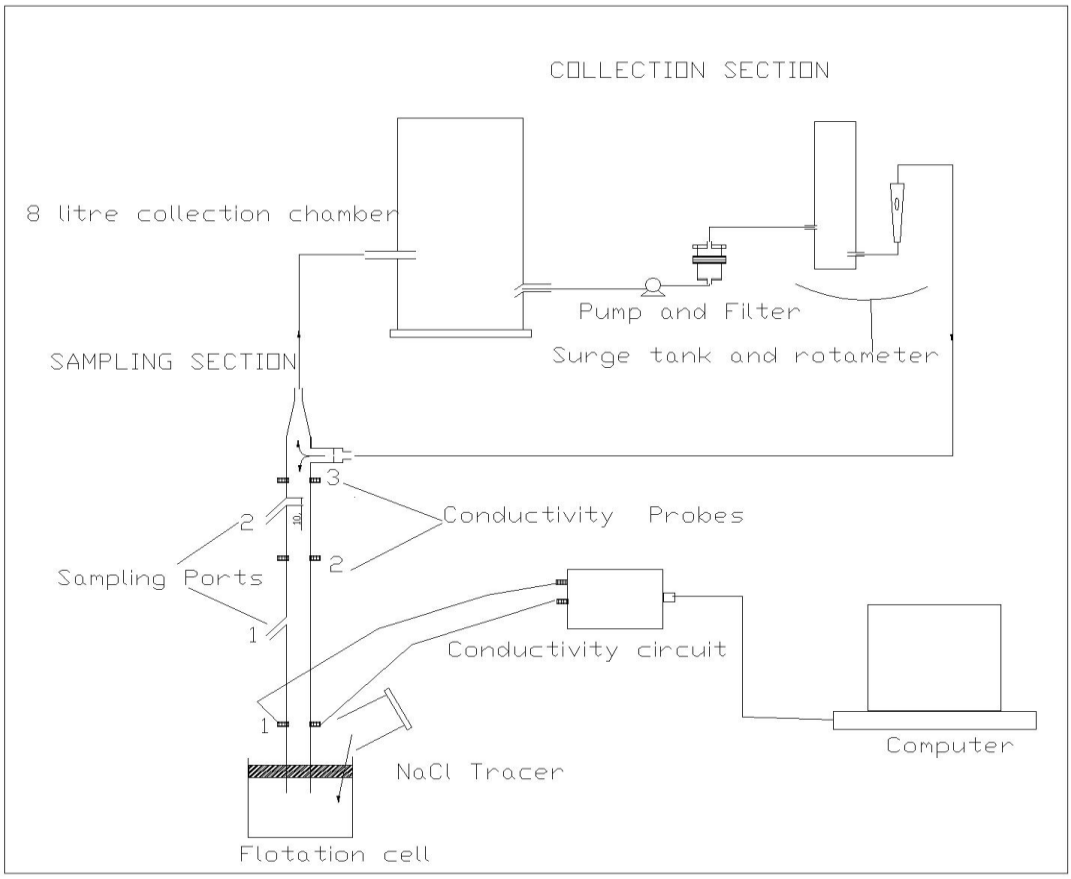

Figure 3.6: Conductivity Experimental setup

Conductivity Data analysis

To quantify the effects of axial mixing on salt transport up the riser of the bubble load meter, careful manipulation of the output response from the conductivity experiments is needed. The use of RTD has been used extensively in chemical engineering literature. Its application in this context was limited by the following factors:

1. The transport of the salt tracer into the bubble load meter riser is by axial mixing (Figure 3.7) and the amount of the injected salt is determined by the intensity of the axial mixing.
2. Salt transport in the riser is not unidirectional because an element of fluid Q_m can rise up to conductivity probe j by axial mixing and back to the flotation cell by the downward water flow.

The peak steady state concentration recorded by each probe was taken as the concentration at that particular probe. To estimate the relative amount of salt at a particular position in the riser a

model that represents the variation of NaCl concentration with height in each riser was used. This variation of NaCl concentrations with height was found to be adequately represented by the empirical equation below.

$$C = C_0 \times e^{-kh^{1.5}} \qquad [3.1]$$

where: C is concentration of NaCl/suspended particles at height h above riser entry point

C_0 is the initial concentration of NaCl/suspended particles in the flotation cell

k is a constant which is a function of bubble size (frother concentration) and the intensity of axial mixing

Integrating equation [3.1] between ($h = 0$ *and* $h = H_j$) gives the total mass of NaCl to a given conductivity probe height H_j, hence the mass of NaCl up to that conductivity probe is calculated. The relative quantity is defined as the ratio of the salt at a particular position to that added to the flotation cell.

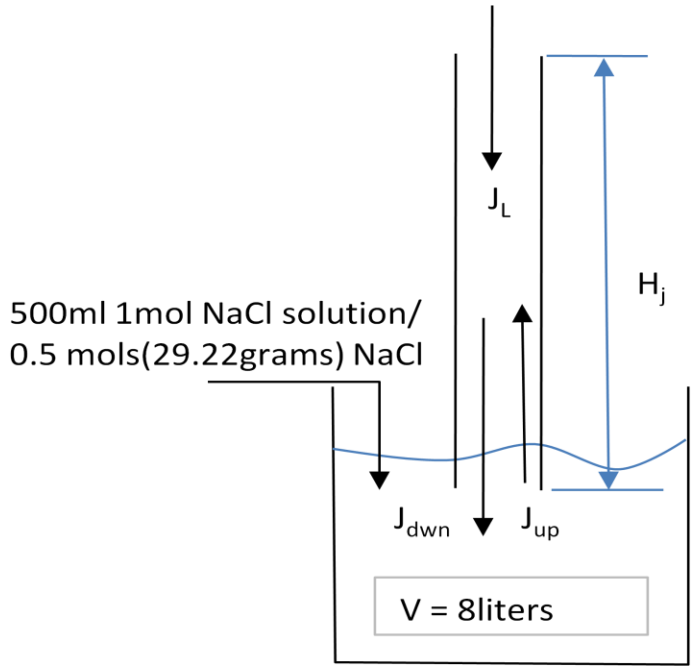

Figure .3.7. Schematic representation of salt transport

3.3.2 Laboratory bubble load measurements

To test the bubble load meter, coal fines flotation was carried out in the flotation machine. The objective of these experiments was to test the bubble load meter when carrying out real froth flotation and also to ascertain whether there is particle drop off. The procedure for coal flotation is based on the Australian Standard – coal preparation AS4156.2.1-2004

Flotation Specifications-coal flotation

800gramms of coal fines was weighed and screened. The solids content used was 100grams per litre of pulp, so that for 8litres, 800grams of dry solids was added maintaining a 10% solids. The level of the pulp in the flotation cell was maintained at about 20mm below the overflow lip with the agitator running. The quantity of the collector (Kerosene) added was 1ml/kg of dry solids and the quantity of the frother was maintained at 0.1ml of MIBC per kilogram of dry solids. The air flow rate was kept at 5 l/min using the air rotameter. The coal was floated for 5 minutes. Table 3.3 shows the typical PSD of the coal feed sample.

Table 3.2: Typical coal particle size distribution

Particle size class	%mass in size class	Cumulative %mass retained
+300	0.00	0.00
-300 + 212	20.61	26.61
-212 + 150	28.58	49.19
-150 + 125	14.50	63.69
-125 +106	13.10	76.79
-106 +90	9.61	86.40
-90 + 75	7.57	93.97
-75 + 45	6.03	100.00
Total	100.00	

Flotation procedure

The 800gram sample was transferred into the flotation cell containing 1000ml of water. A mixing time of 2 minutes was allowed with the agitator running at 1000rpm, before another 2 minutes was added with the agitator now at 2000rpm. This was done to ensure thorough wetting

of the coal. Water was added to the flotation cell up to the 8 litre mark. The collector was added by means of a syringe beneath the surface of the pulp. The pulp was conditioned for 1 minute before adding the frother. The cell contents were then conditioned for a further 1 minute before opening the air valve to begin flotation.

Bubble collection procedure

1) The collection chamber was filled with frother/plant water.

2) The pump was started after making sure that the bottom of the riser section of the device was tightly closed.

3) Circulation was allowed to take place until all the sections of the device were filled with water.

4) Water was added to the collection chamber up to the mark again.

5) The device was lowered into the flotation cell, down to the required level. While the pump was still circulating water, the stopper at the bottom of the device was removed.

6) The timing device was started as the first bubbles entered the collection chamber

7) After 5 minutes the valve to the collection chamber was closed the pump and the agitator were stopped and time and volume recorded

8) Water was filtered from the collection chamber contents and mass of solids collected was recorded.
9) Masses of solids collected as the concentrate and tailings were also recorded.

3.3.3 Testing for particle drop off

Particle detachment occurs as a result of the build up of excessive forces in the bubble skin following the sudden acceleration of the particle-bubble aggregate (Cheng and Holtham, 1995). Klassen and Mokrousov (1963) identified six possible ways by which particles gets detached from bubbles, these includes particle inertia as the bubble rises, pressure of liquid streams on the bubble skin, particle dropping off as bubble changes direction of motion, impact of another particle and impact if the bubbles hit a barrier. There are three possible ways in which particles

can detach from bubbles in the bubble load meter viz. bubble coalescence, sudden acceleration of the bubbles at the T-junction, change of bubble motion as a result of the axial mixing in the bubble load meter.

To verify whether bubbles are losing their load in the riser section of the bubble load meter, samples of inter-bubble liquid were drawn gradually using syringes from the provided sampling ports. The sampling ports are arranged such that one is 50mm below the T-junction, where particles are anticipated to detach due to sudden acceleration of the bubbles and coalescence at the T- junction. The other is 800mm above the entry point to cater for the effect of axial mixing along the riser. The drawn inter-bubble liquid was then analyzed for particles. Figure 3.8 shows the sampling port-syringe arrangement.

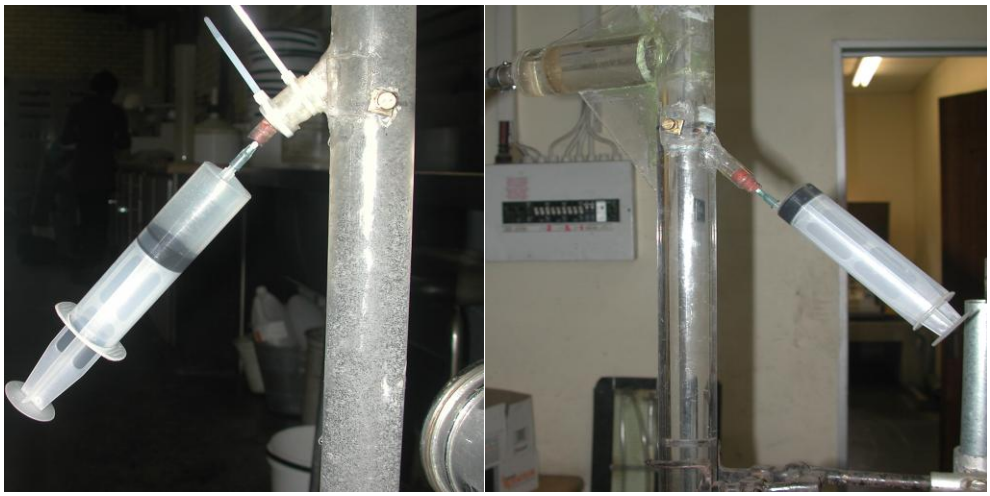

Figure 3.8: Photographs showing the positions of the sampling ports and the associated syringes for sample extraction on the bubble load meter

3.3.4 Flow identification methods

Flow regimes in two phase flow can be identified by visual observation. The use of digital and video cameras can enhance the quality of information that can be obtained from visualization. In order to identify the flow regime existing during bubble load measurements and bubble meter testing, a digital camera Nikon D990 was used. In addition to flow identification, bubble sizes and bubble rise velocities can also be estimated. Adjustment of the camera shutter speed enabled

freezing of the bubbles at high shutter speed and reducing the shutter speed gave an idea of the path being followed by the bubbles as they rise.

3.4 Industrial test set up

The main aim of this thesis is to produce a bubble load meter that is industrially applicable. To fulfil this objective, validation of the equipment was carried out at Lonmin's EPC (Eastern Platinum Concentrator) in Marikana.

3.4.2 EPC basic flotation circuit

Bubble load measurements were done on the first cell of the primary roughers and the first cell of primary cleaners. EPC treats UG2 Ore; with a head grade 0.3% sulphur. Appendix D shows the typical composition of the ore. The ore is initially ground to 80% passing 75µm, and treated with SNPX collector. The pulp is pumped from the primary rougher feed tank at rate of 415tph and 22% solids by mass into the first cell of the primary roughers. The concentrate from the first three cells of the primary roughers goes to the first three cells of the primary cleaners, while the rest goes to the last 6 cells of the primary cleaners. Concentrate from these first three cleaner cells is pumped to the high high grade 'HHG' concentrate cells as shown in the basic EPC flow diagram, Figure 3.9

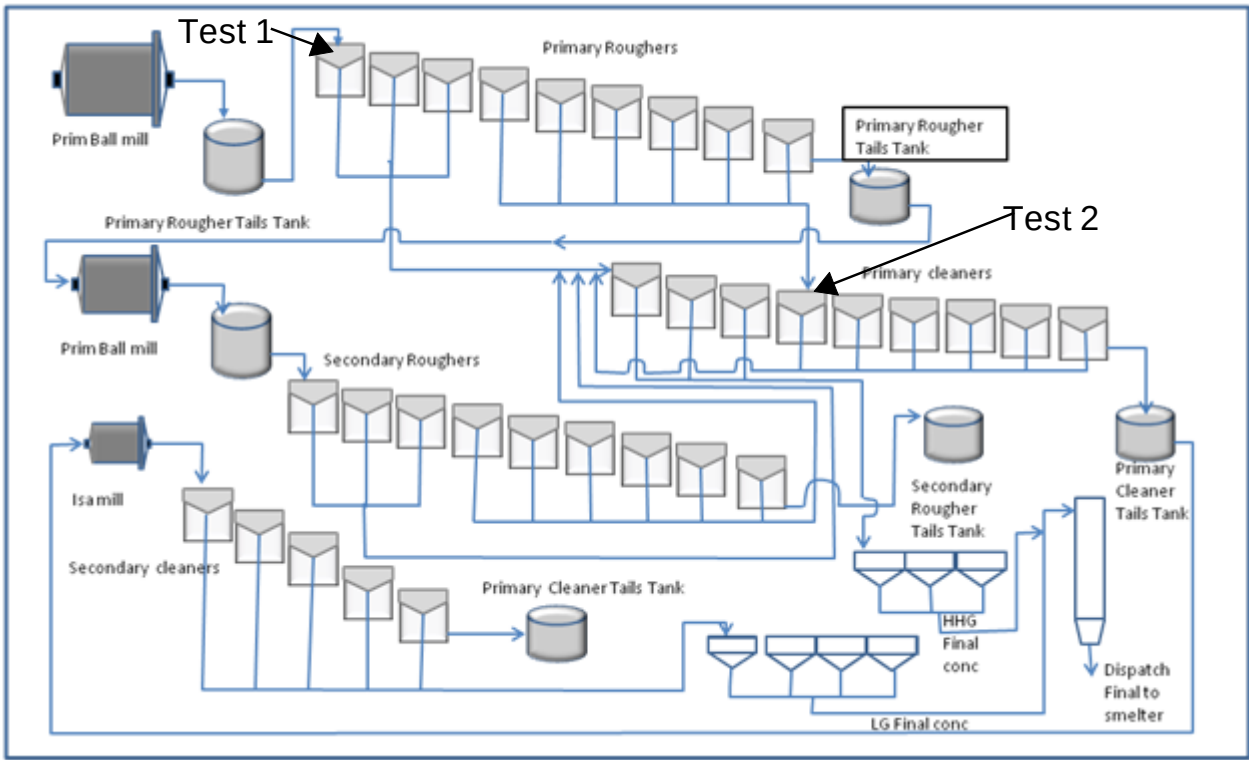

Figure 3.9: Lonmin flotation circuit

3.4.1 Equipment set up: Primary rougher

Figure 3.10 shows the position of the bubble load meter riser stand and the riser-stand arrangement during bubble load measurement. It is important to maintain the riser vertical to avoid bubbles from concentrating on one section of the riser. The use of a spirit level ensured that the riser was vertical. To avoid air accumulation in the tube that connects the riser to the collection chamber, the collection chamber was maintained above the riser by using a table as a stand. Figure 3.11 shows the stand with the collection chamber surge tank and water rotameter.

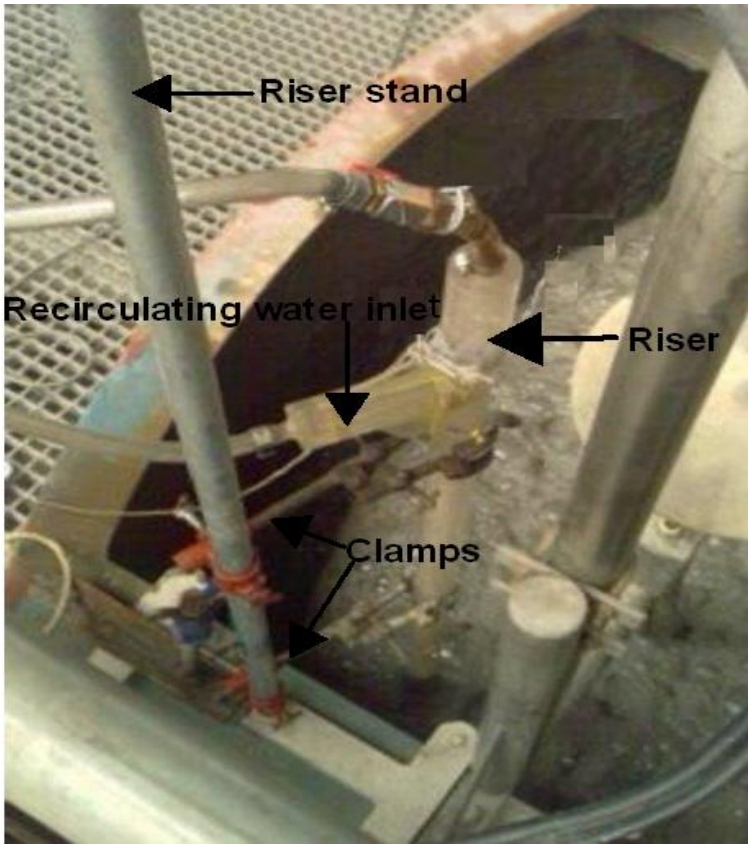

Figure 3.10: Photograph shows position of riser in the flotation cell during bubble measurement

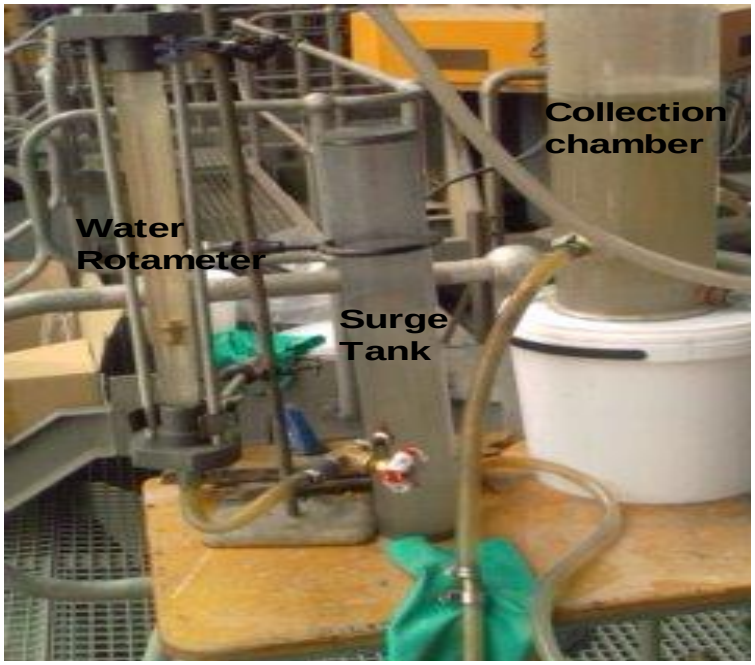

Figure 3.11: Photograph showing the collection chamber, surge tank and water rotameter during bubble load measurement.

3.4.2 Equipment set up: Primary cleaner cell

Equipment set up for the primary rougher cells was also adopted for the primary cleaner cells.

3.4.3 Concentrate and pulp sampling

By using buckets and A3 plastic bags and a timer, concentrate samples from both the primary rougher and primary cleaner cells were obtained. It is important to note that since the sampling method had a high propensity to errors, repeats were done. Samples of the pulp were drawn just below the pulp-froth interface using a beaker. The beaker was dipped to below the pulp froth interface while closed but facing upwards opening was done in the pulp phase. This was done to make sure that only the pulp is sampled without sampling particles attached to bubbles.

3.5 Estimation of gas dispersion parameters

3.5.1 Gas hold up

Gas hold up refers to the volumetric fraction of air in the riser. Hold up can be measured using the bubble load meter by connecting a water manometer to the sampling ports. Gas hold up is then calculated using the equation below, assuming that bubble density is equal to zero.

$$\varepsilon_g = 1 - \frac{\rho_w}{\rho_{sl}}\left[1 - \frac{\Delta h}{\Delta L}\right] \qquad [3.1]$$

where ρ_w is density of water

ρ_{sl} is density of slurry

ΔL is height difference between manometer inlets

Δh is height difference between manometer levels

3.5.2 Superficial gas velocity

Superficial gas velocity can also be measured with the bubble load meter. Superficial gas velocity J_g is calculated from the volume of air collected. The air volume needs to be corrected

to atmospheric pressure since the pressure inside the collection chamber is less than atmospheric. Assuming that all fluids are at atmospheric temperature, the corrected volume (V_{gc}) is given by

$$V_{gc} = V\frac{P_{abb}}{P_{atm}} \qquad [3.2]$$

where: V is the measured volume.

P_{atm} is atmospheric pressure

P_{abb} is absolute pressure at which the volume measurement was taken.

If absolute pressure = gauge pressure +atmospheric pressure, then superficial gas velocity is calculated as

$$J_g = \frac{V}{A_r.t} \qquad [3.3]$$

3.5.3 Bubble load and froth recovery parameter calculation

If M is collected mass, bubble load B_L is calculated as

$$B_L = \frac{M}{V_{gc}} \qquad [3.4]$$

If froth recovery parameter R_f is defined as fraction of particles entering the froth phase attached to the air bubbles that reports to the concentrate launder (Savassi et al., 1997) then R_f is calculated as shown below

$$R_f = \frac{\text{Flowrate of particles to the concentrate via the particle - bubble attachment process}}{\text{Flowrate of particles attached to bubbles entering the froth phase}}$$

$R_f = \frac{M_C}{M}$, where M_C concentrate loading (g/l) (*assuming no entrained particles reports to the concentrate launder*).

3.5.4 Estimation of entrainment

Harris (2000) recognized the contribution of true chromite flotation to the overall chromite recovery. To use Cr_2O_3 as a partially floatable gangue and bubble load information to estimate entrainment in PGM flotation requires data on the liberation of the ore. Where this information is

absent assumption may be made that allows the calculation of the entrainment factor. Yianatos et al. (2010) developed an empirical equation to estimate entrainment factor from bubble load information. After suggesting the relationship between gangue recovery (R_G), entrainment factor (EF) and water recovery (R_w) as

$$EF_{,i} = \frac{R_{G,i}}{R_w} \qquad [3.5]$$

Yianatos et al. (2010) then defined the entrainment factor using the empirical equation given below

$$EF_{,i} = \exp\left(-0.693 \left(\frac{d_{p,i}}{\delta} \right)^{\phi} \right) \qquad [3.6]$$

where (ϕ) is the drainage parameter

δ is the particle size that corresponds to an entrainment factor EF_i of 0.5

The above model in conjunction with bubble load information will be used to estimate the degree of entrainment and gangue recovery.

Chapter 4

Bubble load meter commissioning and improvement

This chapter describes the developmental stages that resulted in the final design of bubble load meter. Problems that were encountered during design and solutions that were implemented are discussed. The main focus of this chapter is to discuss specific experiments that were applied to improve the design and performance of the device. The general description of experiments and procedures was done in chapter 3, however where needed the set-up is duely elaborated upon. The crux of the experiments in this chapter will be to test

1) hydrodynamics in the riser/flow regime identification
2) particle drop off
3) Unattached particle rejection by the wash water
4) Axial mixing intensity and its effects on riser dimensions

The final design of the bubble load meter and its operating procedure is also discussed in this chapter.

4.1 Bubble load meter initial testing

To test viability of the bubble load meter, its conformance to the set performance targets must be verified and ascertained. The acceptable performance criteria include that

1) Bubbly flow should exist in the riser
2) Unattached particles should not report to the collection chamber, or the wash water must be effective in rejecting unattached particles.
3) Attached particles should not drop off from the bubbles.

The design of the bubble load meter makes it possible to test and verify each of these set targets.

4.1.1. Flow regime identification

The initial testing of the 30mm riser bubble load meter was done using an air water system. 0.1ml/litre MIBC was added to both the flotation cell and the collection chamber, the agitator was run at 2000rpm, and air was measured by means of an air rotameter connected to the suction side of the self-aerated Denver flotation machine, as depicted in Figure 4.1. Bubbles rose up the 30mm ID riser, in what was taken to be bubbly flow; this was confirmed with pictures taken on the riser and T-junction with the digital camera (see Figure 4.2).

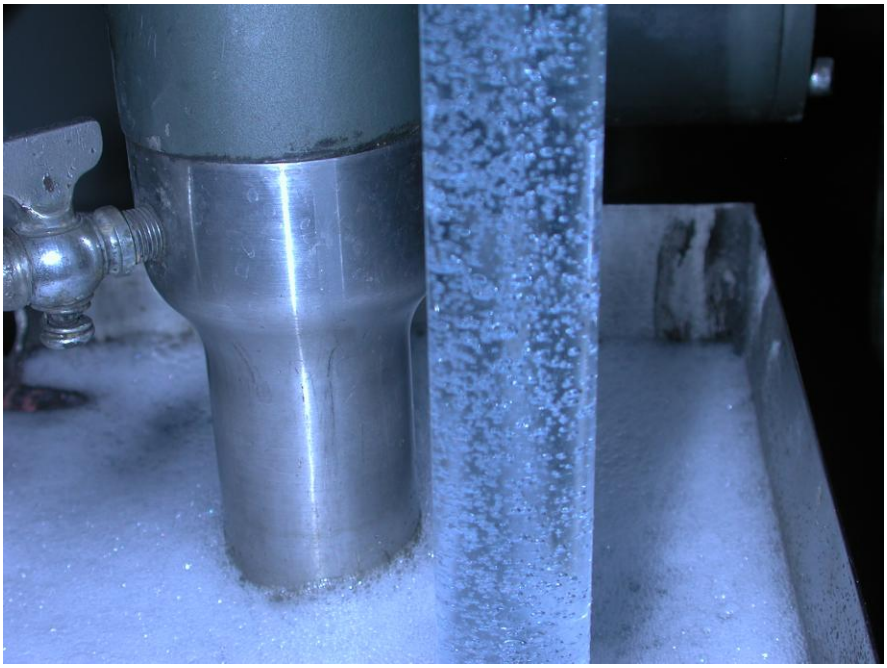

Figure 4.1: Denver flotation cell and riser position

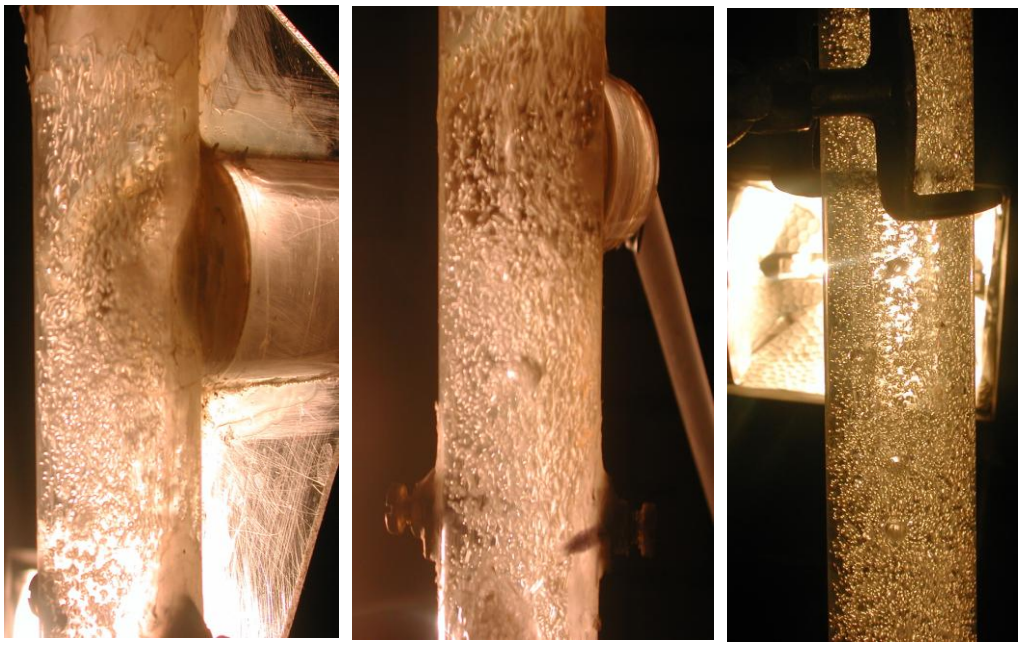

T-junction side view T-junction front view Flow along the riser

Figure 4.2 Flow regimes at the T-junction and along the riser

It is also worth mentioning that air was accumulated on the top part of the horizontal piece of the 90 Deg T-junction, as the bubble load meter was filled with frother water. This presented a problem of trying to get rid of the air before a run. Consequently, this observation prompted the change of the angle at the T-junction.

4.2 Unattached particle rejection in the riser

The bubble load meter works on a positive displacement principle; this means there is always a net downward flow of water which must prevent unattached particles from rising up the bubble load meter riser. To test the effectiveness of the wash water, stimulus-response experiments as described in section 3.4 in chapter 3 were conducted.

4.2.1 Conductivity probes calibration

The output from the Waveview$^{(R)}$ oscilloscope is an inverted voltage signal. This signal must be processed to give the corresponding concentration output. Also, conductivity cell constant depends on the dimensions of the probes and the distance between them. So it follows that if signals from the different probes are to be compared, then the brass probes need to be calibrated.

To calibrate the probes, NaCl solutions of known concentration were prepared (Table 4.1) and poured into the flotation cell. The solution was then sucked from the flotation cell until the whole riser was filled. The probes were then connected to the conductivity circuit, data logger and pc as depicted in Figure 3.6 in chapter 3. The resulting calibration curves are shown in appendix A. From the calibration curves, models that relate output voltage to concentration were developed. Table 4.2 shows the equations that relate output voltage to concentration *Conc* for the three risers.

Table 4.1: 30mm riser typical conductivity probes calibration data

NaCl concentration (mols/litre)	Conductivity (µS/cm)	Voltage (volts) output at different probe positions		
		Conductivity probe 1	Conductivity probe 2	Conductivity probe 3
0	6	3.45	3.45	3.46
Tap water	163	2.80	2.93	3.05
0.0055	504	2.31	2.34	2.45
0.011	1001	1.95	1.97	2.08
0.022	1972	1.58	1.60	1.72
0.044	3880	1.30	1.30	1.42
0.088	7630	1.17	1.15	1.20
0.125	10680	1.07	1.07	1.12
0.25	2080	0.97	1.04	1.06
0.534	39000	0.86	0.83	0.83

Table 4.2: Calibration equations for the three risers

50mm riser	**Equation**	**R^2 Values**
Conductivity probe 1	$Conc = 0.3618 \times v^{-3.986}$	**0.9955**
Conductivity probe 2	$Conc = 0.3504 \times v^{-3.843}$	**0.9962**
Conductivity probe 3	$Conc = 0.7708 \times v^{-4.072}$	**0.9926**
30mm riser		
Conductivity probe 1	$Conc = 0.1353 \times v^{-3.076}$	**0.9950**
Conductivity probe 2	$Conc = 0.1832 \times v^{-4.256}$	**0.9901**
Conductivity probe 3	$Conc = 0.2240 \times v^{-4.205}$	**0.9954**
20mm riser		
Conductivity probe 1	$Conc = 0.2271 \times v^{-3.689}$	**0.9946**
Conductivity probe 2	$Conc = 0.3292 \times v^{-3.611}$	**0.9751**
Conductivity probe 3	$Conc = 0.1653 \times v^{-3.391}$	**0.9929**

4.2.1 Conductivity experimental conditions

The agitator was run at 2000rpm, 500ml of 1mol NaCl was added to the flotation cell and the preliminary results obtained with the 30mm riser are summarized in Figure.4.3. The results indicate that hardly any salt reaches the second probe and none reaches the third conductivity probe. With this result, it was confidently assumed that unattached particles were not reporting to the collection chamber

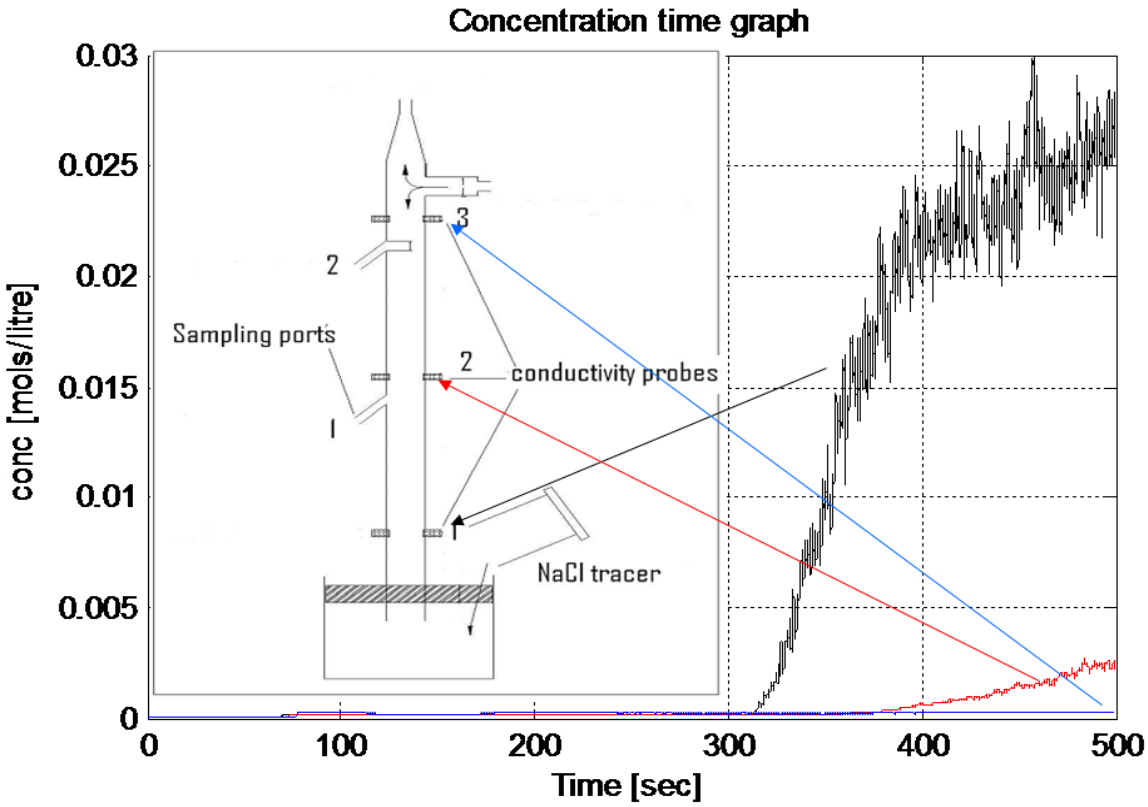

Figure 4.3: Stimulus-response experiments results

4.3 Particle drop off

The air water system testing of the bubble load meter proved that

(i) Bubbly flow exists in the riser at 5litre/min air flowrate and 2000rpm agitator speed.

(ii) It also proved that no inter-bubble liquid reports to the collection chamber and thus unattached particles are completely rejected by the displaced water.

This means that one aspect remains to be tested i.e. particle drop off in the riser. Coal flotation experiments were carried out following the procedure described in section 3.3.2 in chapter 3. Samples of the inter-bubble water were drawn from the riser using 50ml syringes and were analyzed for particles. Figure 3.8 in chapter 3 shows the syringe arrangement.

The results obtained with coal flotation were very low. It is important to note that some fine dust particles rose up the column with the inter-bubble liquid up to the second conductivity probe. This was in agreement with what was observed with the salt tracer experiments. It became

imperative that quantitative instead of qualitative (Figure 4.3) information alone be extracted from the salt tracer experiments. The rise of fine dust up the riser, made it impossible to accurately measure particle drop off at this point.

4.3.1. Coal flotation observation analysis

It was assumed that the rising of fine coal up the bubble load meter riser is caused by a strong axial mixing process taking place as bubble swarms rose up the column. It was also speculated that swarms of bubbles mechanically push water a distance up the column i.e. bubble swarm theory for entrainment (Warren and Smith, 1989). Bubble sizes, bubble rise velocities were envisaged to influence the mixing process in the bubble load meter riser. To what extend does bubbles size and velocity, number of bubble aggregates sampled per unit time, riser diameter affect the axial mixing? This is an important question that needs to be addressed during the bubble load meter design.

4.4 Axial mixing quantification

To quantify the mixing process, conductivity experiments as described in section 3.4 in chapter 3 were carried out. In addition to quantifying the relative amount of salt that reaches each probe up the column, these experiments were also designed to test the effect of bubble size on salt transport up the riser. To control bubble sizes, different amount of frother concentrations were added to both the flotation cell and the collection chamber. The following frother (MIBC) concentrations were investigated: No frother (0ppm), 4ml of 1% MIBC (5ppm), 8ml 1%MIBC (10ppm), 16ml 1%.MIBC (20ppm). The MIBC was added to 8 litres of water in the flotation cell. Salt tracer was introduced 60 seconds after starting the experiments.

4.4.1 Results for the 30mm riser

The following section presents results of the conductivity experiments obtained with the 30mm riser. The results show how the concentration of NaCl varies with height at different frother concentrations. For the purpose of quantitative comparison, the average of the steady state peak NaCl concentration was taken as the concentration at a particular conductivity probe position. The values of the change in NaCl concentration ($\Delta Conc$) at each probe position are shown in

each graph. It is important to note that the ($\Delta Conc$) is the difference between the average concentration recorded when bubbles only are flowing in the riser and the average of the steady state peak concentration after NaCl injection. Qualitative comparison was derived by plotting the responses of each of the three probes on a riser on the same scale.

No frother results

It can be seen from Figure 4.4a that the change in NaCl concentration recorded by conductivity probe 1 is 0.0146moles/ litre, representing 0.62% of the initial 0.5moles/litre introduced into the flotation cell. On conductivity probe 2 hardly any salt was recorded, the change in concentration $\Delta Conc$ is 0 as indicated in Figure 4.4b. In fact the recorded concentration slightly decreased as a result of bubble introduction. It is then safe to conclude that with no frother, no tracer reaches the second conductivity probe and hence there will be no tracer at probe 3, Figure 4.4c confirms this prediction. Figure 4.4d shows the output when the three conductivity probes are plotted on the same scale

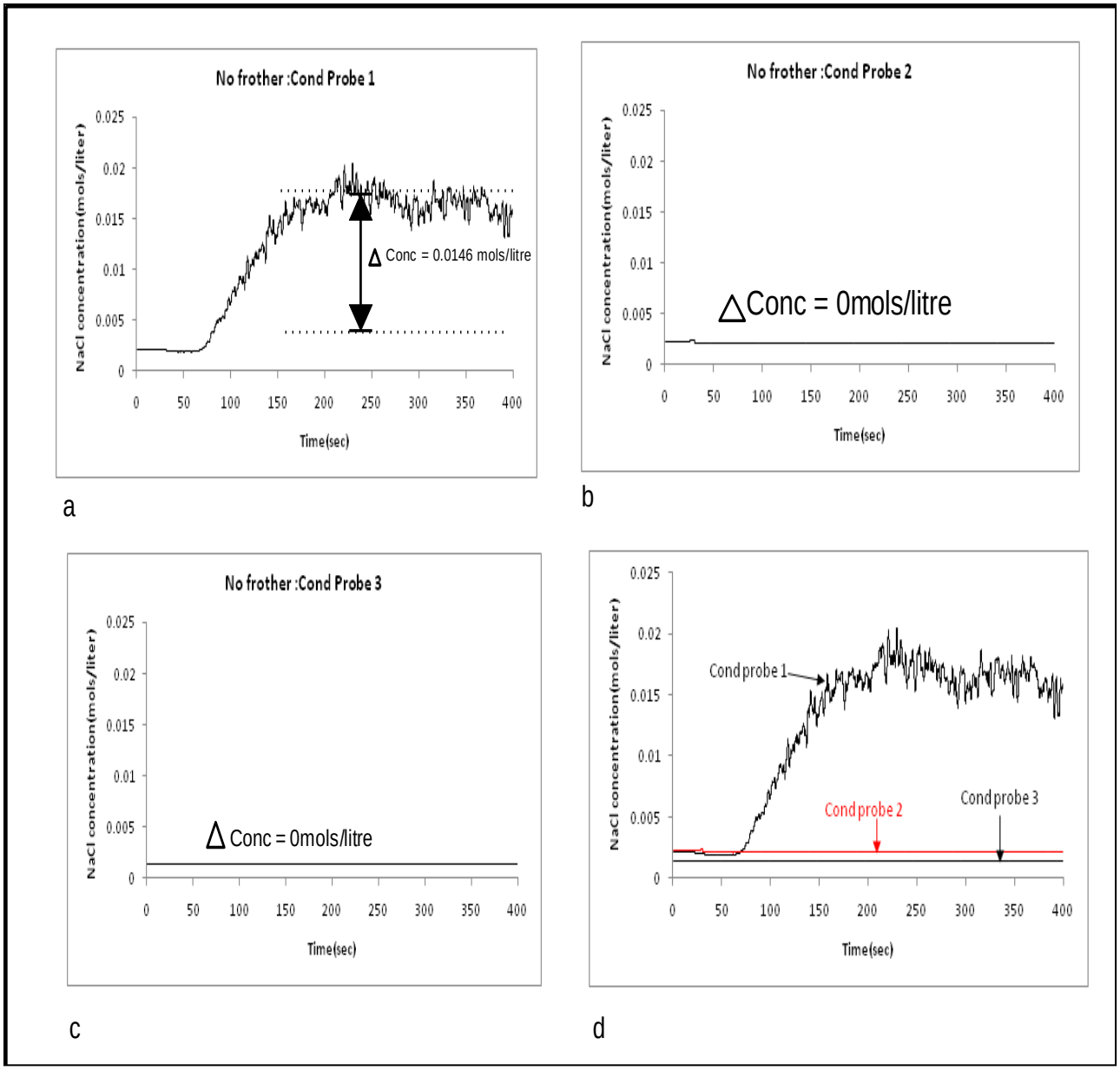

Figure 4.4 Conductivity responses for the 30mm riser when no frother is added to the flotation cell

Conductivity test results for 4ml of 1% v/v MIBC (5ppm)

The response of the conductivity probes in the 30mm riser to 4ml of 1%MIBC are presented in this section. Figure 4.5a shows how the concentration of NaCl changes with time at conductivity probe 1, when 4ml of 1% MIBC was added to the flotation cell. NaCl concentration increased up to an average concentration of about 0.0349mols/litre after 400 seconds. The initial concentration of NaCl in the flotation cell was 0.0588moles per litre. Based on the intial mass of NaCl added to

the flotation cell, this shows that on average 1.5% NaCl reaches the first probe. Figure 4.5b shows that after 400seconds a ΔConc of 0.0044moles/liter NaCl is recorded by Conductivity probe 2. This constitutes 0.19% of the original NaCl concentration set up in the flotation cell.

The ΔConc recorded by conductivity probe 3 is 0mols/ltre (see Figure 4.5c). Again with the 30mm probe, it can be concluded that with 5ppm frother concentration no particles unattached to bubbles would reach the collection chamber. To compare the three graphs, they are plotted on the same axis as shown in Figure 4.5d below

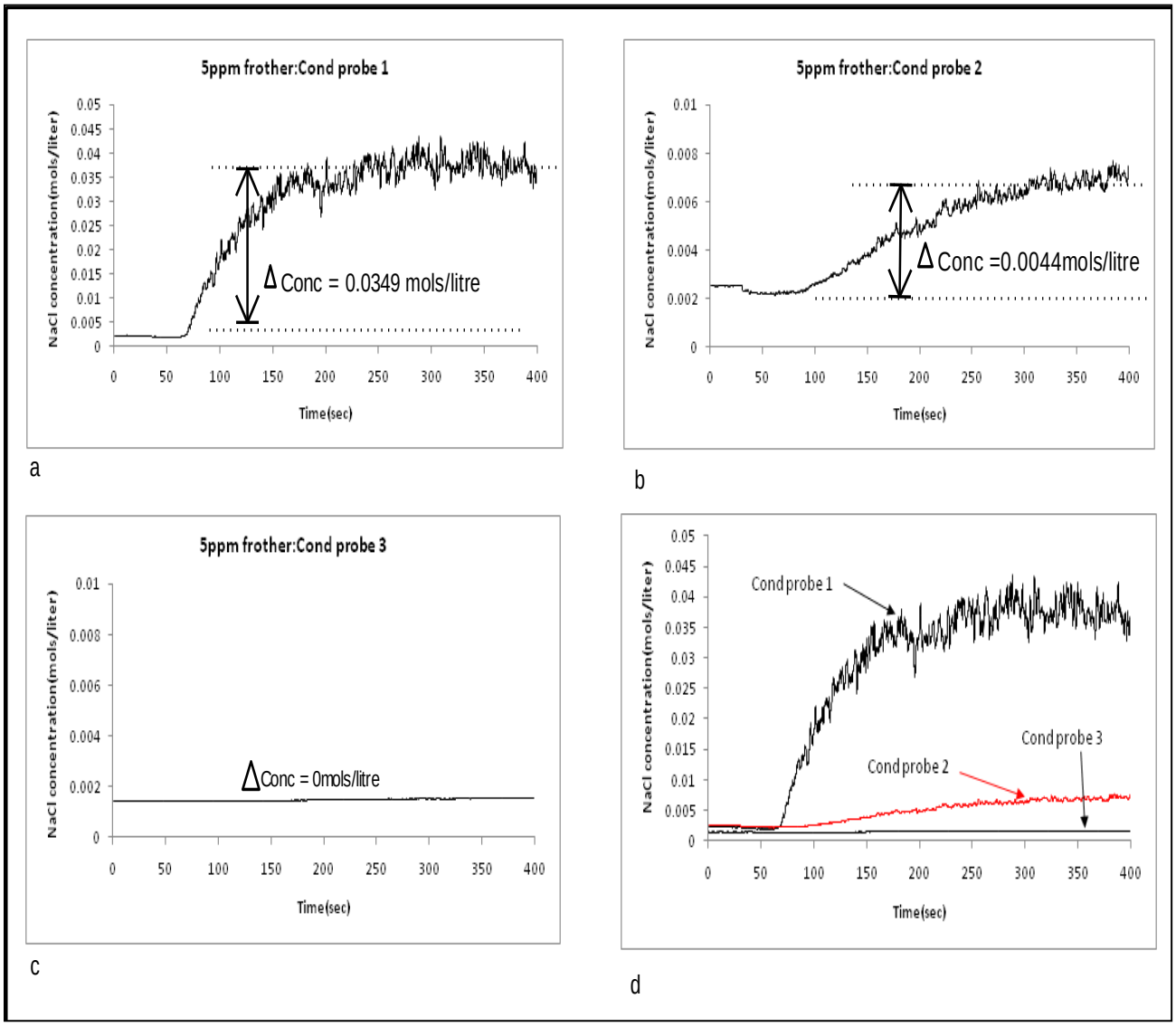

Figure 4.5 Conductivity responses for the 30mm riser when 5ppm frother is added to the flotation cell

Conductivity test results: 8ml of 1% v/v MIBC

The average of the steady state NaCl concentration recorded by conductivity probe 1 was 0.0358mols/litre constituting 1.5% of the original amount of salt tracer introduced into the flotation cell (Figure 4.6a). Conductivity probe 2 recorded an averaged peak value of 0.00220mols/litre see Figure 4.6b and conductivity probe 3 recorded 0.00012mols/litre (Figure 4.6c) representing 0.093 and 0.024% of the original NaCl added respectively. The response of the conductivity probes for 8ml of MIBC when plotted on the same scale is shown in Figure 4.6d.

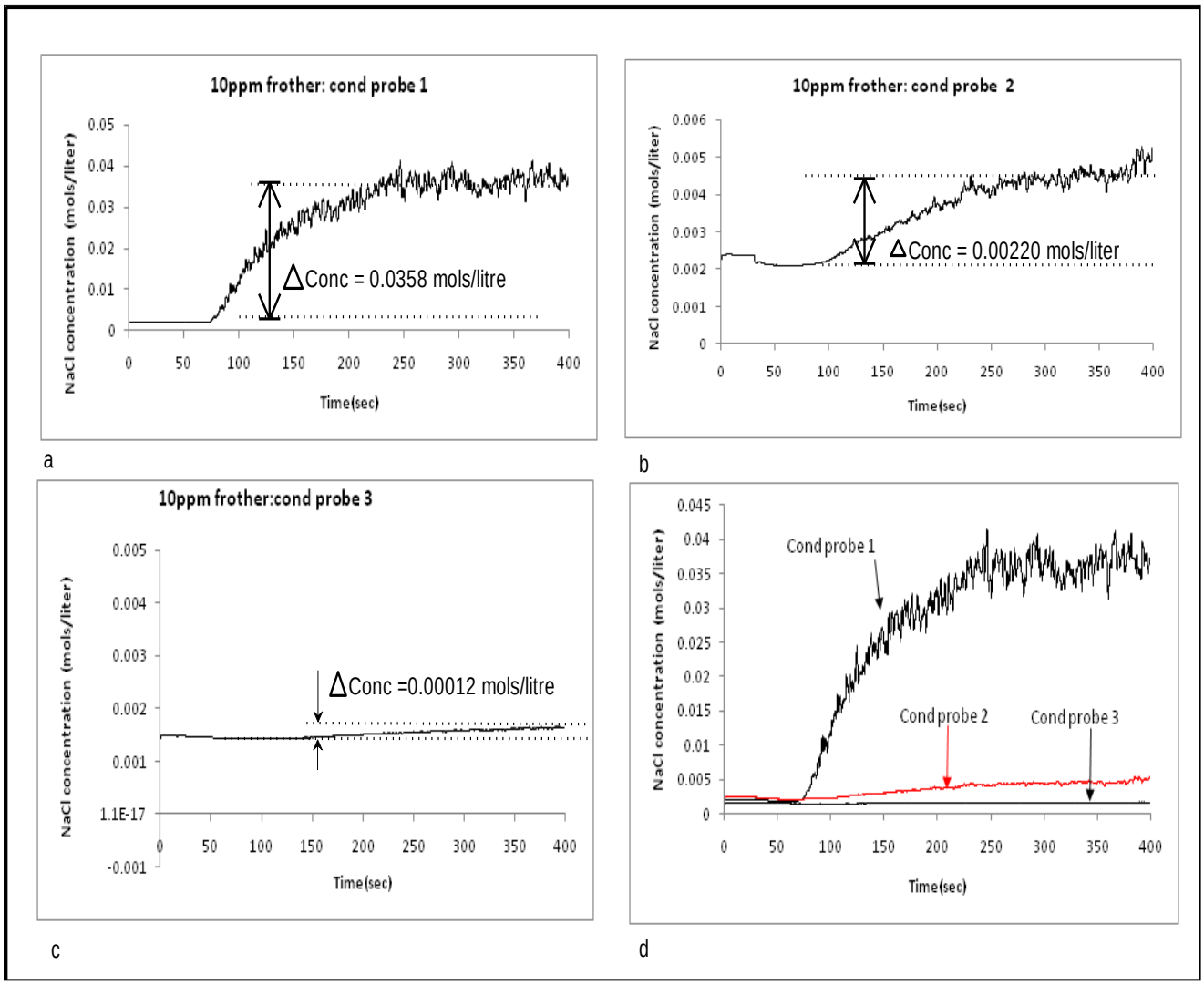

Figure 4.6 Conductivity responses for the 30mm riser when 10ppm frother is added to the flotation cell

Conductivity Results: 20ppm (16ml of 1%MIBC)

No salt was recorded at conductivity probe 3 (Figure 4.7c). Conductivity probe 2 recorded 0.3% of the original salt added into the flotation cell; its concentration-time profile is summarized in Figure 4.7b. Conductivity probe 1, recorded a NaCl peak concentration of 0.039mols/litre(Figure 4.7a) this represents 1.7% of the original NaCl added. A comparison of the three conductivity probes is shown in Figure 4.7d.

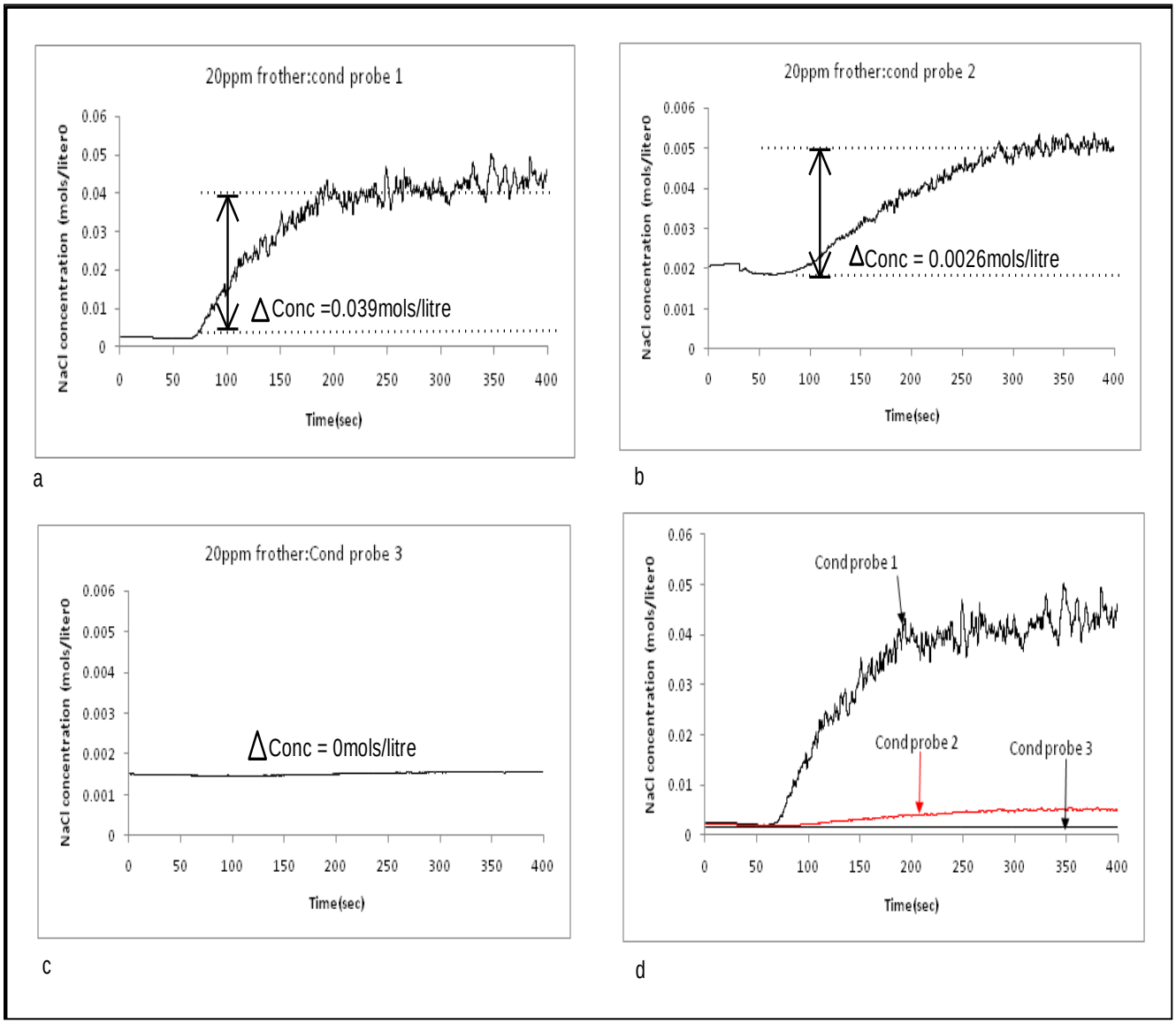

Figure 4.7 Conductivity responses for the 30mm riser when 20ppm frother is added to the flotation cell

4.4.2 Concluding remarks: 30mm riser conductivity experiments

Stimulus response tests on the 30mm bubble load meter has revealed that, though there is an upward salt transport, the wash water is effective in eliminating it from reaching the third probe. Only 0.2% NaCl on average reaches conductivity probe 2, while 1.7% on average reaches probe 1. Hence this bubble load meter riser can be used to measure bubble loads without a chance of sampling unattached particles. The amounts of NaCl recorded at each probe as a function of bubble size/ frother concentration is summarized in Figure 4.8. Conductivity Probe 1 recorded a maximum salt concentration of 1.7% at a frother dosage of 20ppm. The NaCl then decreases with frother concentration up to 0.62% when no frother was injected. Conductivity probe 2 and 3 recorded no salt for all frother concentrations while Conductivity probe 2 recorded a peak value of 0.16% at 5ppm frother

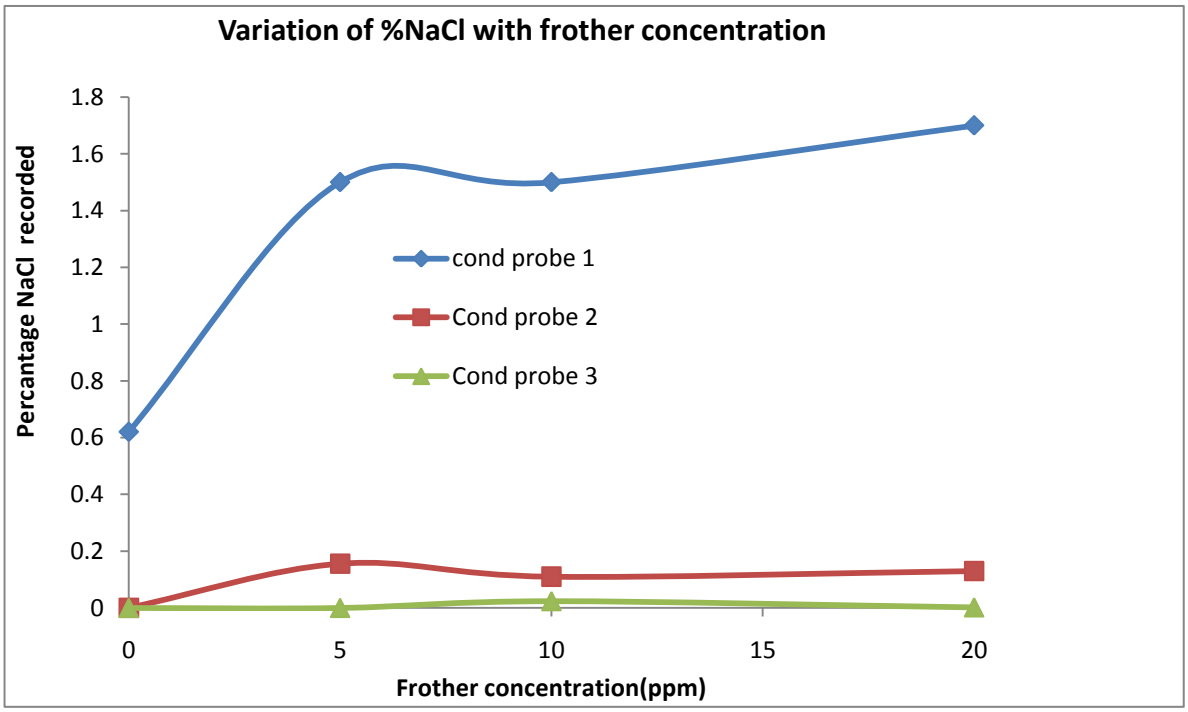

Figure 4.8: Comparison of the effect of frother concentration on %NaCl recorded by each probe

Variation of %NaCl with frother dosage: discussion

Axial mixing is a strong phenomenon in the riser section of the bubble load meter. But the fact that reducing bubble sizes by increasing frother concentration increased the NaCl concentration recorded by conductivity probe 1 requires another explanation in addition to axial mixing. If axial mixing was the only cause for the amount of salt recorded by conductivity probe 1, then the largest amount of NaCl would have been recorded with no frother because of the large bubble sizes that are produced. Large bubbles have superior rise velocities which were expected to induce strong eddies and thus an intense mixing process. Contrary to the expectation, relatively fine bubbles (5ppm MIBC) resulted in more salt at the third probe. This can be explained by:

(1) An increased number of bubbles rising per unit time as a result of the size of the bubbles.

(2) Large number of slowly rising bubbles mechanically pushing inter-bubble liquid up the riser (The bubble swarm theory).

Fine bubbles produced as a result of frother addition will rise at slow velocity, dragging some liquid between them as they are highly packed, whereas large bubbles will rise individually and are not as intensively packed as fine bubbles. Figure 4.19 shows a comparison of the flow of bubbles when No frother, 4ml of 1%MIBC and 16ml of 1%MIBC were added to the flotation cell. It is also important to note that the number of bubbles sampled per unit time increase with frother concentration if gas rate and agitator speed are held constant as is the situation here.

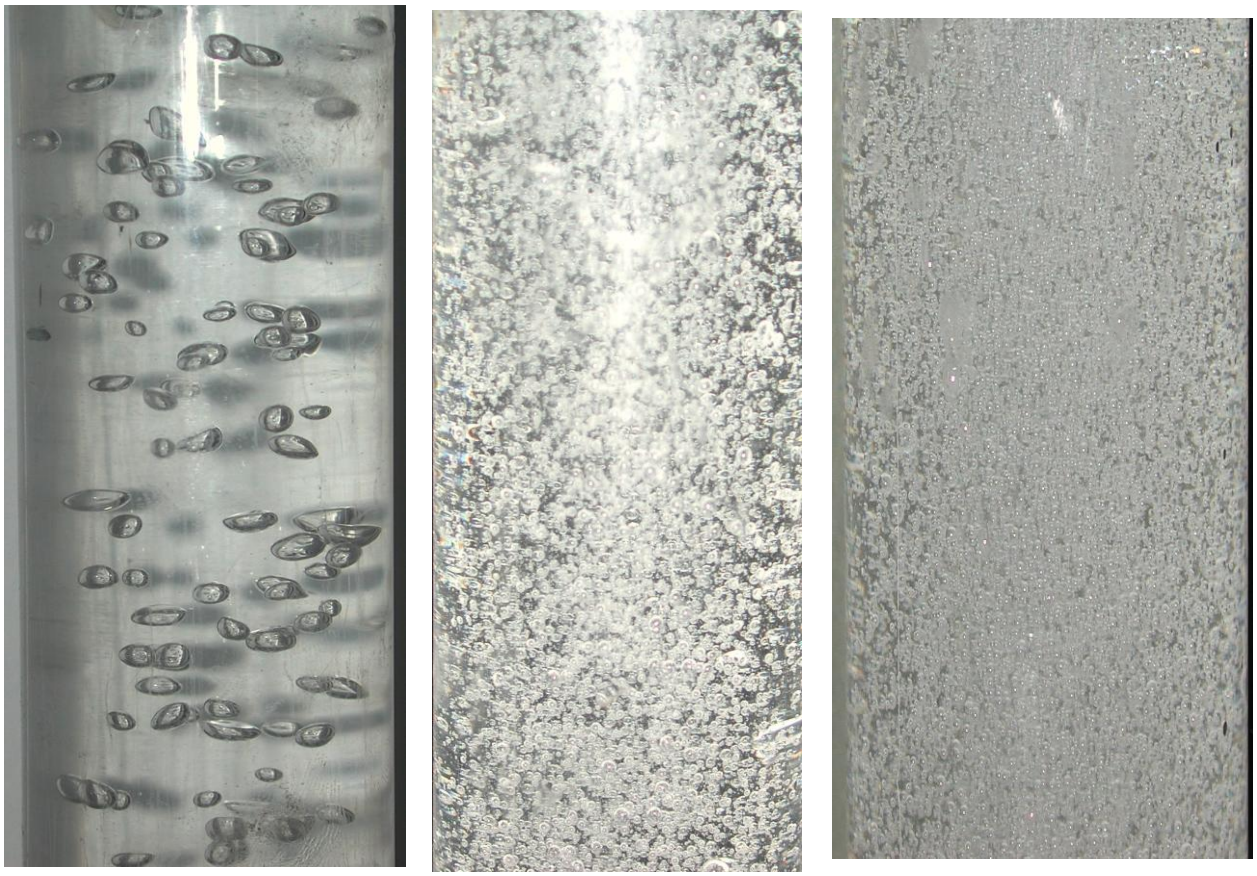

Figure 4.9: Comparison of bubbly flows for No frother, 4ml of 1%frother, and 16ml of 1% MIBC.

4.5 Bubble load meter redesign

Armed with evidence from conductivity experiments that the 30mm pipe is effective to work as a bubble load meter riser, more ideas to improve the load per unit time were explored. These methods include: making two more risers of diameters 20mm and 50mm respectively. The 50mm pipe riser was intended to verify if it was possible to increase riser diameter without compromising the quality of the load obtained. Increasing riser diameter would be advantageous in that it would increase the bubble load per unit time. The 20mm pipe was constructed to verify the effect of pipe diameter on axial mixing when the three risers' responses to salt experiments are compared.

4.5.1. The 20 and 50mm risers' description

Liquid back mixing intensity increases with column diameter (Alvare and Dahhan, 2006). To investigate the effect of riser diameter, sampling risers with IDs of 20mm and 50mm were constructed out of Perspex. Their design is similar to the 30mm ID pipe except for the T-junction were the angle was increased from 90 degrees to 120 degrees, this was done to eliminate air accumulation at the T-junction. The schematic of the new devices is shown in Figure 4.10.

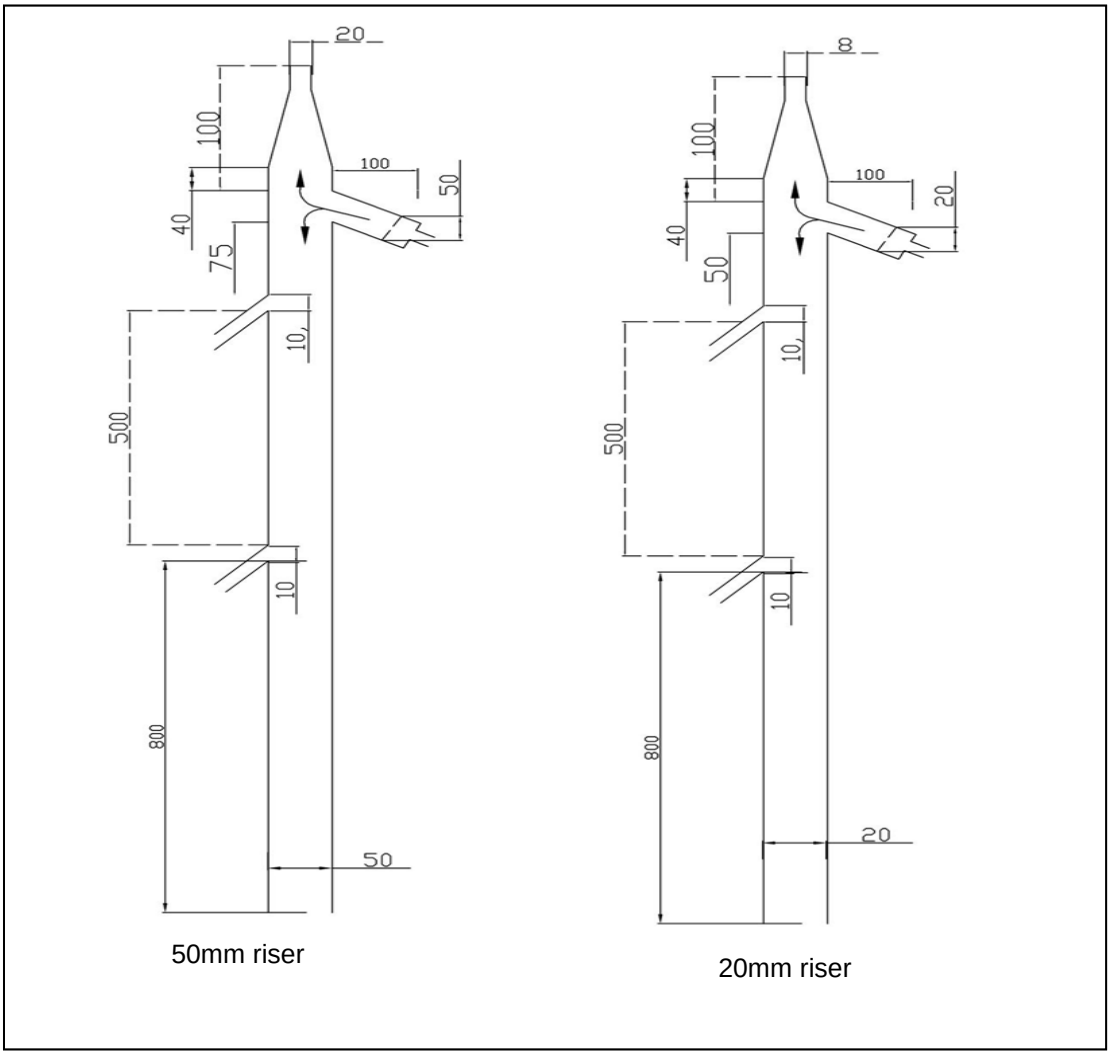

Figure.4.10: Schematic of the 20 and 50mm risers.

4.5.2. Conductivity probe results for the 50mm riser

This section presents the filtered output signal response from the conductivity probes on the 50mm riser. A brief description of the results is also given. The voltage output signal was converted into the corresponding concentration-time output using equations in Table 4.2. A moving average of 22 steps was used to remove noise from the voltage output signal. Comprehensive analysis of the output response of the 20 and 50mm risers are shown in Appendix B, a summary of the results are presented in this section. Figure 4.11 is a summary of the conductivity experiments response for the 20 and 50mm risers

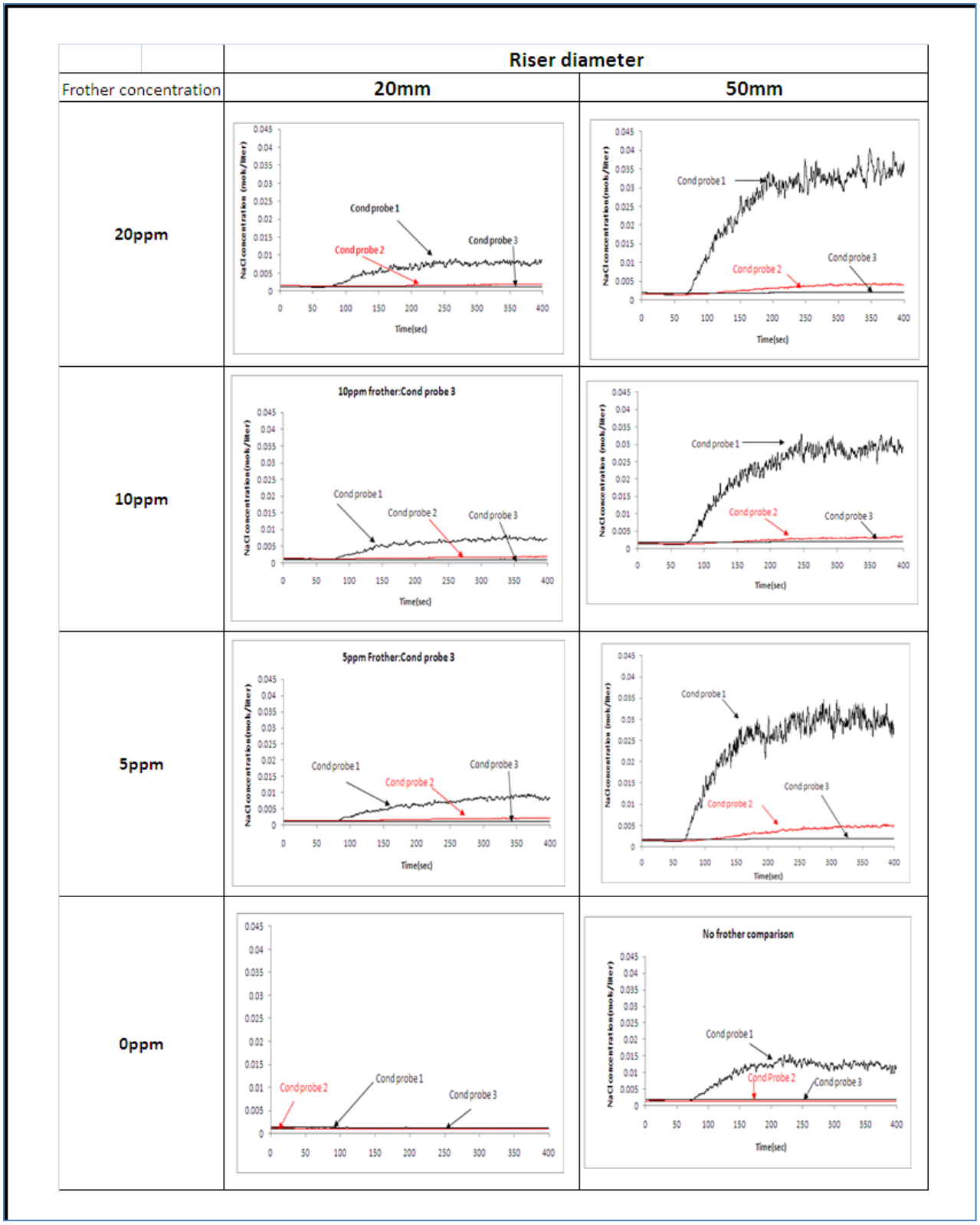

Figure 4.11 Summary of the 20 and 50mm riser for all frother concentrations

4.6 Comparison of the three risers: conductivity experiments

To decide on the final design of the conductivity probe, the proper riser diameter need to be decided. Three aspects were addressed by the conductivity experiments done in this research, these are:

1) The effect of riser diameter on salt transport
2) The effect of frother (bubble size) on salt transport up the risers
3) The general variation of NaCl concentration with height above the riser entry point.

This section compares and summarises the results obtained with the three risers with the ultimate objective of coming up with the correct diameter for the bubble load meter riser.

4.6.1 Effect of riser diameter on salt transport

It has been acknowledged that riser diameter influences the axial mixing in the riser. The more intense the axial mixing the greater the amount of salt transported up the column hence the higher the chance of it reporting to the collection chamber. Figure 4.12 to Figure 4.15 shows how %NaCl that reached a particular probe varies with riser diameter. For all frother concentrations investigated, the %NaCl increased with riser diameter. The 50mm riser recorded the highest amount of NaCl while the 20mm recorded the lowest

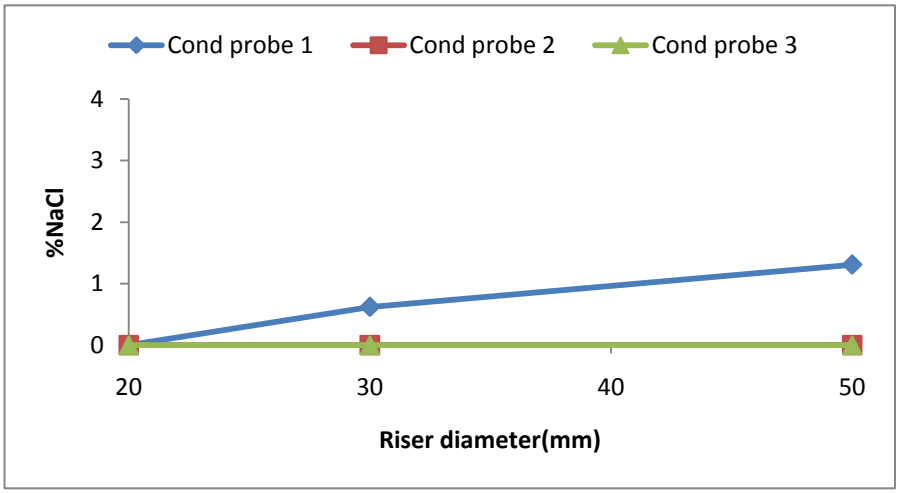

Figure 4.12: Change in %NaCl with riser diameter at 0ppm MIBC

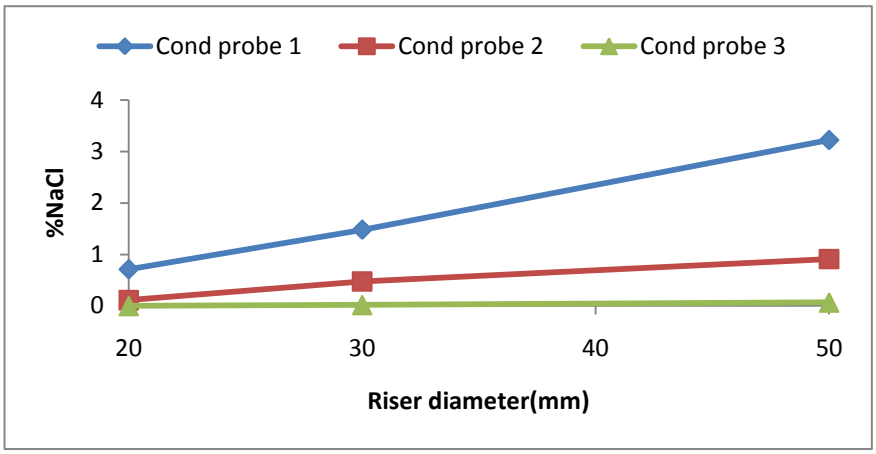

Figure 4.13: Change in %NaCl with riser diameter at 5ppm MIBC

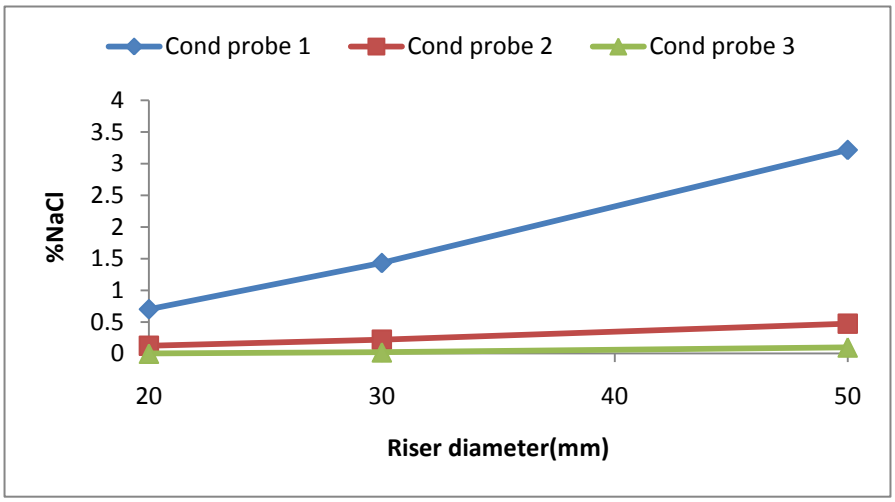

Figure 4.14: Change in %NaCl with riser diameter at 10ppm MIBC

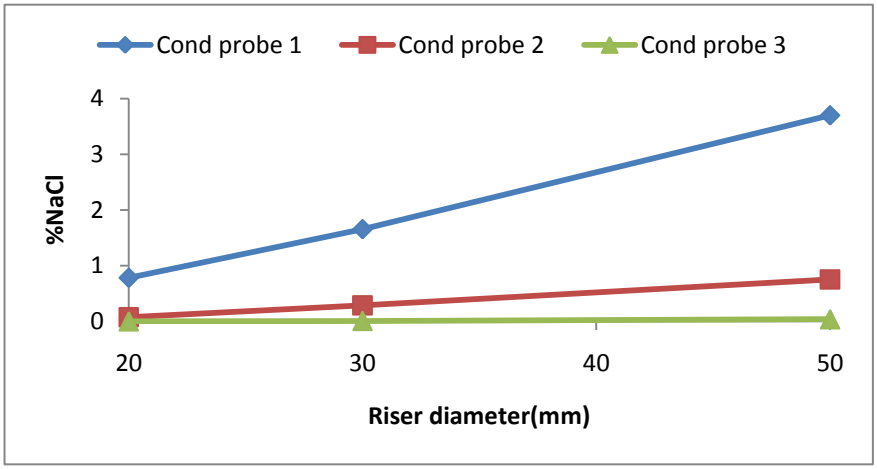

Figure 4.15: Change in %NaCl with riser diameter at 20ppm MIBC

4.6.2 The effect of frother (bubble size) on salt transport

The intensity of axial mixing in two phase systems is dependent on the relative velocities of the two phases. The higher the velocity of the dispersed phase (bubbles in this case) the more intense the mixing phenomenon. If agitation rate is maintained constant, addition of frother will decrease the mean bubble size produced in the flotation cell. The effect of bubble size and hence bubble rise velocity on salt transport was investigated. The results are summarised in Figure 4.16. These results show a general increase in %NaCl as frother dosage is increased from 0ppm to 20ppm. It is interesting to note that addition of 5ppm MIBC resulted in more NaCl rising up to the second conductivity probe for all the risers. The rate at which NaCl transport up the column changes with frother addition seems to gradually decrease after 10ppm was added. This was explained by acknowledging that

1) Adding frother will affect bubble sizes up to a concentration known as the Critical Coalescence concentration (CCC), beyond which addition of more frother will not change the bubble sizes.
2) Secondly NaCl transport up the column is a strong function of axial mixing and the number of bubble aggregates entering the riser per given time. Increasing frother concentration will also increase the bubble aggregates sampled per unit time up to a point where adding more will not change the number of bubble aggregates sampled.

Taking the above points into consideration, it can speculated that addition of 5ppm MIBC produced bubbles of a relatively large mean size to induce strong axial mixing as a result of high velocity, while at the same time the bubbles produced are still small enough to allow a large number of them to be sampled per unit time. After the addition of 10ppm frother, the slowing down of the rate of %NaCl change can be attributed to the small change in bubble sizes as the frother concentration approaches the CCC. The effect of frother on bubble size is thoroughly discussed by Laskowski et al. (2003) and Finch et al. (2008).

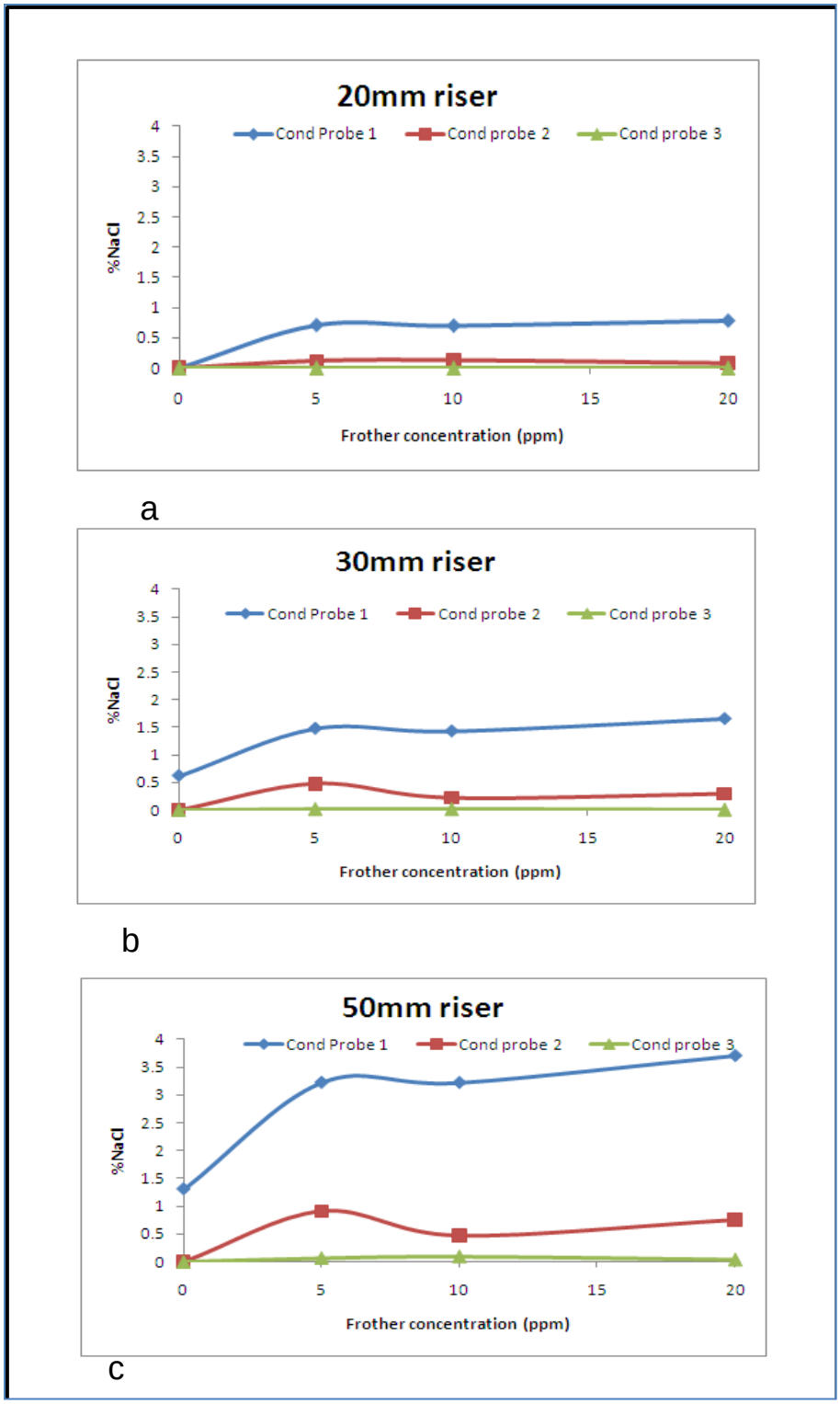

Figure 4.16: Variation of %NaCl with rising up the column with frother concentration

4.6.3 Variation of %NaCl with height above riser entry point

Determination of the height of the riser is an integral part of the bubble load meter design. Figure 4.17 to Figure 4.19 shows how concentration of NaCl varies with height above the entry point. For the three risers %NaCl recorded by each probe decreased with height, meaning that the higher the riser the less likely it is to get NaCl/unattached particles to collection chamber.

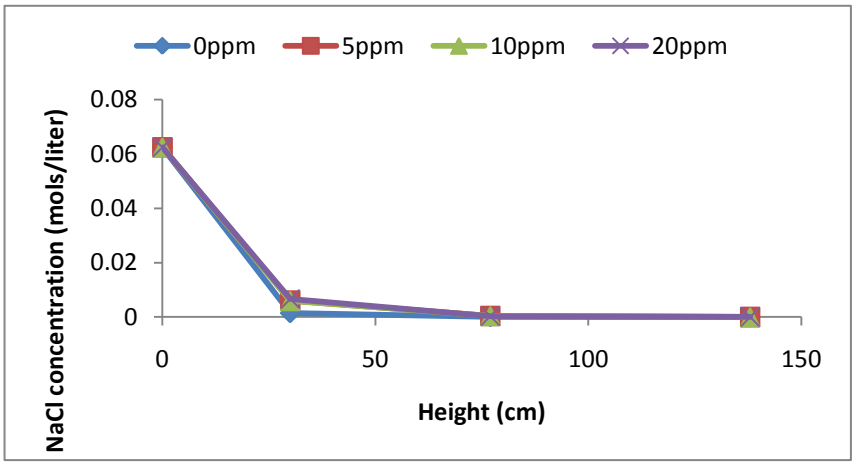

Figure 4.17: Variation of NaCl concentration with height (20 mm riser).

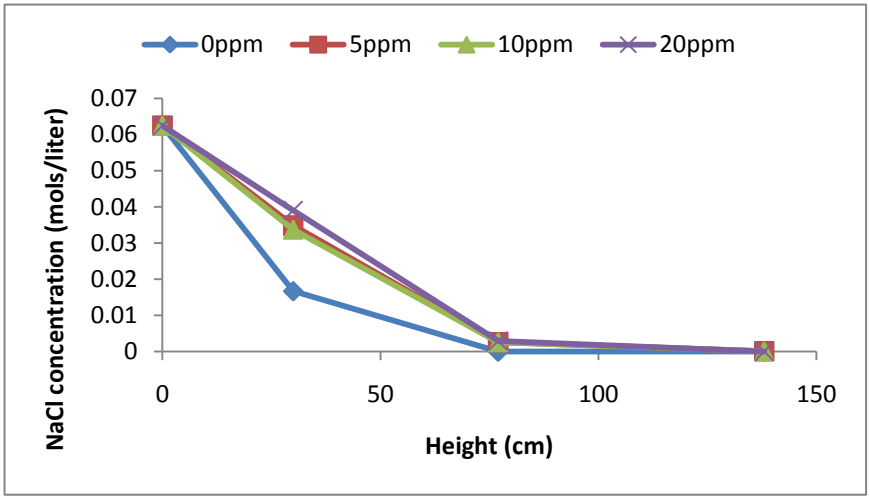

Figure 4.18: Variation of NaCl concentration with height (30 mm riser)

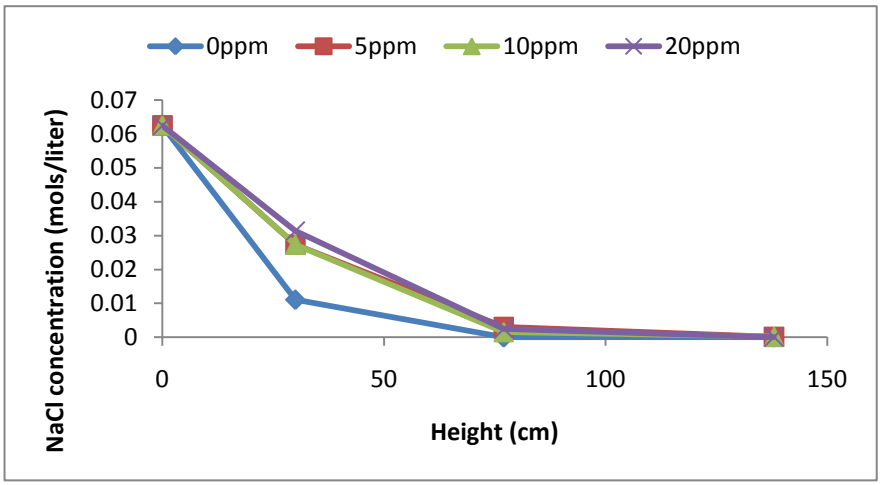

Figure 4.19: Variation of NaCl concentration with height (50 mm riser)

4.7. Summary conductivity experiments

The purpose of the conductivity experiments was to choose the best riser for the bubble load meter. It was verified that increasing the riser diameter increases the amount of NaCl transport up the column Figure 4.12 to Figure 4.15. The 50mm riser recorded highest amount of NaCl (3.7%) at conductivity probe 1(30cm above the entry point) and 20mm riser recording the lowest amount of NaCl (0%) at conductivity probe 1. Conductivity probe 3 (138cm from entry point) provides the most important information since any salt it records will eventually report to the collection chamber. The 30mm and 20mm risers recorded no salt on conductivity probe 3; while the 50mm riser recorded 0.1% of the original salt at conductivity probe 3, implying that the mixing was more turbulent in the 50mm riser. From the trends discussed in this chapter, it is evident that, 20mm and 30mm risers can be used as bubble load meter risers with confidence. The best choice is the 30mm meter since it can offer a high load per unit time i.e. its cross sectional area is 2.25 times the 20mm riser. Though the 50mmID riser offers a high load per unit time, there are chances that bubble load that would be obtained will not be true representative of true flotation because of a more turbulent mixing process.

It is interesting to note that only 0.1% of the original salt that was added to the flotation cell rose up to the third conductivity probe on the 50mm riser. Also, salt was only recorded when frother was added, with no frother addition no salt reached probe 3. It is thus proposed that the 50mm riser can still be used if a method of reducing axial mixing is devised. It is also interesting to note

that NaCl concentration decreases with increase in height of the riser. Increasing the height of the 50mm riser to above 150cm may reduce or eliminate salt/inter-bubble liquid from reaching probe 3. Secondly baffling and the use of packing may reduce the intensity of axial mixing thus inter-bubble liquid can be eliminated from reaching probe 3

4.8. Use of Baffles

It is important to bear in mind that reducing pipe diameter effectively reduces the mass of particles collected per unit time. This is undesirable. The objective of this thesis is to get a dry bubble load sample in excess of 200grams in a reasonable time (15minutes). Though the 20mm and 30mm risers gave satisfactory results in as far as mixing is concerned, other methods that reduce axial mixing without changing much the effective volume of the sampling section were explored.

Baffles can be used to reduce axial mixing although their use in industrial flotation columns has been abandoned because they did not work (Moys et al., 1995). Analysis by Moys et al. (1993) clearly shows why this is so. Non uniform gas distribution in columns was pointed as the main reason of the poor performance of baffling. Non uniform gas distribution results in different gas hold up values which subsequently results in liquid circulation due to pressure differences. To try and create a pressure balance the use of flexible baffles was assessed. Results from Moys et al. (1993) indicate that use of flexible baffles can substantially reduce the water circulation. It is from Moys et al. (1993) that the idea of using flexible baffle inside the 50mm pipe was introduced. A thin (0.5mm) piece of flexible Perspex was cut and inserted into the 50mm column effectively dividing it into two sections as shown in Figure 4.20. The Perspex was inserted such that it was 30mm from the column entry point and 30mm below the T-junction. Tests were carried out with an air-water system. Circulation reported by Moys et al. (1993) was also observed. The circulation process was more pronounced on the rise velocity of the bubbles in each section, in one section the bubbles appeared stationery whereas on the other section they rose at a relatively large velocity. The intended effect of flexible baffling could not be achieved. It was assumed that the baffle inserted actually acted more like a rigid baffle, thus benefits that are accrued by using flexible bubbles could not be realized. This result led to the abandoning of baffling. Use of packing to reduce axial mixing was proposed.

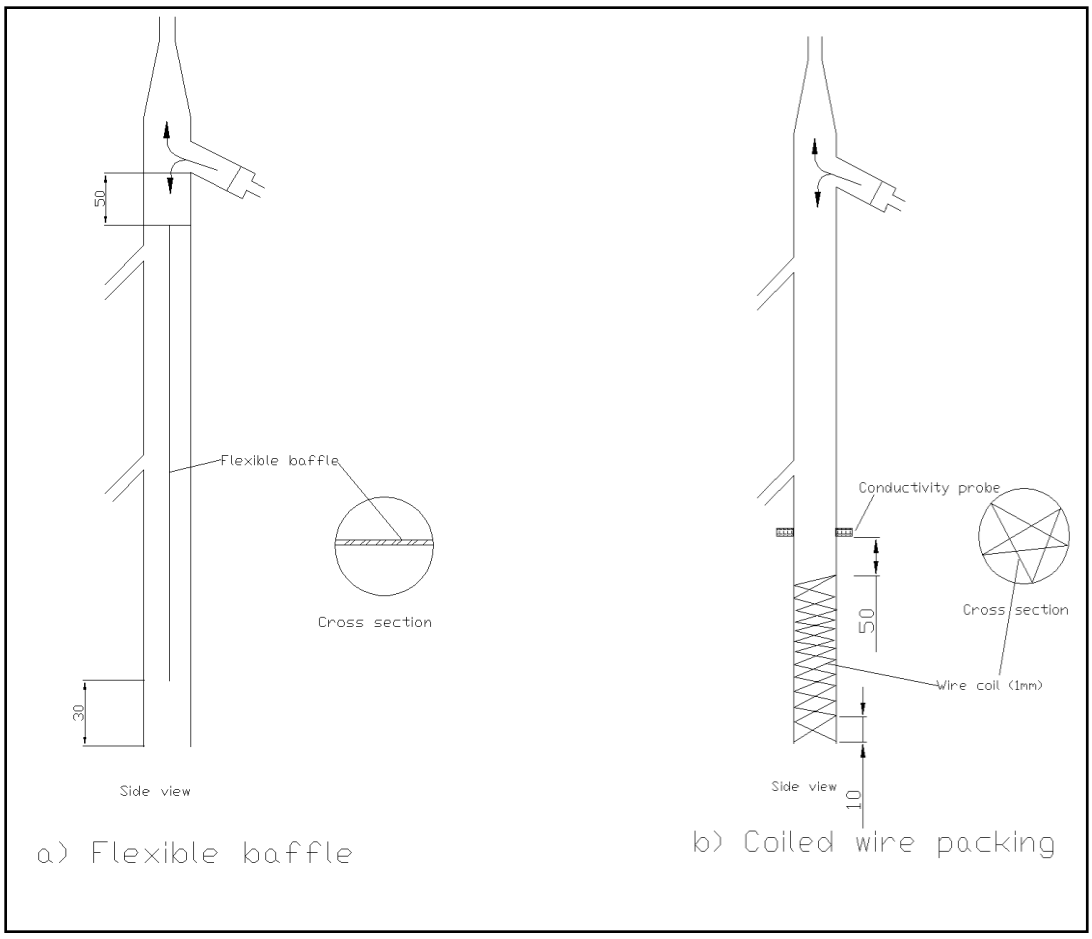

Figure 4.20: Axial mixing reducing methods; a) use of flexible baffle b) Packing-coiled thin wire

4.9. Operating the bubble load meter

The operation of the bubble load meter requires careful control of the water recirculation rate. Pressure drop across the filter also needs to be monitored. As discussed above the bubble load meter that gives good results has been designed, however to obtain reliable results the following procedure must be adhered. Establish the average superficial velocity in the flotation cell using a superficial gas velocity probe first before taking any measurements.

1) Since the superficial gas velocity is equal to the superficial liquid velocity, liquid flowrate can be calculated. For convenience, Tables in Appendix C are used to establish flowrate and water rotameter reading for all the risers tested in this thesis.
2) Mount the riser such that it is exactly vertical (use of spirit level can be convenient) before taking a measurement.

3) Depending on the particle sizes and the specific cakes resistance of the particular ore, sampling times are determined. Pressure drop across the filter and flowrate of water as indicated by the water rotameter should also give an indication of when to stop a run. Normally when the pressure gauge on the filter records a pressure that exceeds one bar then a run should be stopped.
4) Getting the entire sample out of the collection volume is an integral part of bubble load measurement, so it is important to use wash bottles to ensure that all particles are collected. Water inside the tube between the collection chamber and the pump should also be removed by pumping clean water from the collection chamber to the filter.

Chapter 5

Pressure prediction theory and axial mixing model and parameter estimation for the bubble load meter

This chapter initially presents the basic theory that predicts pressure drop in the riser based on standard chemical engineering principles. It goes on to discuss the axial mixing model which is used to describe the mixing taking place in the riser section of the bubble load meter. The model predicts the salt concentration in salt impulse tests and hence models the rise of inter-bubble particle concentration as a function of height above the bubble entry point. The model assumes that the mixing taking place in the riser can be approximated by a large number of mixers in series. Parameter estimation is achieved using Simulink, a simulation toolbox in Matlab.

5.1 Pressure prediction model in the bubble load meter.

The following section presents a simple model for predicting the flowrates in the various channels in the bubble load meter. The hydrodynamic model is based on standard chemical engineering equations for pressure drops in various parts of the equipment. Pressure drop in fluid systems is one of the fundamental parameters of interest to design engineers (Vassallo and Keller, 2006), it is important that theory that predicts pressure drop across the various channels of the bubble load meter be developed if its design is to be considered complete. The theory developed is based on two phase systems (gas and liquid) ignoring the presence of particles attached to bubbles. Fundamental laws of two-phase pressure drop prediction are adopted.

5.1.1. Brief pressure drop prediction literature

The pressure drop in two-phase systems is usually higher than pure liquid flow at the same mass flux (Vassallo et al., 2006). The earliest and simplest analysis of two phase flow is the homogeneous approximation where both phases are assumed to flow with the same average

velocity. The homogenous application is suitable for high mass flux or high pressure where slip ratio is low. The downside of the homogenous model is that it under predicts the actual pressure drop in real systems (Vassallo et al., 2006). Adopting the homogeneous approximation in this analysis, the pressure gradient in the riser can be thought of as arising from three additive contributions (i) frictional (ii) flow acceleration (iii) hydrostatic head

$$\frac{dp}{dz}=\left(\frac{dp}{dz}\right)_{fr}+\left(\frac{dp}{dz}\right)_{acc}+\left(\frac{dp}{dz}\right)_{gr} \qquad [5.1]$$

(1) Pressure drop due to flow acceleration

For homogenous model, pressure drop due to flow acceleration is given by

$$\left(\frac{dp}{dz}\right)_{acc}=\frac{d}{dz}\left(\frac{1}{A}\int_{A}\rho u^{2}\right)=m^{2}\,\frac{d}{dz}\left(\frac{1}{\rho_{H}}\right) \qquad [5.2]$$

where: m is the total rate of mass flow per unit area in the pipe

u is the velocity, ρ_H is the effective density which can be calculated as follows

$$\rho_{H}=\varepsilon_{g}\rho_{g}+(1-\varepsilon_{g})\rho_{L} \qquad [5.3]$$

(ii) Pressure drop due to gravity

Pressure gradient due to gravity is given by

$$\left(\frac{dp}{dz}\right)_{gr}=g\rho_{H}=g\left[\varepsilon_{g}\rho_{g}+(1-\varepsilon_{g})\rho_{L}\right] \qquad [5.4]$$

(iii) Pressure drop due to wall friction

The frictional pressure drop due to shear stress exerted by the tube wall is the most problematic term in two-phase pressure drop. It is related to the wall shear stress τ_w by

$$\left(\frac{dp}{dz}\right)_{fr}=\frac{2\tau_{w}}{R} \qquad [5.5]$$

where R is the radius of the pipe in metres

5.2 Model development

The bubble load meter was divided into various sections as indicated in Figure 5.1 and expressions for estimating pressure drop across each section were developed.

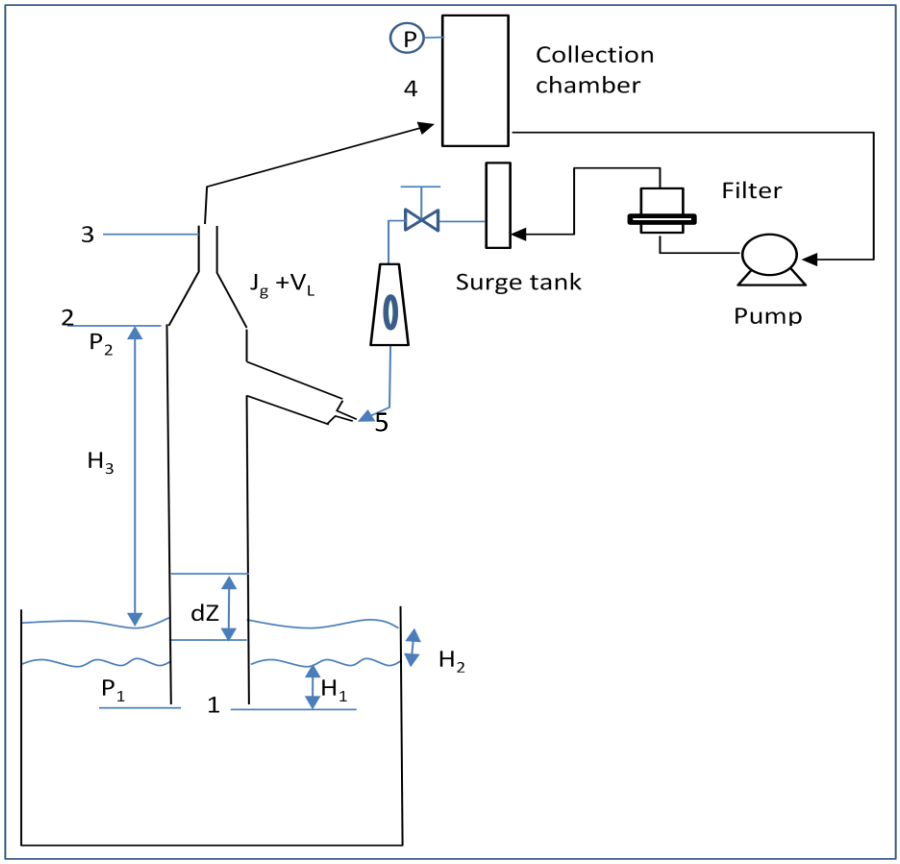

Figure 5.1: Model development schematic diagram

5.2.1. Section 1 to 2

In this section air bubbles are flowing countercurrently to water which is a flowing at superficial velocity J_L equal to the superficial gas velocity J_g. It was assumed that

a. Air bubbles are uniformly distributed across cross sectional area of the riser
b. Homogenous flow is taking place along the riser
c. The rise velocity of the air bubbles in the water air mixture flow is constant and does not change with height H.

Flowrates in this section are also very low and the superficial liquid velocity is typically less than 2cm/s, thus pressure drop due to friction and flow acceleration were considered insignificant, and hydrostatic pressure was considered to be dominant.

By integrating equation [5.4] pressure drop across this section is calculated as shown by the expression given below.

$$\Delta P_{gr} = g\Delta z\left[\varepsilon_g \rho_g + (1-\varepsilon_g)\rho_L\right] \qquad [5.6]$$

where ε_g is gas hold up and Δz is the difference in height between two points in this section.

If froth height is taken as H_2 and H_1 as the depth of the riser below the pulp-froth interface (see Figure 4.55), then pressure at the riser entry point is calculated as follows

$$P_1 = P_{atm} + g\left[\rho_p(1-\varepsilon_g) + \varepsilon_g\rho_g\right]H_1 + \rho_f H_2 \qquad [5.7]$$

where: ρ_p is the density of the pulp and ρ_f density of the froth.

Now considering all upward distances from the froth surface as negative and downward distances as positive, pressure at point 2 is calculated as shown below.

$$P_2 = P_{atm} + \Delta P_{H_3} \qquad [5.8]$$

Substituting equations [5.6] and [5.7] into [5.8] and taking Δz as $-H_3$ (see Figure 5.1) it reduces to the expression given below

$$P_1 = P_{atm} - H_3 g\left[\varepsilon_g\rho_g + (1-\varepsilon_g)\rho_L\right] \qquad [5.9]$$

Thus,

$$\Delta P_{H_3} = -gH_3\left[\varepsilon_g\rho_g + (1-\varepsilon_g)\rho_L\right] \qquad [5.10]$$

5.2.2. Section 2 to 3

Flow in this section can be described as flow through a sudden contraction. Cross sectional area of the pipe decreases from d_1 to d_2. Pressure drop across this component can be estimated by equation [5.11] (Moys et al., 2010).

$$\Delta P_{SC} = -0.75\rho u^2 \qquad [5.11]$$

where: ρ_L is the liquid density and u is the velocity, u_{SC} after the sudden contraction or the velocity u_{SE} before the sudden enlargement;

5.2.3. Section 3 to 4

Pressure drop in this section where contents are flowing under laminar conditions can be calculated using equation [5.12] as suggested by (Moys et al., 2010).

$$\Delta P_{pipe} = \frac{-32\mu L u}{d^2}\ , \qquad [5.12]$$

where: μ is liquid viscosity and, L, u and d are pipe length, liquid velocity and pipe diameter.

Thus pressure indicated by the pressure gauge on the collection chamber is a sum of all pressure drops across the various components from the entry point of the riser to the collection chamber. Equation [5.13] below predicts the pressure in the collection chamber P_{CC}.

$$P_{CC} = P_{atm} + \Delta P_{H_3} + \Delta P_{SC} + \Delta P_{pipe} \qquad [5.13]$$

5.2.4. Section 4 to 5

Pressure drop in this section is mainly due to, the filter, valve and pipe friction. Driving force for flow is provided by the pump. Equation [5.11] is used to estimate pressure drop due to the pipe. The equation to estimate pressure drop across the filter is developed in the following section.

(i) Pressure drop across the filter

This is the most important component contributing to pressure drop on the collection section of the bubble load meter. To estimate pressure drop, the cake filtration theory for pressure filtration

operating at a constant rate is adopted. Constant rate mode is adopted since a positive displacement pump is used to circulate water in the bubble load meter.

The basic equation for filtration: Poiseulle's Law is

$$\frac{1}{A}\frac{dV}{dt}=\frac{\Delta P}{\mu(R_m+R_c)} \qquad [5.14]$$

$$R_m=\frac{\alpha W}{A} \qquad [5.15]$$

$$\alpha=\alpha'\Delta P^s \qquad [5.16]$$

where: V is filtrate volume, A is area, t is time, ΔP is pressure drop across the filter, μ is broth viscosity, W mass of filter cake, R_m media resistance, R_c cake resistance, α is specific cake resistance, S is compressibility factor.

where the filter media resistance $R_m << R_c$ then for incompressible cake $S=0$ and for constant rate filtration, the pressure drop is given by

$$\mu\frac{Q}{A^2}(\alpha W)=\Delta P_{filter} \qquad [5.17]$$

ii. Pressure drop across the valve

Pressure drop across the valve can be estimated as the difference in pressure between the inlet and the outlet of the valve. It is calculated from the equation below

$$\Delta P_{valve}=\rho.\sqrt{\left(\frac{Q}{Kv}\right)} \qquad [5.18]$$

where Q is flowrate in m^3/hr

ρ is density kg/m^3

Kv is coefficient of flow

The total pressure drop on the collection section is also a sum of the pressure drops across the filter, pressure drop on the sudden expansion and pressure drop due to the pipe i.e.

$$\Delta P_{CS}=\Delta P_{filter}+\Delta P_{pipe}+\Delta P_{valve}+\Delta P_{SE} \quad [5.19]$$

5.2.5. Concluding remarks

Most of the parameters in these equations can easily be evaluated; superficial gas velocity is calculated from the volume of air collected in the collection chamber. Superficial liquid velocity is equal to the superficial gas velocity, thus water flowrate in an out of the collection chamber is calculated. For verification, the water rotameter connected to the bubble load meter is used. Gas hold up inside the bubble load meter can easily be measured experimentally by connecting water manometer to the sampling ports on the bubble load meter riser. The coefficient of flow can be obtained from the manufacturer of the valve. The only parameter which remains is the specific cake resistance which depends on the ore being floated. The average specific cake resistance can vary from 1×10^{9} which is considered very easy to separate up to $1\times10^{13}\ m/kg$ which is very difficult to separate (Leu, 1986)

5.3 Axial mixing in two-phase systems

The effectiveness of the bubble load meter in eliminating inter-bubble liquid and thus preventing unattached particles from reaching the collection chamber is dependent on the mixing taking place in the riser. To quantify the extent of the axial mixing in each riser, stimulus-response experiments using NaCl as a tracer as described in chapter 4 were done. The experiments involved introducing 0.5moles NaCl in 500ml of water into the flotation cell and using conductivity probes to measure the amount of salt recorded at different heights above the entry point. Where flow is assumed to be plug flow, then particle entrainment is completely eliminated and no NaCl should be recorded by conductivity probes and when perfect mixing is assumed, then inter-bubble salt tracer will report to the collection chamber. Conductivity experiments were done to quantify the extent to which salt tracer is transported up the riser as a function of riser diameter and bubble rise velocity. In order to predict the response of different risers, a model based on the tanks–in–series model is proposed and parameter estimation done. The main

objective of the model is to predict salt concentrations at different levels in the riser. It is also important to mention that the intensity of mixing in the riser influences phenomena like bubble coalescence and particle drop off which are inimical to accurate bubble load measurement

5.3.1 Model development

If the riser is divided into a number of equally sized cells or tanks as depicted in Figure 5.3, the rate of change of species in tank i is given by equation [5.20]

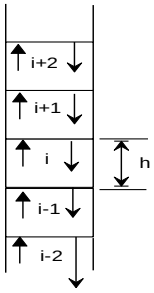

Figure 5.2: Cell arrangement in riser

$$V_i \frac{dc_i}{dt} = F_{i,in} - F_{i,out} \qquad [5.20]$$

And if we define J_{dwn} as the mean downward liquid velocity and J_{up} as the average liquid rise velocity as a result of the axial mixing, and if all flows are defined as positive i.e.

$$J_{up} \geq 0$$
$$J_{dwn} \geq 0$$

Then the superficial liquid velocity J_L is defined by equation below.

$$J_L = J_{dwn} - J_{up} \qquad [5.21]$$

J_{dwn} is related to J_{up} as follows

$$kJ_{dwn} = J_{up}, 0 \leq k < 1 \qquad [5.22]$$

If the concentration of NaCl in each of the tanks is depicted by c_i then for cell i equation [5.20] reduces to

$$V_i \frac{dc_i}{dt} = A(J_{up}.c_{i-1} + J_{dwn}.c_{i+1}) - A(J_{up}.c_i + J_{dwn}.c_i) \quad [5.23]$$

By substituting equations [5.21] and [5.22] into [5.23], the change in concentration becomes

$$\frac{dc_i}{dt} = \frac{J_L.k}{h_i(1-k)}(c_{i-1} - c_i) + \frac{J_L}{h_i(1-k)}(c_{i+1} - c_i) \quad [5.24]$$

5.3.2 Flotation cell NaCl concentration change

The displacement of water from the collection chamber by air results in a net down flow of water into the flotation cell. This water will dilute the NaCl concentration in the flotation cell. A model to depict this change in concentration in flotation cell is important. Figure 5.3 shows what happens in the flotation cell

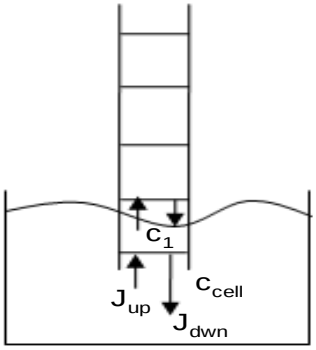

Figure 5.3:Transport process in the flotation cell

The rate of change of concentration in the flotation cell, can also be defined as

$$\frac{dVc_{cell}}{dt} = F_{i,in} - F_{i,out} \quad [5.25]$$

If c_{cell} is the concentration of NaCl in the flotation cell and J_{dwn} and J_{up} are defined as by equation [5.22], then equation [5.25] becomes

$$V\frac{dc_{cell}}{dt} + c_{cell}\frac{dV}{dt} = A_i(J_{dwn}.c_1 - J_{up}.c_{cell}) \quad [5.26]$$

And, if $J_{dwn} = \frac{J_L}{(1-k)}$, then equation [5.26] reduces to equation given below

$$V_{cell}\frac{dc_{cell}}{dt}+C_{cell}\frac{dV_{cell}}{dt}=\frac{A_i.J_L}{(1-k)}\left(c_i-k.c_{cell}\right) \quad [5.27]$$

The volume in the flotation cell is also changing with time as a result of the downward flow of water displaced from the collection chamber by air. This dilution need to be incorporated into equation [5.27]. The rate of change of volume in the flotation cell is given by

$$\frac{dV_{cell}}{dt}=A_i(J_{dwn}-J_{up}) \quad [5.28]$$

$$\frac{dV_{cell}}{dt}=A_iJ_L \quad ,Vcell=8000cm^3, t=0 \quad [5.29]$$

5.3.3: Parameter estimation

In order to verify the applicability of this model, equations [5.24], [5.27] and [5.29] are simulated using Matlab 7.1's simulink toolbox. The number of cells N_i up to a given conductivity probe j is given by

$$N_i=\frac{H_j}{(dz)} \quad [5.30]$$

H_j is the height of the riser from the entry point to conductivity probe j.

5.3.4 Superficial liquid velocity

The superficial liquid velocity J_L is approximately equal to the uncorrected superficial gas velocity J_{gu} and is calculated from the volume of air collected i.e. Corrected volume (V_{gc}) using equation [3.2] in chapter 3. Superficial gas velocity is then calculated from the equation given below

$$J_g=\frac{V_{gc}}{A.t} \quad [5.31a]$$

where t is the time in seconds taken to collect the gas.

A is the cross sectional area of the riser.

It is important to note that the J_g calculated using equation [5.31] will be lower than the actual J_L, because of expansion of the gas as it rises in the riser due to decrease in pressure. To get the

actual amount of water displaced from the collection chamber, a new uncorrected superficial gas velocity based on the measured volume of air is defined as given below

$$J_{gu} = \frac{V}{A.t} \qquad [5.31b]$$

Form the value J_{gu}, the superficial liquid velocity J_L is calculated the only parameters that need to be estimated are k and the height of each tank h_i

5.4 Model simulation example

The following section presents the steps taken to develop a Simulink model for the axial mixing in the riser of the bubble load meter. An illustration of the Simulink model development for 4 tanks in series and the flotation cell is presented below.

The basic equation for each tank is given by equation [5.32] up to equation [5.36].

Now letting:

$$K = \frac{J_L}{h_i(1-k)}$$

$$M = \frac{J_L.k}{h_i(1-k)}$$

Equation [5.24] reduces to

$$\frac{dc_i}{dt} = M(c_{i-1} - c_i) + k(c_{i+1} - c_{i-1}) \qquad [5.32]$$

For $i = 4, 3, 2 \ and \ 1$ we have

$$\frac{dc_4}{dt} = M(c_3 - c_4) + k(c_5 - c_4) \qquad [5.33]$$

$$\frac{dc_3}{dt} = M(c_2 - c_3) + k(c_4 - c_3) \qquad [5.34]$$

$$\frac{dc_2}{dt} = M(c_1 - c_2) + k(c_3 - c_2) \qquad [5.35]$$

$$\frac{dc_1}{dt} = M(c_{cell} - c_1) + k(c_2 - c_{cell}) \quad [5.36]$$

Now since the flotation cell has different cross sectional area and volume than the other four tanks, the changes in its salt concentration is given by combining equations [5.27] and [5.30].

By substituting K as defined above, equation [5.27] reduces to the equation given below

$$V_{cell}\frac{dc_{cell}}{dt} + C_{cell}\frac{dV_{cell}}{dt} = K.A_i(c_1 - k.c_{cell}) \quad [5.37]$$

The concentration in the flotation cell is also changing with time as a result of the downward flow of water displaced from the flotation cell by air. This dilution needs to be incorporated into equation [5.38]. The change in the volume of the flotation cell is given by

$$\frac{dV_{cell}}{dt} = A_i.J_L \quad [5.38]$$

Note that $V_{cell} = 8000cm^3, t = 0$

And A_i is the cross sectional area of the riser of diameter 3cm.

5.5 Simulink model diagrams

5.5.1 Flotation cell Simulink model Diagram

Modelling of the flotation cell is a combination of equation [5.37] and [5.38], the initial volume of the flotation cell is 8liters and it increases with time. The initial concentration in the flotation cell is 0.05289mol/litre. The model is depicted in Figure 5.4

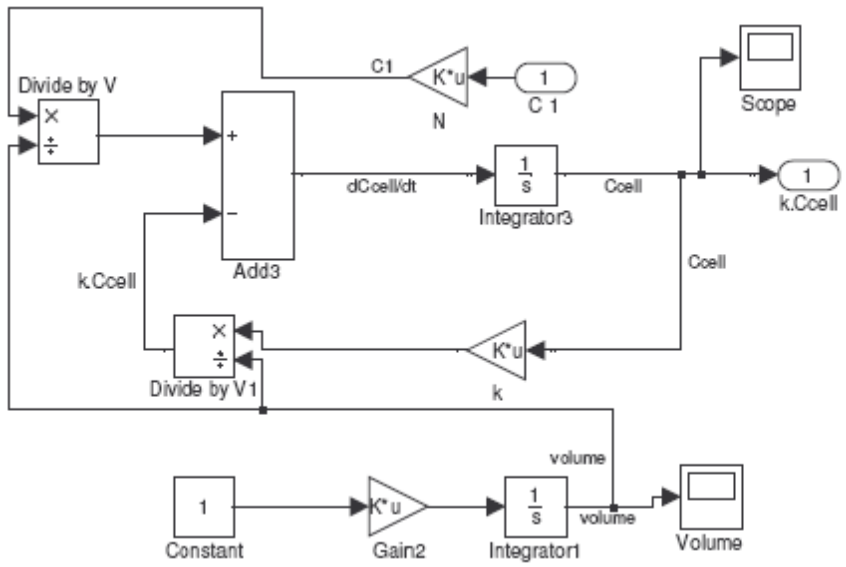

Figure 5.4 Flotation cell Simulink model

5.5.2 Simulink model diagrams for riser tank i =4, 3, 2 and 1

Equations [5.34] to [5.37] models the changes that take place in each tank, the corresponding Simulink model diagrams are given in Figures 5.5, 5.6, 5.7 and 5.8 below. It is important to note that c_{cell} is equivalent to $C0$ in the Simulink diagram for the flotation cell and the first tank.

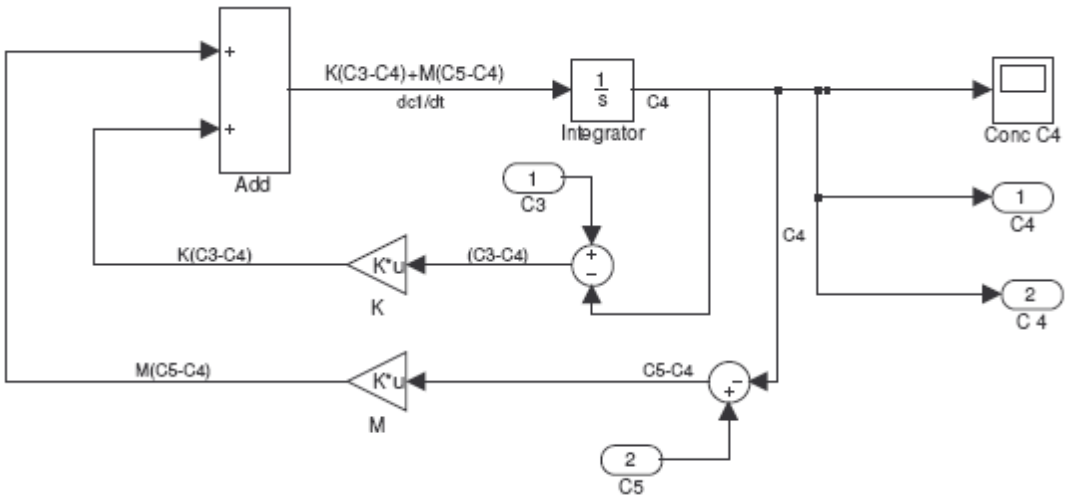

Figure 5.5 Tank i =4 Simulink model

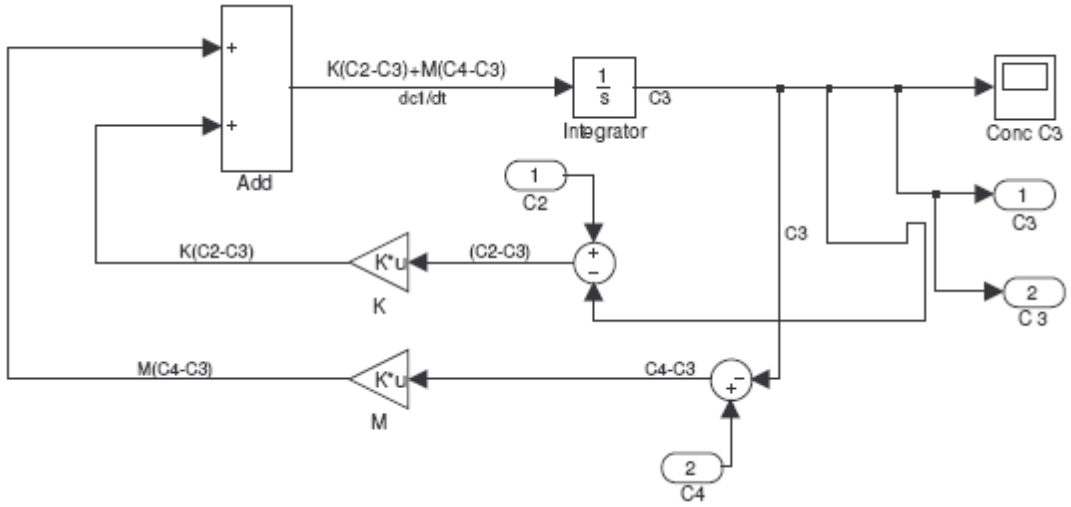

Figure 5.6 Tank i =3 Simulink model diagram

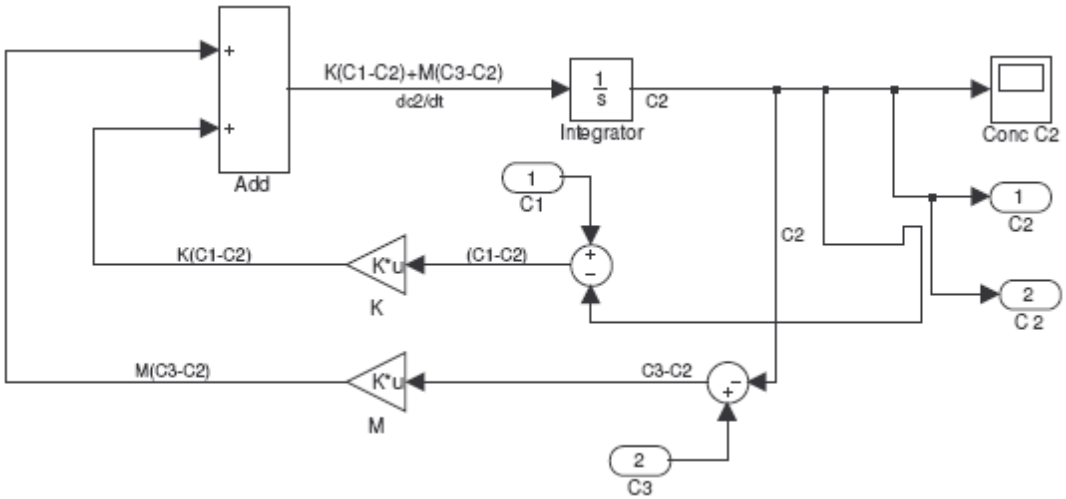

Figure 5.7 Tank i =2 Simulink model

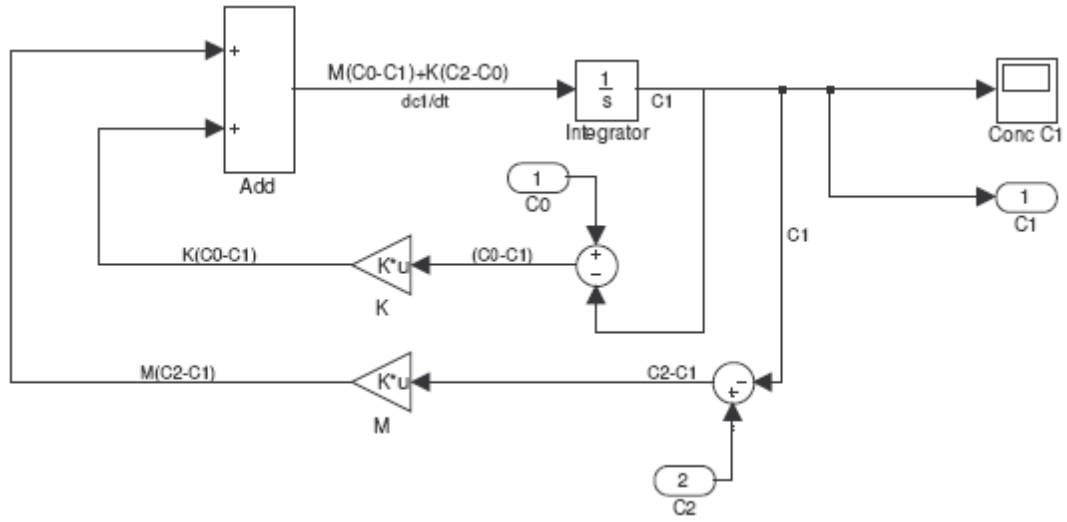

Figure 5.8 Tank i = 1 Simulink model

5.6. Determination of number of tanks for the model

The ultimate objective of this axial model is to determine the number of cells in series that result in a response approximating the experimental results. Determination of the number of cells for this model was achieved by comparing the model to the standard axial dispersion model after establishing the relationship between the model coefficients and the axial dispersion coefficient. The set hypothesis was that for a given riser diameter and frother concentration the value of the axial dispersion coefficient should be approximately constant after finding the optimum number of tanks in the model. The relationship between the axial dispersion equation [5.39] and the basic model equation [5.24] was established by comparing coefficients

$$A.dz.\frac{dc_i}{dt} = A_i.J_L.c_{i+1} - A_i.D.\frac{dci}{dz}\bigg|_{z+dz} - \left[A_i.J_L.c_i - A_i.D\frac{dc_i}{dz}\bigg|_z\right] \qquad [5.39]$$

where dz is the height of each cell

D is axial mixing coefficient

Expanding equation [5.39] and approximating $\frac{dc_i}{dz}$ with equation [5.40] and then comparing its coefficients to equation [5.24] yields relationships given below equation [5.41 to 5.43]

$$\frac{dc_i}{dz} = \left[\frac{c_i - c_{i+1}}{\Delta z} \right] \qquad [5.40]$$

$$J_{dwn} = J_L + \frac{D}{\Delta z} \qquad [5.41]$$

$$J_{dwn} + J_{up} = J_L + \frac{2D}{\Delta z} \qquad [5.42]$$

$$J_{up} = \frac{D}{\Delta z} \qquad [5.43]$$

If Δz is also defined by equation [5.31], then D is related to the axial mixing parameter (k) as given below

$$\frac{k}{1-k} = \frac{N}{J_L.H}.D \qquad [5.44]$$

By choosing an initial k-value for a fixed number of tanks N, a value for the axial dispersion coefficient ◐ was calculated. From this D-value, corresponding k-values for different number of tanks were calculated. The model was then run with these different k and N values and the output from the models was compared. Table 5.1 shows the model parameters and the calculated k-values. Figure 5.9 is a plot of concentration versus time for the different number of tanks which were varied from 8 (N8) to 23 tanks (N23). It is evident from this figure that the change from N16 and N23 is insignificant, thus it was decided that 16 tanks in-series were adequate for this model.

Table 5.1 Model parameters

Number of cells	8	11	16	23
Axial mixing parameter(k)	0.83	0.90	0.93	0.95
Superficial liquid velocity (J_L)	0.7	0.7	0.7	0.7
Riser diameter (d) cm	3	3	3	3
Height of cell (h) cm	3.75	2.72	1.875	1.30

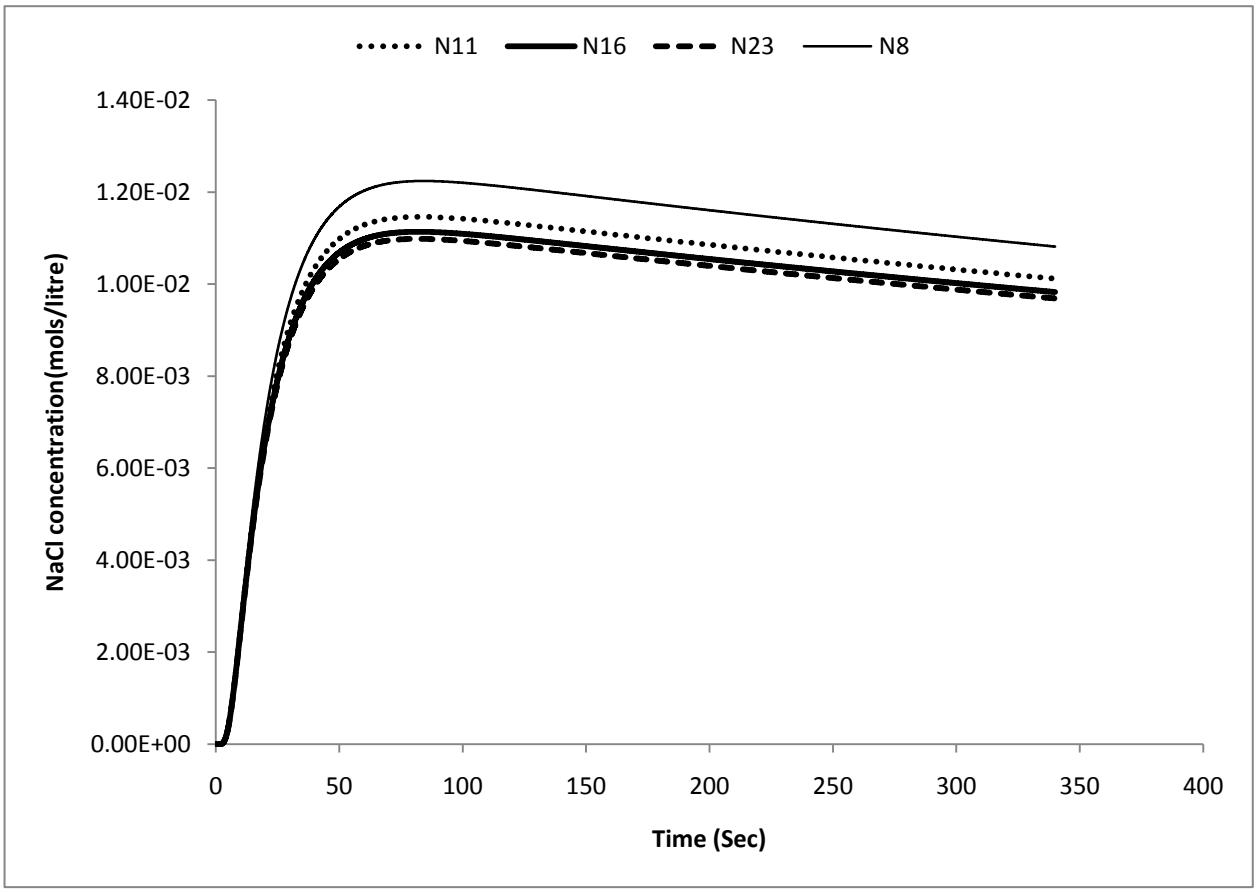

Figure 5.9: Change in NaCl concentration with time for different number of tanks

5.7 Comparison of experimental results with the model output

The importance of the axial mixing model is in its ability to predict salt transport i.e. extent of axial mixing in the bubble load meter riser. To validate the developed model, the simulated model output response was compared to the experimental data. Only results of conductivity probe 1 for all risers are shown in the section, conductivity probe 2 and 3 results are not shown since the important parameters are equal to those for conductivity probe 1.

Preliminary model fit was done on the 30mm riser; the results are shown in Figure 5.10 below. The result compares the model output to experimental data for the 30mm pipe at conductivity probe 1 when 5ppm, 10ppm and 20ppm MIBC was added to flotation cell. Model parameters are shown in Table 5.2.

Table 5.2: Model parameters for conductivity probe 1 for the 30mm riser

Number of cells	16	16	16	16
Axial mixing parameter(k)	0.79	0.85	0.85	0.87
Superficial liquid velocity (J_L)	0.7	0.7	0.7	0.7
Riser diameter (d) cm	3	3	3	3
Height of cell (h) cm	1.875	1.875	1.875	1.875

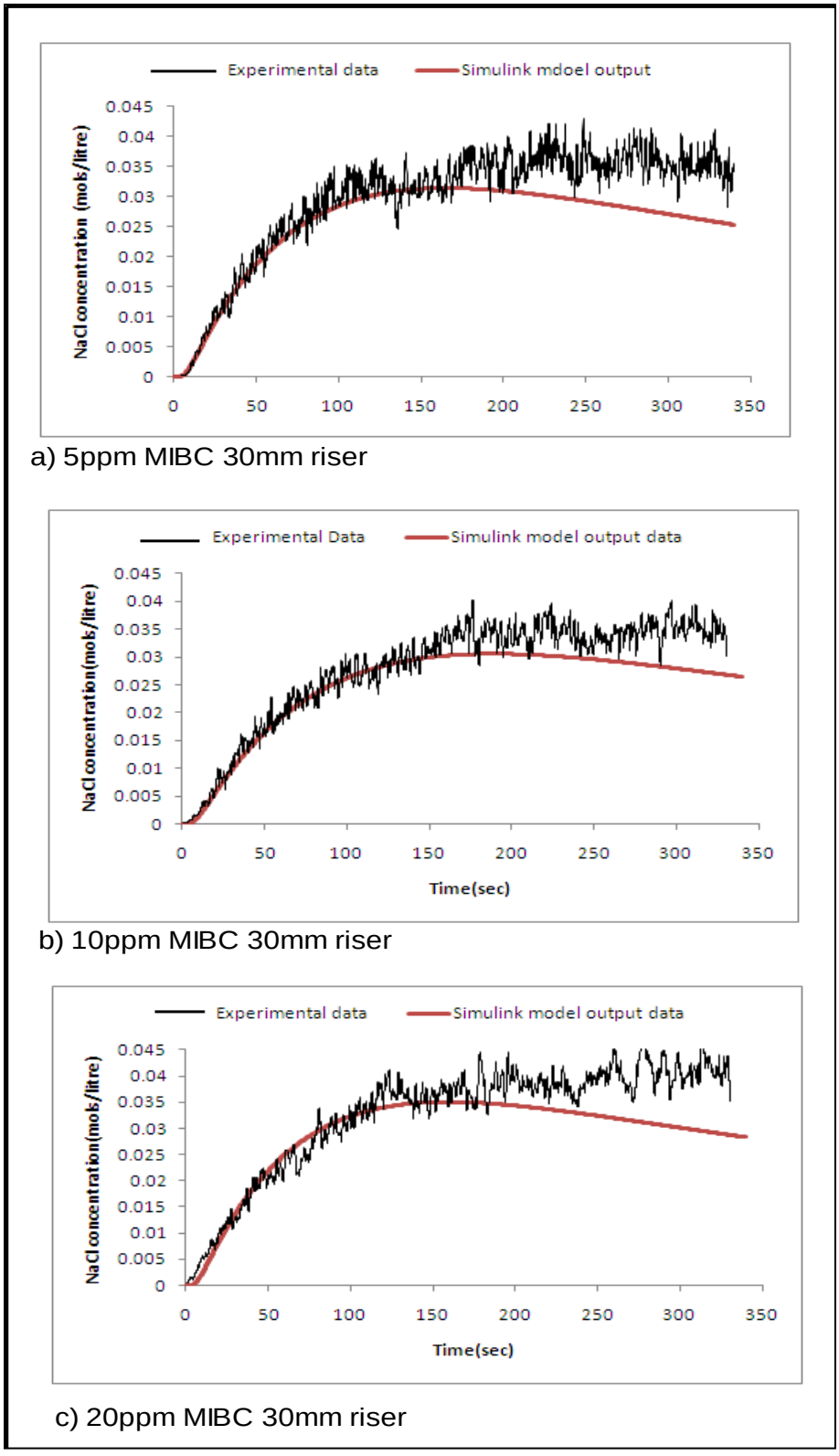

Figure 5.10: Comparison of experimental data with simulink model output results for conductivity probe 1 on the 50mm riser for 5, 10 and 20ppm MIBC

Additional parameter (α)

Figure 5.10 shows that the model tends to under predict the experimental data after 150 seconds of running. This was expected as the analysis of conductivity experiments done in chapter 4 had indicated that, there is an additional amount of salt that is moving up the riser as a result of another process which is not axial mixing. To account for this additional NaCl, an additional parameter (α) was added to the basic model.

This parameter accounts for the additional NaCl that rises up the column as a result of:-

1) Mechanical push of inter-bubble liquid by slow rising air bubbles (bubble swarms), it also accounts for the NaCl that also goes up the first few cells of the riser as a result of the turbulence in the flotation cell.
2) Accounts for the salt that is adsorbed on the bubble lamella

In order to incorporate this additional parameter into the basic axial mixing model, the parameter was defined as the fraction of the bubble lamella that is covered by NaCl. This means that the parameter is a surface area fraction and is depended on bubble size (MIBC concentration) and the number of bubble aggregates sampled per unit time (riser diameter). This also means that this parameter is related to the superficial gas velocity (J_g).

Addition of this parameter, changed the basic model equations for the riser cells and the flotation cell from [5.24] and [5.27] to [5.45] and [5.46] respectively.

$$\frac{dc_i}{dt} = \left[\frac{J_L.k}{h_i(1-k)} + \frac{\alpha.J_g}{h_i}\right](c_{i-1} - c_i) + \frac{J_L}{h_i(1-k)}(c_{i+1} - c_i) \qquad [5.45]$$

$$C_{cell}\frac{dV_{cell}}{dt} = \frac{A_i.J_L}{(1-k)}.c_1 - \frac{A_i.J_L.k}{(1-k)}.c_{cell} - J_g.A_i.\alpha.c_{cell} - V\frac{dc_{cell}}{dt} \qquad [5.46]$$

Data fit and parameter estimation was done using equations [5.45] and [5.46] and results are presented in the following section.

5.7.1 50mm riser model and experimental data comparison for conductivity probe 1

Figure 5.11 below shows the results of the comparison for the 50mm pipe at conductivity probe 1 when 0ppm, 5ppm, 10ppm and 20ppm MIBC was added to flotation cell. Model parameters are shown in Table 5.3.

Table 5.3: Model parameters for conductivity probe 1 for the 50mm riser

Parameter	0 ppm MIBC	5 ppm MIBC	10 ppm MIBC	200 ppm MIBC
Axial mixing parameter(k)	0.80	0.83	0.82	0.84
Superficial liquid velocity (J_L)	0.7	0.7	0.7	0.7
Riser diameter (d) cm	5cm	5cm	5cm	5cm
Height of cell (h) cm	1.875	1.875	1.875	1.875
α value	0.90	0.94	0.935	0.96
Number of cells	16	16	16	16

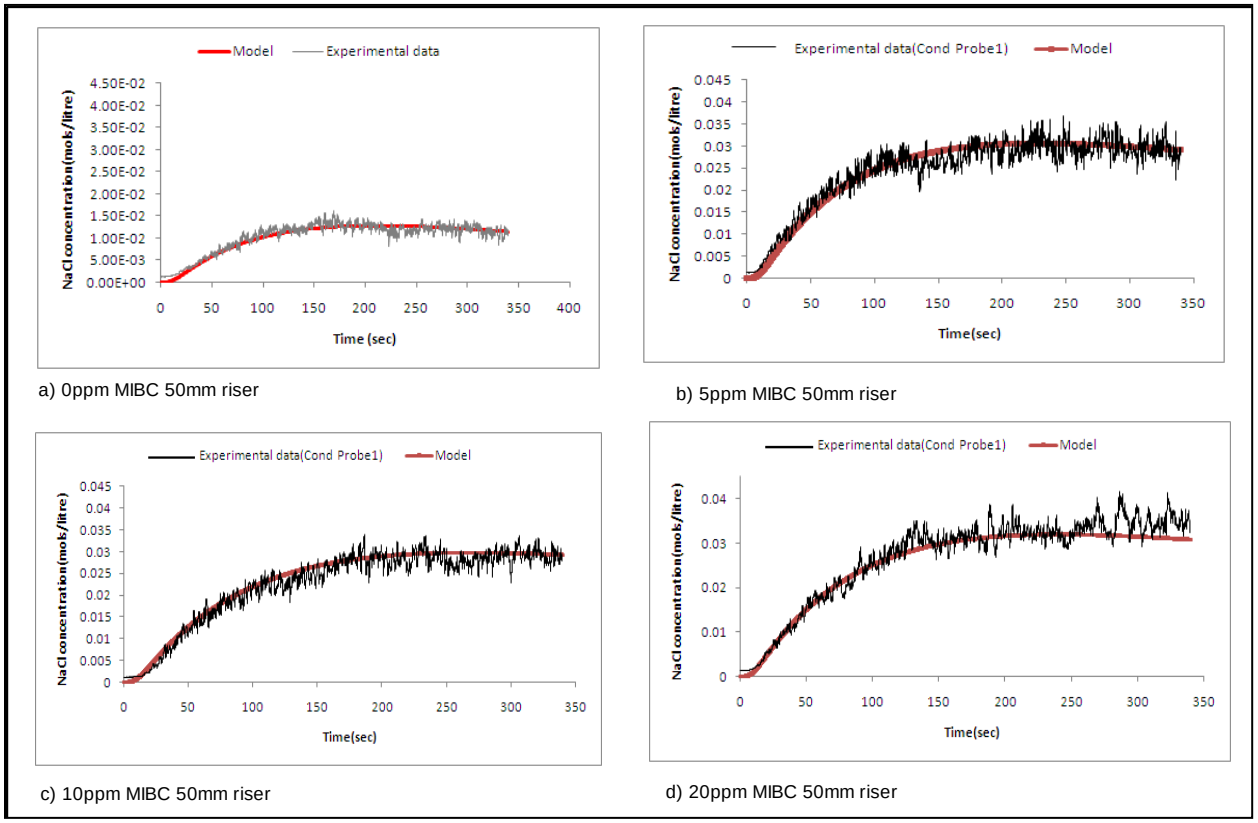

Figure 5.11: Comparison of experimental data with Simulink model output results for conductivity probe 1 on the 50mm riser for 0, 5, 10 and 20ppm MIBC

5.7.2 30mm riser model and experimental data comparison for conductivity probe 1

Table 5.4: Model parameters for conductivity probe 1 for the 30mm riser

Parameter	0 ppm MIBC	5 ppm MIBC	10 ppm MIBC	200 ppm MIBC
Axial mixing parameter(k)	0.77	0.83	0.83	0.84
Superficial liquid velocity (J_L)	0.7	0.7	0.7	0.7
Riser diameter (d) cm	3cm	3cm	3cm	3cm
Height of cell (h) cm	1.875	1.875	1.875	1.875
α value	0.45	0.93	0.94	0.95
Number of cells	16	16	16	16

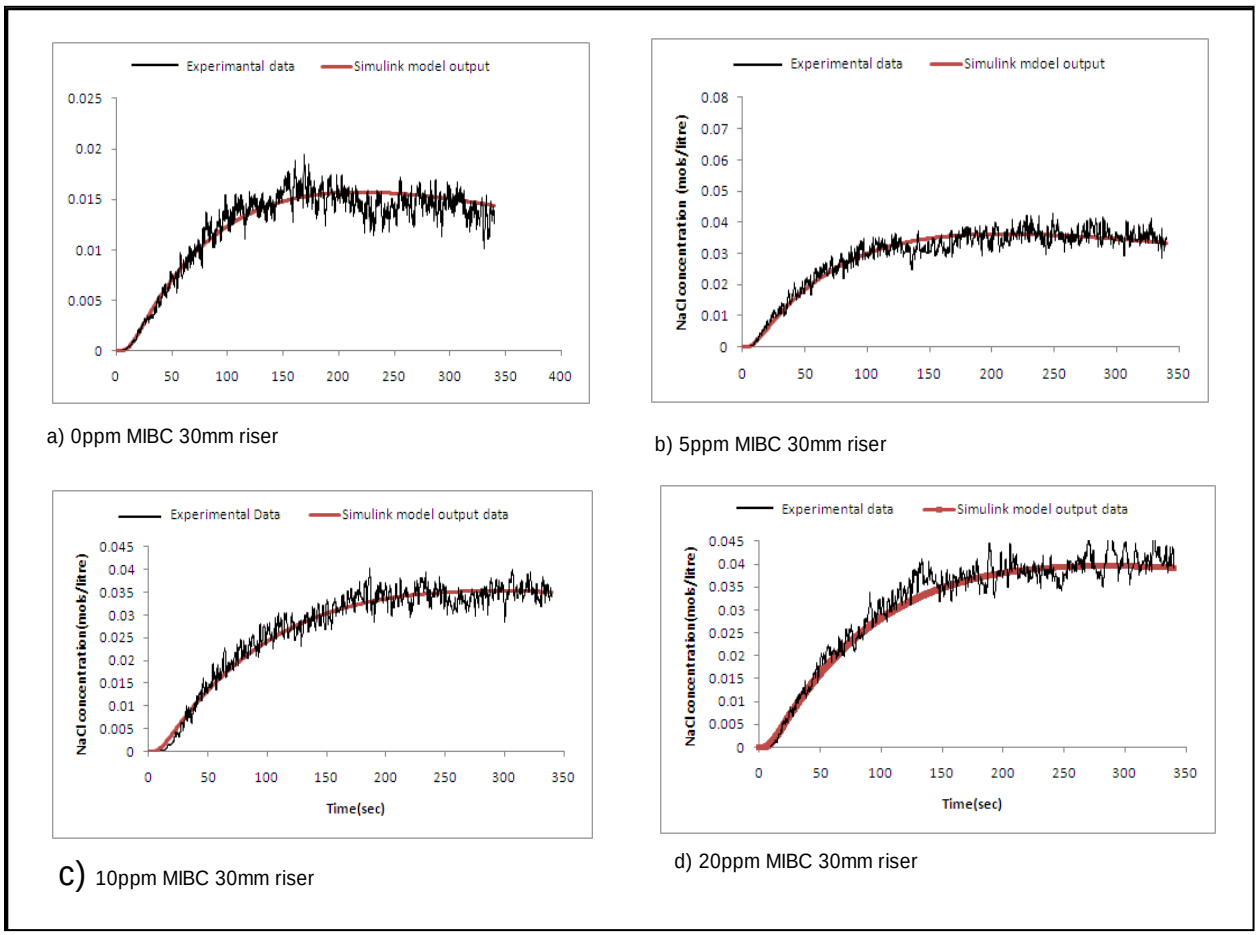

Figure 5.12: Comparison of experimental data with Simulink model output results for conductivity probe 1 on the 30mm riser for 0, 5, 10 and 20ppm MIBC

5.7.3 20mm riser model and experimental data comparison for conductivity probe 1

5.5 Model parameters for conductivity probe 1 for the 20mm riser

Parameter	0 ppm MIBC	5 ppm MIBC	10 ppm MIBC	200 ppm MIBC
Axial mixing parameter(k)	0.4	0.75	0.74	0.76
Superficial liquid velocity (J_L)	0.7	0.7	0.7	0.7
Riser diameter (d) cm	2	2	2	2
Height of cell (h) cm	1.875	1.875	1.875	1.875
α value	0.11	0.15	0.13	0.13

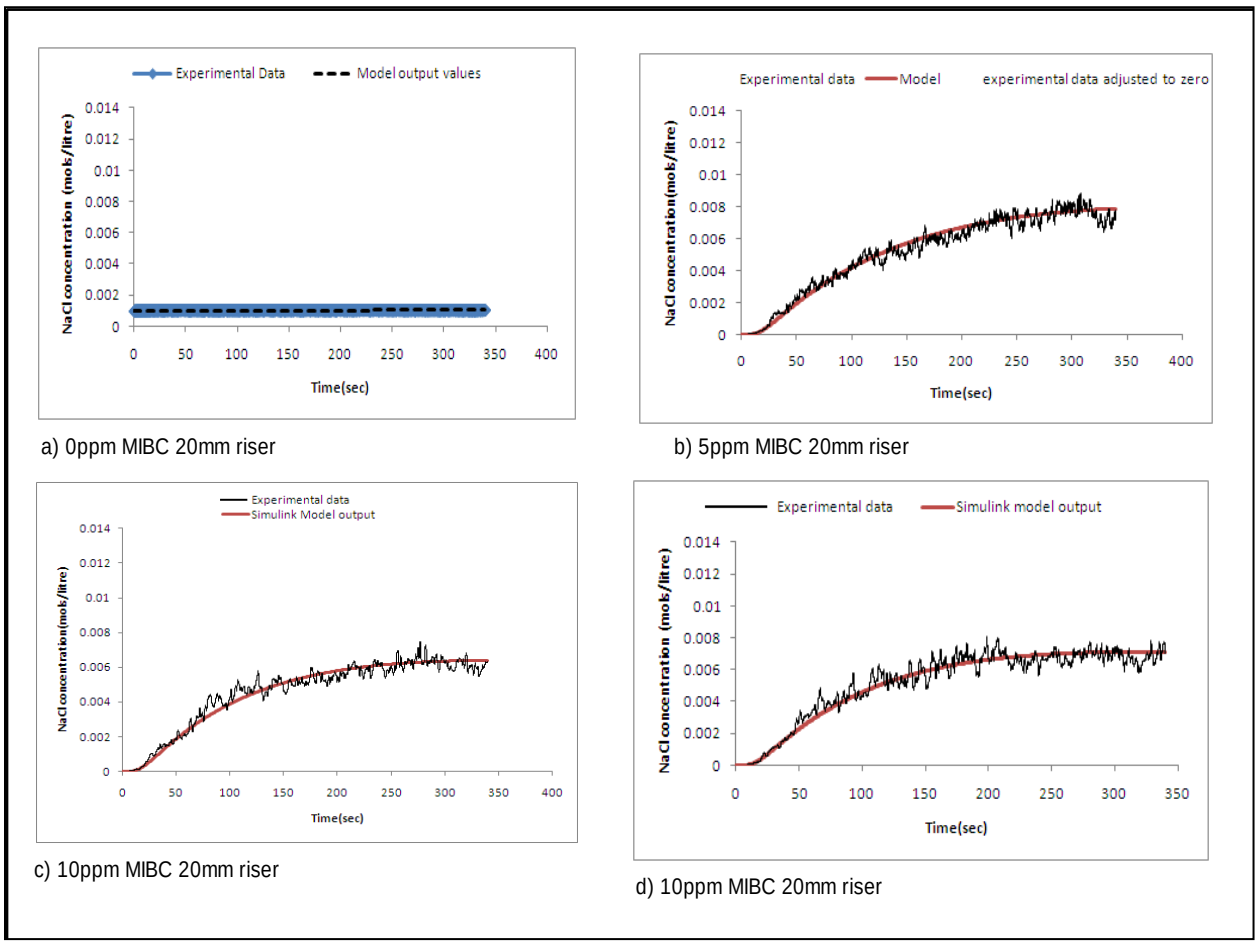

Figure 5.13: Comparison of experimental data with Simulink model output results for conductivity probe 1 on the 20mm riser for 0, 5, 10 and 20ppm MIBC

5.8 Axial mixing model parameter estimation results summary

The model developed fits the experimental data well. Figure 5.14 shows the variation of the axial mixing parameter with frother concentration for a particular riser, what is notable is the general increase of k values with increase in riser diameter, also the change in the k-values with increase in frother concentration for all riser diameters with a tendency of attaining an almost constant value from 5ppm and above. The large changes in the axial mixing parameter (k) from 0ppm to 5ppm is explained by realizing that when no frother was added, the bubble aggregates sampled were large and fewer and they rose almost independent of each other thus the mixing intensity was low. Further addition of MIBC above 5ppm resulted in an increase in the number of the bubbles sampled per unit time for a particular riser diameter, but had a slight effect on the axial mixing coefficient. An average k-value of 0.83 was obtained for 50mm rise. The mean k-values for MIBC concentration range of 5ppm to 20ppm for the 30mm and 20mm riser are 0.83 and 0.75 respectively.

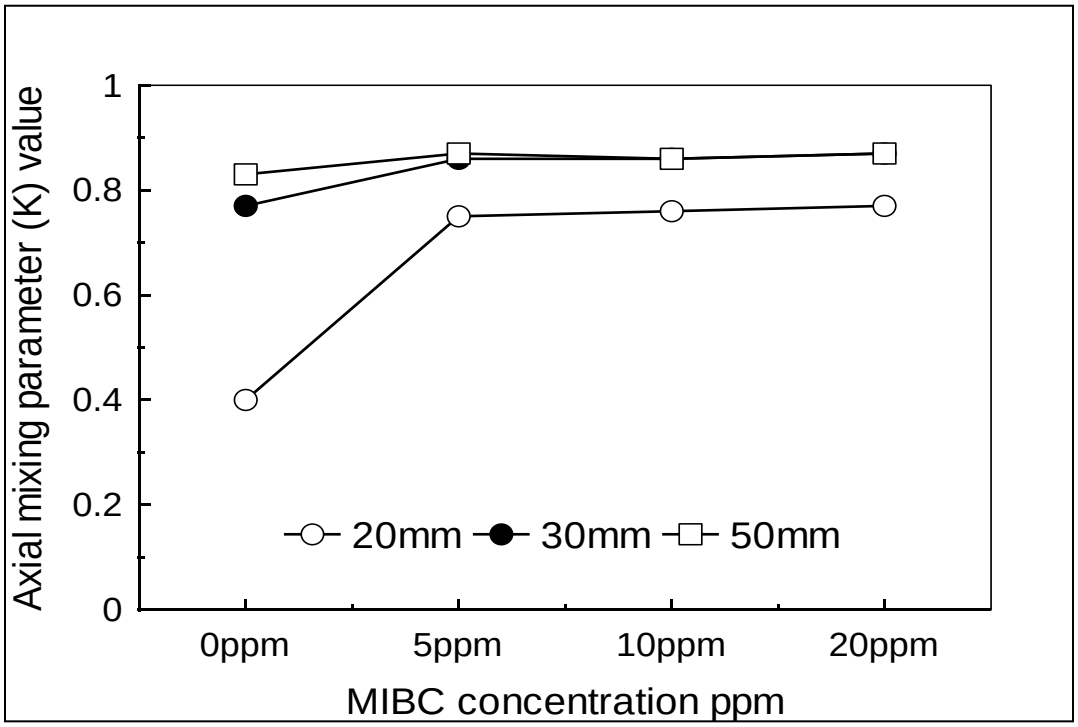

Figure 5.14 Variation of axial mixing parameter (k) with MIBC concentration

5.8.1 Additional model parameter (α)

It was acknowledged in chapter 4 that the transport of salt up the riser is a combination of axial mixing, mechanical push by a slow rising swarm of bubbles and NaCl adsorbed on the bubble lamella. This theory was also confirmed by the model. Figure 5.15 shows the output from the two models i.e. one without the α -parameter and the one with this parameter for the 50mm riser. The model without the α -parameter tends to under predict the experimental data, introducing the α -parameter improves the fit. The under prediction by the model without the α -parameter is expected because it does not take into account the salt that moves up as a result of the mechanical push by bubble swarms and the salt that is adsorbed on the bubble lamella. The α -parameter accounts for this additional NaCl.

Figure 5.16 shows the variation of the α -parameter with concentration for the three different risers. It is interesting to note again that it increases with riser diameter and with MIBC concentration for a particular riser.

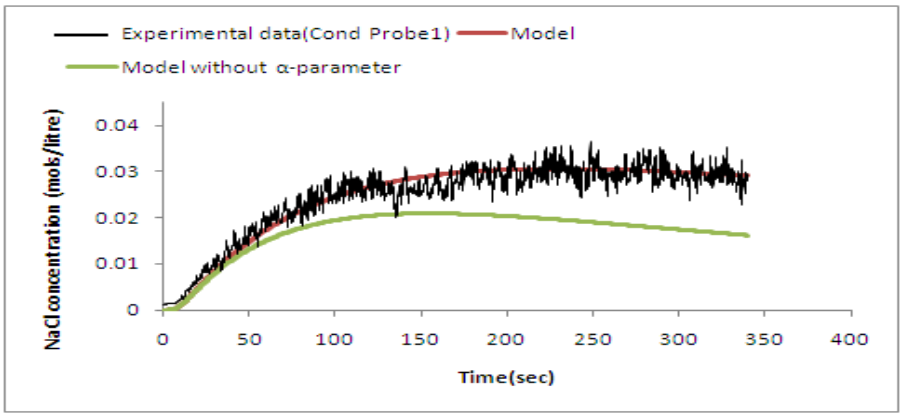

a) 5ppm MIBC 50mm riser, α = 0.94

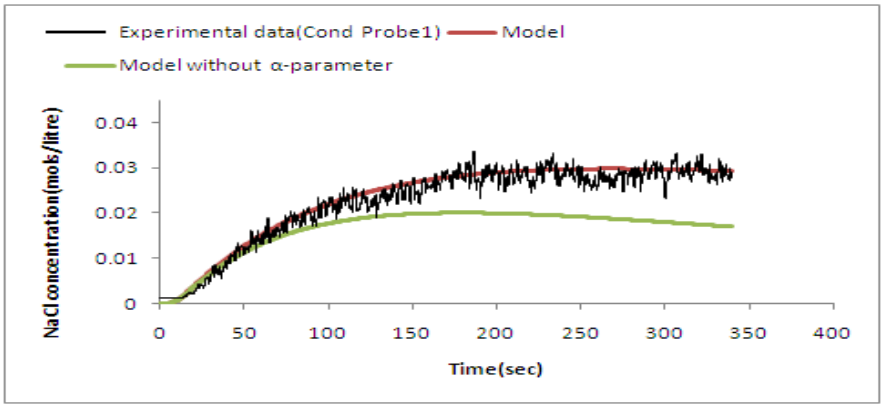

a) 10ppm MIBC 50mm riser, α = 0.935

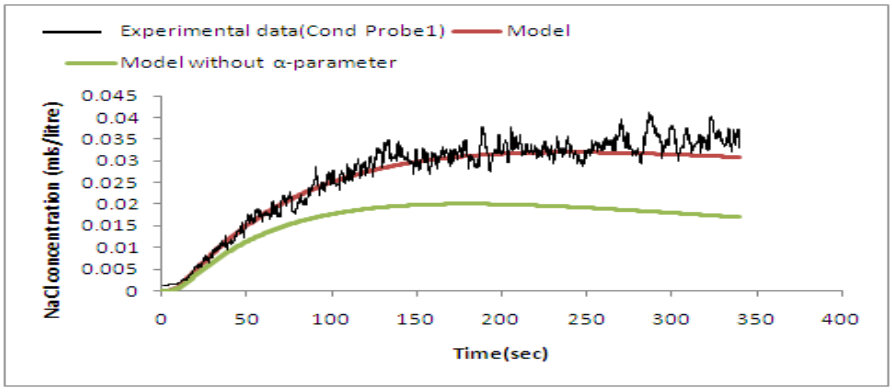

a) 20ppm MIBC 50mm riser, α = 0.96

Figure 5.15: Comparison of response of the model with and without the α-parameter for the 50mm riser

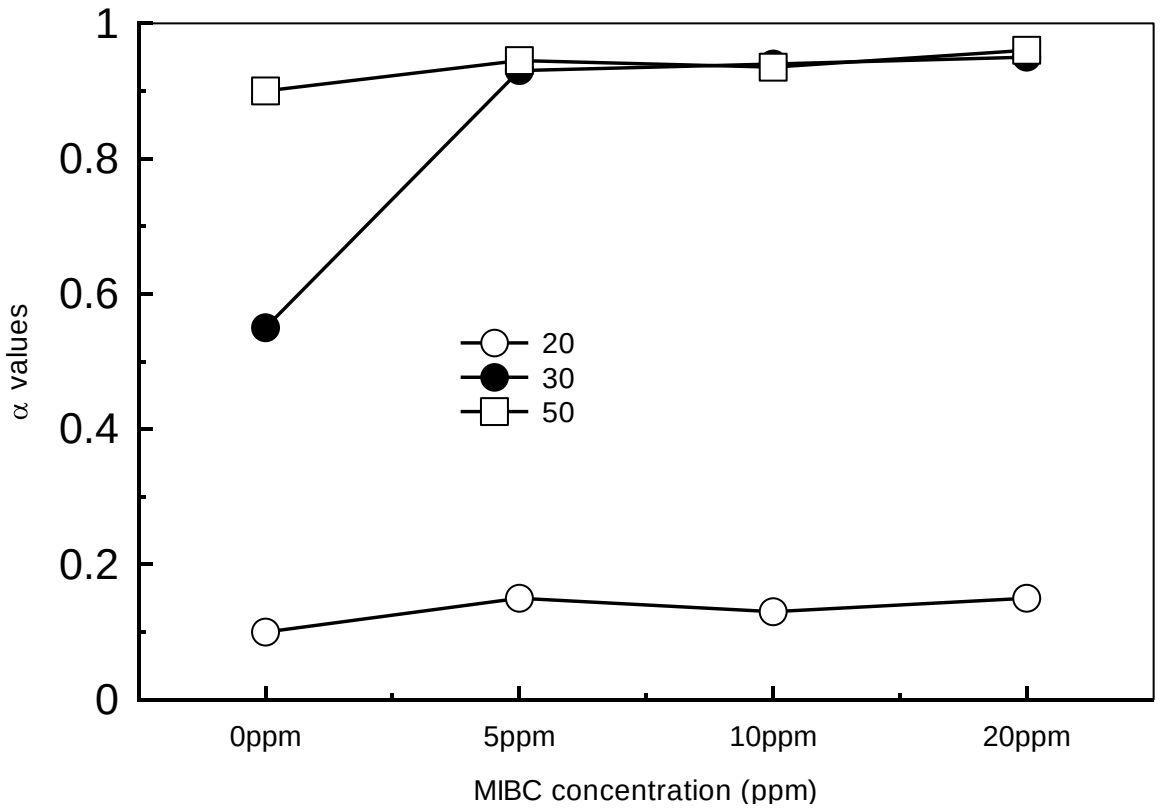

Figure 5.16 variation of α -parameter with concentration for the three risers

5.8.2 Axial mixing parameter estimation conclusion

A model which adequately predicts salt changes in the risers of the bubble load meter was successfully developed, two important parameters one for the axial mixing and the other accounting for the mechanical push were established. All the parameters are strong functions of riser diameter; they tend to increase with riser diameter. The α -parameter is also a strong function of bubble size (frother concentration in this case). Though the axial mixing parameter increased from 0ppm to 5ppm the increase thereafter is minimal, this may imply that the salt increase after 5ppm came as result of α -parameter (bubble swarm effect).

Chapter 6

Results and discussion

In this chapter bubble load results are presented. The basic design features of the bubble load meter and their impacts on an industrial plant are evaluated. The chapter also presents the results on the validation of performance targets for the bubble load meter. A discussion on how the bubble load results can be used to interpret flotation kinetics such as estimation of froth recovery and entrainment is also included.

Using bubble load data to estimate entrainment will is important in the modelling of entrainment. A section that demonstrates the possibility of using this data to calculate entrainment is included. To facilitate the calculations, a number of assumptions were made some of which needs further investigation, section 6.7 is dedicated to highlighting these assumptions and their limitations. It also includes the kind of measurements that should have been done to facilitate the calculations.

The main objectives of this research were to:-

1. Develop an instrument or device to measure bubble loading in industrial flotation machines based on the Dyer (1995) concept. The device should measure bubble loads accurately without particle losses as a result of bubble coalescence, or break up. The instrument should also be capable of collecting a solid sample in excess of 200 grams for PGM analysis
2. Verify the applicability of the device in industrial flotation machines and the effectiveness of bubble load data in evaluating flotation kinetic data such as froth recovery and estimation of entrainment.

The chapter will discuss the results that were obtained and how they were used to meet the main objectives. The results are divided into two i.e. those focusing on the design aspects and those focusing on the industrial applicability and flotation kinetics interpretation

6.1. Bubble load meter: Design aspects

A bubble load meter was successfully designed; its design features and operating procedures and limitations were discussed in chapter 4, and in this chapter a brief summary is given. The summary will focus more on the conclusions that were drawn on the effects of riser diameter, effect of riser height, and effect of water recirculation rate and water quality on the performance of the bubble load meter.

6.1.1 Riser diameter

As discussed in chapter 4, a bubble load meter with riser diameters of 20mm, 30mm and 50mm was developed. The design and operational aspects of the bubble load meter that were tested have been discussed in chapter 4. From the results presented in chapter 4 (Figure 4.12 to Figure 4.15), it was seen that NaCl concentration recorded by each conductivity probe increased with riser diameter. For the 20 and 30mm riser columns, NaCl hardly reached conductivity probe 2 and consequently nothing was recorded at the third conductivity probe. The 50mm riser recorded salt (0.1% of the original salt) at conductivity probe 3 indicating that under normal operation, unattached particles may reach the collection chamber. It was therefore safe to conclude that from these three risers tested, constructing the bubble load meter with the 20mm and 30mm ID pipes was adequate. To maximize the mass of sample per unit time the 30mm ID riser was opted for (*cross sectional area is 2.25 times larger than the 20mm*).

6.1.2 Riser column height

The bubble load meter was designed with a height of 1.5m for all the three risers. This height was chosen for convenience of operation and to allow bubble load measurements to be taken at different depths below the pulp-froth interface. Using conductivity experiments, the effect of height on salt transport (inter-bubble liquid) was investigated. Comprehensive results are shown in chapter 4. The results indicate that NaCl concentration decreases with increase in height for a particular riser diameter. This implies that increasing the height of the bubble load meter for the 50mm ID may eliminate the problem of particles reaching conductivity probe 3. Figure 6.1

shows the variation of NaCl concentration with height for 5ppm and 10ppm frother concentrations on the 50mm riser. This variation of NaCl concentrations with height was found to be adequately represented by the empirical equation given below

$$C = C_0 \times e^{-k.h^{1.5}} \qquad [6.1]$$

where C is concentration of NaCl/suspended particles at height h above riser entry point

C_0 is the initial concentration of NaCl/suspended particles in the flotation cell

k is a constant which is a function of bubble size (frother concentration) and the intensity of axial mixing

Thus, provided the column is long enough, the 50mm riser could still be used. Its height however should be determined experimentally. The current length of the 20 and 30mm risers is adequate.

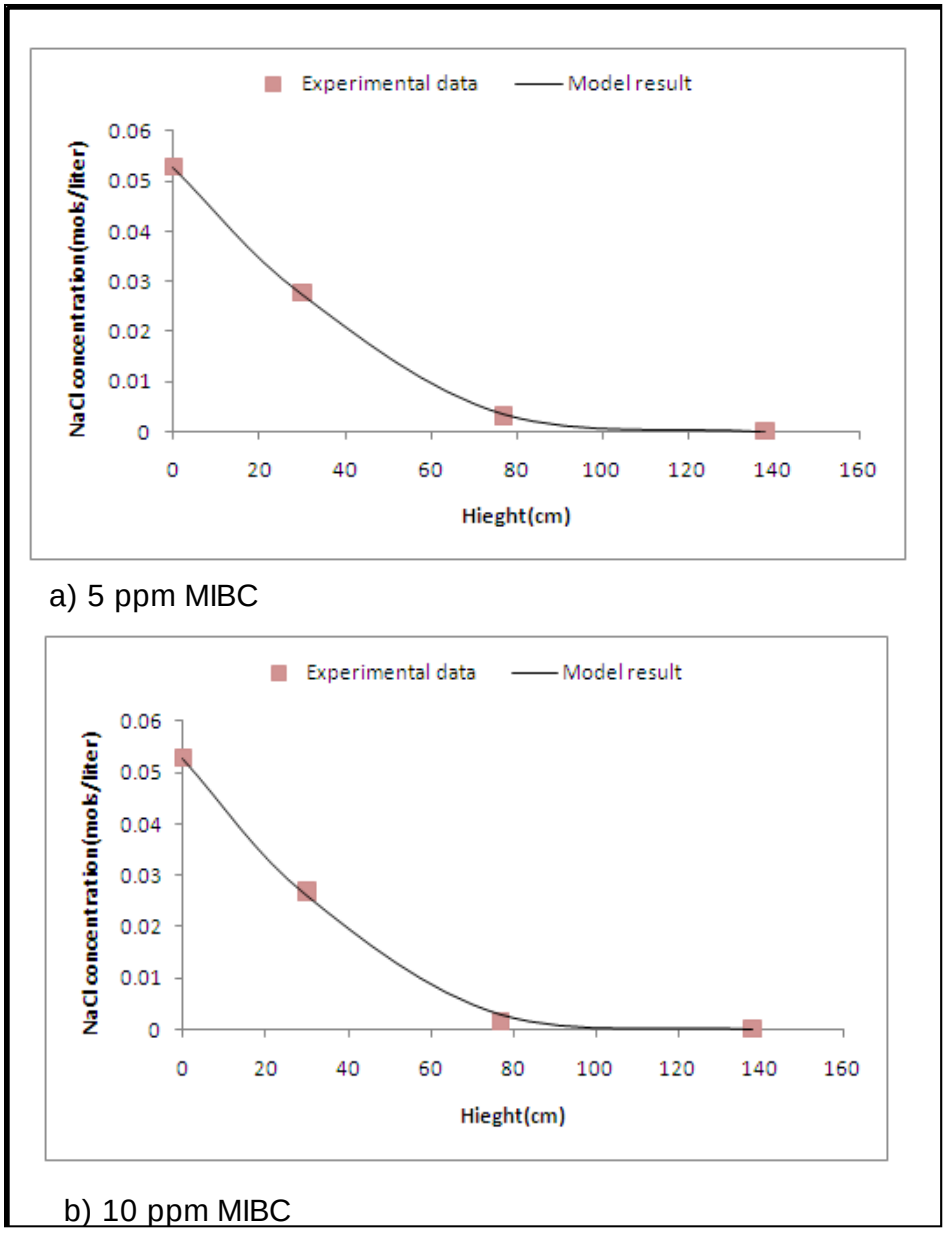

Figure 6.1: Variation of concentration with height on the 50mm riser for 5 and 10ppm MIBC

6.1.3 Water flowrate control

Water flowrate is an important parameter for the smooth operation of the bubble load meter. It provides the medium in which particle-bubble aggregate flows to the collection chamber. It also determines the stability of the bubble-particle aggregate. It must neither be too high nor too low. Very high water flowrate result in the bubbles being pushed too much out of their natural trajectory at the T-junction increasing shear forces that lead to particle detachment and eventual

drop off. Figure 6.2 shows the effect of increasing the water recirculation velocity at the T-junction from 1.85cm/s to 3.7cm/s for the 20mm riser.

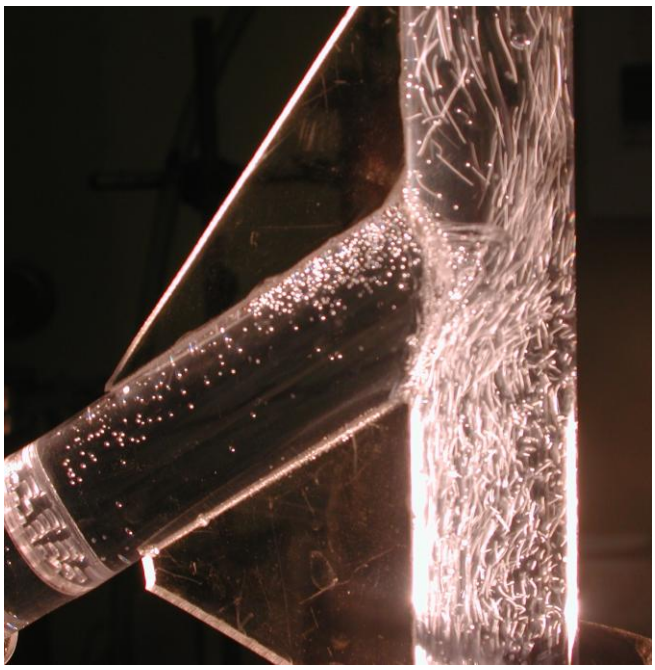

a) Velocity at T-junction = 3.7cm/s

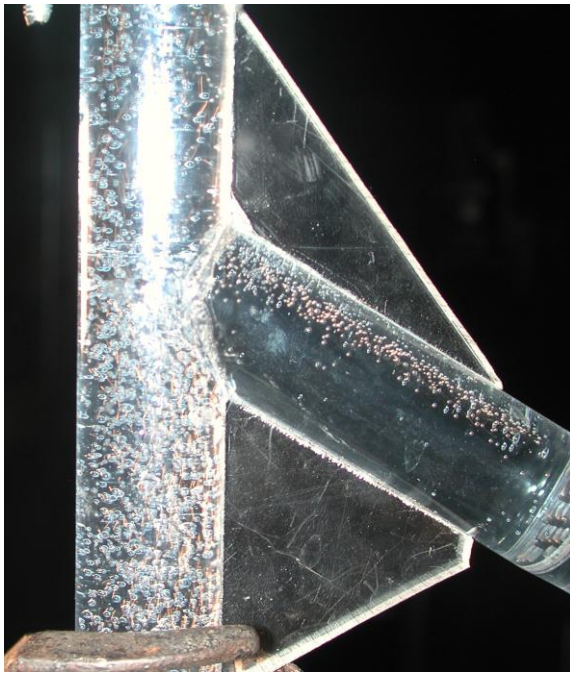

b) Velocity at T-junction = 1.85cm/s

Figure 6.2: Effect of water flowrate at the T-junction

Low water flowrate is also detrimental to the operation of the bubble load meter. Particles detach at the sudden contraction above the T-piece because of the following reasons:

- After the sudden contraction, bubbles would coalesce and hence particles may detach from the bubbles.
- The sudden change in the kinetic energy of the bubbles due to change in cross sectional area of the flow channel at the sudden contraction would result in particle detachment.

The water recirculation rate should be high enough to elutriate all the detached particles to the collection chamber. If the water velocity is too low then particles would settle in the tube that connects the riser to the collection chamber. Figure 6.3 shows particles settling in the tube that connects the 20mm riser to the collection chamber.

Figure 6.3: Picture showing particles settling in the tube that connects the riser to the collection chamber

In summary an optimum flowrate that makes sure that particles do not detach at the T-junction and at the same time ensuring that particles that detach from bubbles after the sudden contraction are pushed to the collection chamber is needed. As a rule of thumb setting the pump flowrate such that it is twice the gas flowrate in the bubble load meter may eliminate particle settling as well as minimising the deviation of bubbles from their natural trajectory at the T-junction. Reducing the horizontal length on the section shown in Figure 6.3 will also reduce the need for high water recirculation velocities.

6.2. Bubble load meter: Verification of set performance targets.

6.2.1 Rejection of suspended material

As discussed in chapter 4, the 20 and 30mm risers are effective in rejecting unattached particles or suspended particles from reaching the collection chamber, results are summarised in Figure 4.17 and Figure 4.18. Conductivity tests with the 50mm ID indicated that indeed NaCl reached

conductivity probe 3, this means that inter-bubble liquid (unattached particles) is not completely eliminated/ rejected by the wash water and had a high chance of reaching the collection chamber.

6.2.2 Particle drop off testing results

To test for particle drop off, coal flotation experiments were carried out in accordance with the procedure in section 3.3. Samples of inter-bubble liquid were drawn from the riser at the sampling port above conductivity probe 2 using syringes as depicted in Figure 3.8 in chapter 3. The liquid samples were filtered and checked for coal particles. Results obtained with the 30mm riser are summarized in Table 6.1 and shows that no particles were dropping off in the riser. With this result, it was concluded that in the riser section below the T-junction no particles were dropping off from the bubbles.

Table 6.1: Particle drop off test results.

	Volume of inter-bubble liquid(ml)	Mass of coal(g)
1	50	0
2	50	0
3	50	0
4	50	0

6.2.3 Design objectives: Brief summary

In conclusion, an effective bubble load meter was designed. A riser diameter of 30mm and height of 1.5m were proved experimentally to be adequate for the bubble load meter. Experiments to test particle drop off and bubble coalescence, rejection of suspended particles were done and proved that the 20 and 30mm are quite effective as bubble load meter risers.

6.4. Industrial applicability of the bubble load meter

The second and most important objective of the research was to verify the industrial applicability of the bubble load meter. This encompasses the set up in an industrial flotation cell, the robustness of the designed equipment and its ease of use. A target sample mass of 200grams was set. The effectiveness of the obtained bubble load data in interpreting froth recovery and entrainment in PGM plant was also set as an objective. The industrial verification/testing of the bubble load meter was carried out at Lonmin's EPC concentrator in Marikana, on the first primary rougher and first primary cleaner cells. Results are presented in this section. The EPC basic flotation circuit is shown in Figure 3.9.

6.4.1 Bubble load: First primary rougher cell

Four separate measurements were successfully taken on the first primary rougher cell. Bubble size and superficial gas velocity measurements were also done on the same cell; results are summarized in Table 6.2.

The bubble load results obtained were very low (*average 2.97g/l*) and an average sample mass of 8.25grams (*average of run 3 and 4*) was obtained. This sample mass was far less than the objective mass of 200grams. The results also show a froth flow number (R_{fn}), greater than 1, implying that entrainment was unusually high or particles were lost in the device. In the absence of entrainment an R_{fn} value of 1 implies there is no particle drop back, while that less than 1 implies particle drop back.

Table 6.2: Bubble load measurement results: First primary rougher cell

Experimental run	Time(sec)	Air volume (cm^3)	Jg(cm/s)	Mass(g)	Bubble load(g\l)	Conc loadin(g/l)	R_f
1	404.00	4658.02	1.63	2.00	0.43	5	11.65
2	452.00	5140.80	1.61	12.50	2.43	5	2.06
3	260.00	2612.32	1.42	8.50	3.25	5	1.54
4	265.00	2478.18	1.32	8.00	3.23	5	1.55
Average(2 to 4)			1.45		2.97	5	1.71
Relative SD			8.19				

Effect of water quality

Table 6.2 above, shows the results obtained from the 4 measurements done on the first primary rougher cell. Experiment 1 was done with plant water while run 2 to 4 were done using concentrate filtered water. These measurements were taken at the same position and depth below the pulp-froth interface. The bubble load value (0.43g/l) obtained on run 1 is very low as compared to the result obtained using concentrate filtered water (*2.97g/l average of run 2 to 4).* Experimental run 1 was done using plant water, which is recycle water from the water treatment plant. It is evident that this plant water was inimical to the existence of the particle-bubble aggregate if the bubble load value of run 1 is compared to the average bubble load value of run 2 to run 4. The chemistry of the water that is added to the bubble load meter is very important for successful bubble load measurement. This water should have the same chemistry as the water in the flotation cell, to avoid particle detachment in the bubble load meter.

6.4.2 Demonstration of the effect of pressure drop across the filter

Experimental runs 2 to 4 were done using concentrate filtered water; comparing their bubble load results shows that, experimental run 2 has a lower bubble load value (2.43grams/litre) than experimental runs 3 and 4 which has an average value of 3.24grams/litre. As seen in Table 6.2 experimental run 2 was run for 452seconds while experiments 2 to 4 were run for about 265seconds. This prolonged sampling time on run 2 led to increase in pressure drop across the filter which led to filter paper breakage resulting in the possibility of loss of particles. Pressure drop across the filter increased as a result of cake formation, the thickness of the cake is a direct function of sampling time. High pressure drop across the filter led to filter paper breakage and particle loss, Figure 6.4 shows a typical loaded filter paper. In experimental runs 3 and 4 sampling times were reduced from 450seconds (*experiment run 2*) to an average time of 265seconds (*experiment 3 and 4*). In addition to reducing sampling times, pressure drop across the filter was also monitored and maintained below 1 bar using the pressure gauge connected to the filter. The average bubble load obtained on these two experimental runs is 3.24g/l (Table 6.2).

Importance of filter on the bubble load meter

Results in this section helps to demonstrate the effect of pressure drop across the filter which is a function of cake thickness on the filter paper. It also demonstrates the importance of the filter in capturing particles that are carried down by the wash water from the collection chamber. In fact, the filter is one of the most important components of the current bubble load meter; it distinguishes it from the previous devices mentioned in literature i.e. (Seaman et al. 2004) and Dyer (1995)). Its main function is to capture particles that are carried with the recirculating water. The fact that particles were actually lost with the wash water on experimental run 2, because of filter paper breakage helps to demonstrate the importance of the filter. In addition, this result also points to the possibility of loss of particles with the wash water in bubble load measuring methods that utilise the positive displacement principle but without a filter that are described in literature e.g. (Seaman et al., 2004 and Dyer, 1995). The process of particle loss with wash water may be more pronounced in situations where these devices are used to measure bubble load in a flotation process with highly brittle froths.

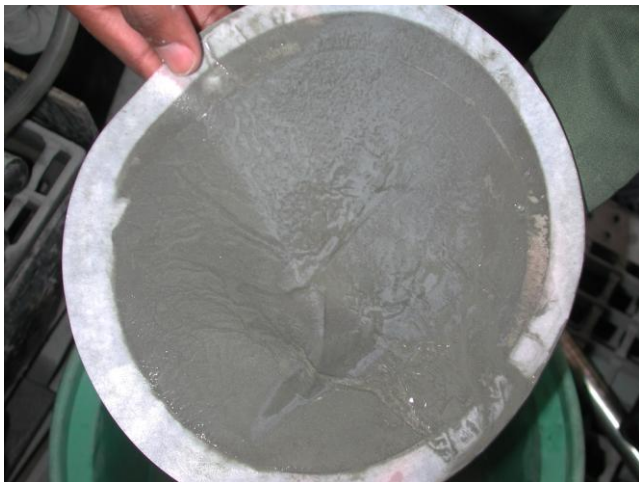

Figure 6.4: Picture of a loaded filter paper

Froth flow number

The values of froth flow number (R_{fn}) calculated, assumed negligible entrainment. The average value for R_{fn} is 1.55 for experimental runs 3 and 4. This R_{fn} indicated in Table 6.2, was calculated by

$$R_{fn} = \frac{Mass\ of\ particles\ in\ the\ concentrate\ per\ liter\ of\ gas\ fed\ to\ cell}{Mass\ of\ particles\ attached\ to\ the\ bubbles\ per\ liter\ of\ gas\ entering\ the\ froth\ phase}$$

Froth flow number can assume any value equal to or greater than zero, depending on the intensity of entrainment, true flotation and dropback of material. So in situations where there is high entrainment, froth flow number (R_{fn}) value cannot be compared to the froth recovery parameter (R_f) as defined by equations [2.7 and 2.8]. The froth recovery number gives an indication of how true flotation is comparable to entrainment and can assume any value greater than, equal to or less than one.

6.5. Using bubble loads to interpret flotation performance

6.5.1 Bubble load rate

The results of the second testing of the bubble load meter on the primary cleaner cell are summarized in Table 6.4. The experiment was run for about 10minutes with strict monitoring of pressure drop across the filter, a bubble load of 10.45g/litre was obtained and froth recovery parameter was 0.69. While the low bubble load value was attributed to the difficulty in floating PGMs, the froth recovery parameter seems more sensible and it indicates that particles were draining from the froth phase back to the pulp phase. A dry sample mass of 35.58 grams was obtained, lower than the set target of 200grams. This lower than target mass was attributed to a number of factors including the fact that this sample was taken using 20mm ID pipe which means fewer bubbles were sampled per unit cross sectional area of riser. If it is assumed that the bubble load is constant at the point of measurement, i.e. steady state operation then it would require 56 minutes and a 50 litre collection chamber to get 200grams of sample. Sampling time can be reduced by using a riser with larger ID. This sample was taken using the 20mm riser, switching to the 30mm riser would reduce the sampling time by a factor of 2.25. Sampling times in the magnitude of one hour results in filter paper blinding, filter paper breakage and lower water recirculation rate which compromises the bubble load quality.

Table 6.3: Primary cleaner cell results

Time(sec)	Air volume (cm^3)	Jg(cm/s)	Mass(g)	Bubble load(g\l)	Conc loading(g/l)	Rf
592.00	3404.00	0.81	35.58	10.45	2.46	0.24

6.5.2 Comparison of variation of grade in the bubble load, concentrate and pulp

The variation of mineral content in the bubble load and concentrate can help understand the phenomenon that takes place in the pulp phase as well as the froth phase. Figure 6.6b is a plot of percentage sulphur content against particle size in bubble load, concentrate and pulp samples respectively. Its main purpose is to demonstrate the differences in grade in these samples. It shows that the percentage of sulphur increases with the particles sizes in each of the three respective samples; the bubble load has higher sulphur content for all size classes while the pulp has the lowest. This trend is also seen for Cu and Ni, Figure 6.6a and Figure 6.6c

It is interesting to note that the bubble load has higher grade of the floatable species for all size classes, indicating the upgrading and selective nature of flotation process. The decrease in concentrate grade is attributed to entrainment of gangue.

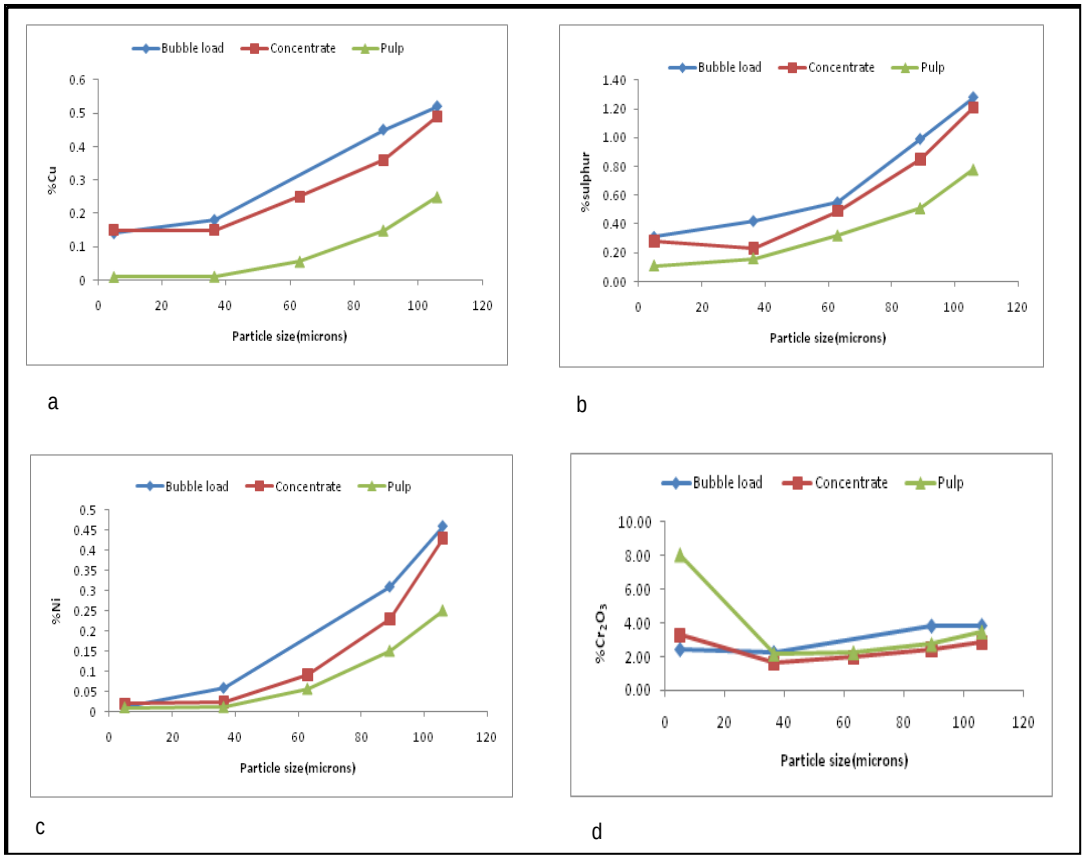

Figure 6.6 Variation of (a) %Cu (b) %Sulphide (c) %Ni (d) %Cr_2O_3 with particle size in bubble load, concentrate and pulp samples.

6.5.3 Estimation of entrainment

Since this analysis is a demonstration of how bubble load data can be used to estimate entrainment in PGM flotation, primary focus will be on chromite since it is when fully liberated and in the absence of activation it is non floatable.

Preliminary conclusions in the rougher cell had indicated that entrainment was high due to the fine grind (55% less than 25µm); a method to estimate entrainment on the primary cleaner cell was devised. Chromite (Cr_2O_3) was used as partially floatable gangue. Figure 6.6d shows the variation of %Cr_2O_3 with particle size in the bubble load, pulp and concentrate. It is interesting to note the presence of significant amounts of Cr_2O_3 in the bubble load (3.83% in +106µm and 3.80% in (-75+53µm) indicating that Cr_2O_3 was reporting to the concentrate not only by entrainment but also by true flotation. In the absence of activation, chromite an oxide is generally

considered naturally hydrophilic; it can be activated when it adsorbs copper in the form of Cu $(OH)^{+}$ at pH 9 (Wesseldijk et al., 1999), or can be recovered owing to locking to the other minerals. Copper sulphate has been identified as one reagent that results in chromite activation when it is used as an activator in PGM flotation (Ekmekci et al., 2003).

The recovery of chromite by true flotation implies that chromite can no longer be considered as a completely non floatable gangue in the estimation of entrainment. It brings forward the fact that chromite recovery to the concentrate is a combination of both true flotation and entrainment. The following section presents the results and procedure to estimate entrainment using bubble load data.

1. Calculation of chromite flowrates in bubble load, tailings and feed streams

The total mass of chromite in the feed and in each size class was calculated using mass balance method after assuming that the concentration of particles in each size class in the pulp is similar to that in the tailings. The rate at which particles are transferred from the pulp phase to the froth phase i.e. true flotation rate was calculated from the bubble load and superficial gas velocity and the cross sectional area of the flotation cell. Inherent in this calculation is the assumption that superficial gas velocity (J_g) was uniform across the flotation cell. Table 6.5 shows the mass flowrate in each size class and chromite content in each size class in the bubble load, feed, tailings and concentrate streams. These flowrates were obtained from mass balances and the chromite content of each stream that was sampled. From Table 6.5, 3.3% (41.35g/s) of the total chromite in the feed is reporting to the concentrate, 5.34% (66.03 g/s) is attaching to bubbles and 96.65% (1195.89g/s) of the original chromite in the feed is reporting to the tailings and 2.4% of the total concentrate flow is chromite. In the absence of activation the floatable chromite (on the bubble load) is taken as the ‘locked’ chromite, and the non floatable chromite (gangue) is the fully liberated chromite.

Table 6.5: Mass distribution of chromite in the feed, bubble load, concentrate and tailings

Feed flowrate			24750.97	g/s	
Size class	**Geo mean particle size**	Mass % in Size Class	Mass flowrate in Size Class (g/s)	**%Cr_2O_3 in Size Class**	Mass flowrate Cr_2O_3 in Size class (g/s)
-150 + 106	126	6.59	1632.28	3.40	55.47
-106 +75	89	10.01	2477.76	2.71	67.11
-53 + 25	36	35.78	8856.28	2.14	189.49
-25	13	47.61	11784.65	7.85	925.18
Total		**100.00**	**24750.97**		**1237.25**

Concentrate flowrate			1703.75	g/s	
Size class	**Geo mean particle size**	Mass % in Size Class	Mass flowrate in Size Class (g/s)	**%Cr_2O_3 in Size Class**	Mass flowrate Cr_2O_3 in Size class (g/s)
-150 + 106	126	13.51	230.10	2.84	6.53
-106 +75	89	19.38	330.16	2.44	8.06
-53 + 25	36	38.21	651.06	1.63	10.61
-25	13	28.90	492.43	3.28	16.15
Total		**100.00**	**1703.75**		**41.35**

Tailings flowrate			23047.22	g/s	
Size class	**Geo mean particle size**	Mass % in Size Class	Mass flowrate in Size Class (g/s)	**%Cr_2O_3 in Size Class**	Mass flowrate Cr_2O_3 in Size class (g/s)
-150 + 106	126	6.08	1402.18	3.49	48.94
-106 +75	89	9.32	2147.60	2.75	59.06
-53 + 25	36	35.60	8205.22	2.18	178.87
-25	13	49.00	11292.22	8.05	909.02
Total		**100.00**	**23047.22**		**1195.89**

Bubble load rate		2484.48	g/s		
Size class	**Geo mean particle size**	Mass % in Size Class	Mass flowrate in Size Class (g/s)	**%Cr_2O_3 in Size Class**	Mass flowrate Cr_2O_3 in Size class (g/s)
-150 + 106	106	10.04	249.44	3.83	9.55
-106 +75	89	13.27	329.75	3.8	12.53
-53 + 25	36	56.97	1415.52	2.26	31.99
-25	13	19.72	489.88	2.44	11.95
Total		**100.00**	2484.60		**66.03**

2. Comparison of bubble load and concentrate Chromite compositions per size class

Taking a basis of one second, it is seen from Table 6.6 that the mass flowrate of chromite in each size class in the bubble load is higher than in the concentrate for all size classes except for the -25µm size class where 35% more chromite reported to the concentrate. If drop back for true flotation is defined as the fraction of the chromite that was collected by true flotation that does not report to the concentrate and if it is assumed that

1) The chromite particles that are recovered by true flotation have a higher chance of reporting to the concentrate than entrained chromite particles for each size class i.e. entrained chromite (gangue) particles will drain back to the pulp phase
2) Drop back for true flotation is the difference between bubble load per size class and the mass of chromite per size class in concentrate
3) If the mass of chromite in the concentrate is higher than the mass of chromite in the bubble load per size class the difference is taken as the amount of entrained chromite particles

then Table 6.6 shows that the percentage of drop back increases with increase in particle size i.e. from 31.60% for the -25 µm up to 66.83% for (-53+25) µm. This increase in drop back can be explained by acknowledging that the degree of 'locking' of the chromite would decrease with particle size, meaning that smaller particles have a higher degree of Cr_2O_3 liberation (see Figure 6.4d variation of the $\%Cr_2O_3$). Minerals with a high grade of Cr_2O_3 are more likely to be less hydrophobic and thus less floatable. These less floatable particles are weakly attached to bubbles and are easily rejected in the froth phase. This phenomenon seems to counteract the effect of particle settling velocity, finer particles have inferior settling velocities than coarser particles of the same mineral, thus it was expected that the drop back would increase with particle sizes. This observation may mean that the froth phase is selective towards the more hydrophobic particles, in this case the floatable mineral with a low degree of liberation of chromite particles.

The negative value for -25 µm size class indicates a parallel phenomenon that is also adding particles of chromite in this size class to the froth phase and hence the concentrate. Table 6.8 shows an extra 35.13% of the -25 µm particles that is reporting to the concentrate by a phenomenon which is not true flotation. The negative 4.20grams/sec mass flowrate implies that particles are being added to the froth phase instead of dropping back to the pulp phase. If this

contribution is termed entrainment, then this observation is in tandem with the generally accepted view that entrainment or degree of entrainment increases with decrease in particle sizes i.e. (Zheng et al., 2006; Savassi et al., 1998).

Table 6.6: Comparison of the chromite content of bubble load and concentrate

Size class	Geo mean particle size	Mass flowrate Cr2O3 in Size class (g/s) in concentrate	Mass flowrate Cr2O3 in Size class (g/s) in bubble load	Drop back rate of Cr2O3 in Size class (g/s)	%Drop back rate of Cr2O3 per Size class
-150 + 106	126	6.53	9.55	3.02	31.60
-106 +75	89	8.06	12.53	4.47	35.71
-53 + 25	36	10.61	31.99	21.38	66.83
-25	**13**	**16.15**	**11.95**	**-4.20**	**-35.13**
Total		**41.35**	**66.03**		

3. Calculation of chromite froth recovery per size class

Froth recovery is an important parameter in analysing the phenomenon that takes place in the froth phase. Its calculation can help in the optimisation of the flotation process. Table 6.7 shows how chromite froth recovery to the concentrate varies with particle size. It is important to note that chromite recovery for -25µm size class is greater than 1 i.e. 1.35, while the overall froth recovery parameter is 0.69, see Table 6.2. It is also interesting to note the general decrease of the froth recovery parameter with decrease in particle size. This observation suggests that the froth in this primary cleaner cell is selective; it rejects the less hydrophobic particles which in this case are represented by the nearly fully liberated chromite (fine particle sizes). Another interesting observation is the froth recovery parameter of the -25µm particles which is greater than 1. This observation raises the point that though chromite might be reporting to the concentrate by true flotation, entrainment in -25µm size class is very high such that it cannot be assumed to be negligible. A R_{fn} greater than 1 was also noticed in the overall froth recovery for experiments done on the first primary rougher cell (Table 6.1), suggesting that entrainment might have been very high also.

Table 6.7: Results of the chromite froth recovery per size class calculation

Size class	Geo mean particle size	Mass flowrate Cr2O3 in Size class (g/s) in concentrate	Mass flowrate Cr2O3 in Size class (g/s) in bubble load	Froth recovery for each chromite size class
-150 + 106	126	6.53	9.55	0.68
-106 +75	89	8.06	12.53	0.64
-53 + 25	36	10.61	31.99	0.33
-25	**13**	**16.15**	**11.95**	1.35
Total		**41.35**	**66.03**	0.63

4. Estimation of entrainment and degree of entrainment

The degree of entrainment is essentially a classification function and is defined herein by equation [6.2] below

$$ENT_i = \frac{mass\ of\ free\ gangue\ particles\ of\ the\ ith\ size\ class\ per\ unit\ of\ water\ in\ the\ concentrate}{mass\ of\ free\ gaunge\ of\ the\ ith\ size\ class\ per\ unit\ of\ water\ in\ the\ pulp}$$

[6.2]

To estimate entrainment or fit an entrainment model, it is essential to know the amount of gangue material in both the pulp and the concentrate. The amount of gangue material (entrainable chromite) in the feed is the difference between the total chromite in the feed and the amount of floatable chromite in the feed. Since the chromite in the concentrate is a sum of floatable and entrainable chromite, the total recovery of chromite is also a sum of the entrainable/non floatable (fully liberated) and floatable (locked/activated) chromite.

Estimation of floatable chromite in the feed

To correctly model or estimate entrainment, liberation data is essential, in the absence of the liberation data then artificial non floatable material/tracer has been used to get model parameters (Savassi et al., 1998). In the absence of both liberation data and non floatable tracer information then bubble load information, with certain assumptions can be used to estimate the flowrate of non floatable particles per size class in the feed. Yianatos et al. (2010) used bubble load information with some assumptions to estimate the degree of entrainment in an industrial

flotation cell. To estimate the gangue flowrate in the feed it was essential that they assume that the valuable species of the floatable mineral in the feed has the same grade as the floatable mineral in the bubble load. The authors acknowledged that this assumption is not strictly valid because some of the valuable mineral in the feed is non floatable. They however went on to state that since the recovery of valuable mineral is usually higher than 90%, then the error that results from this assumption when estimating the flowrate of gangue in the feed is minimal i.e. 3-5% for coarser particles size classes and less than 1% for the finer classes.

In this case where there is no liberation information of the ore as well as non floatable tracer information, it became imperative that we use bubble load information in conjunction with assumptions to estimate the flowrate of gangue in the feed per size class. The following set of assumptions were made

1. Floatable mineral locked to chromite has the same Cr_2O_3 grade per size class in the feed as the Cr_2O_3 grade of the floatable mineral on the bubble load.
2. Assume a minimum collection zone recovery by true flotation (bubble load) of 90% per each size class of the floatable mineral on which chromite is locked.

These assumptions are not strictly valid as was noted by Yianatos et al. (2010), because of non floatability of some of floatable mineral where chromite might be locked and also the realisation that the collection zone recovery by true flotation (bubble load) of finer size classes might be less than 90% as a result of the increase in chromite liberation with decrease in particle sizes. Table 6.8 shows the flowrates of floatable (locked) chromite per size class. Notable is the decrease in chromite floatability for particles less than 53 µm, see Figure 6.7

Table 6.8: Mass of floatable chromite in each size class in the feed

Size class	**Geo mean particle size**	Mass flowrate Cr_2O_3 in Size class (gram/s) in bubble load	Mass flowrate floatble Cr_2O_3 in Size class (gram/s) in feed	%floatable chromite per size class in the feed
-150 + 106	126	9.55	10.62	19.14
-106 +75	89	12.53	13.92	20.74
-53 + 25	36	31.99	35.55	18.76
-25	**13**	**11.95**	13.28	1.44
Total		**66.03**	73.36	5.93

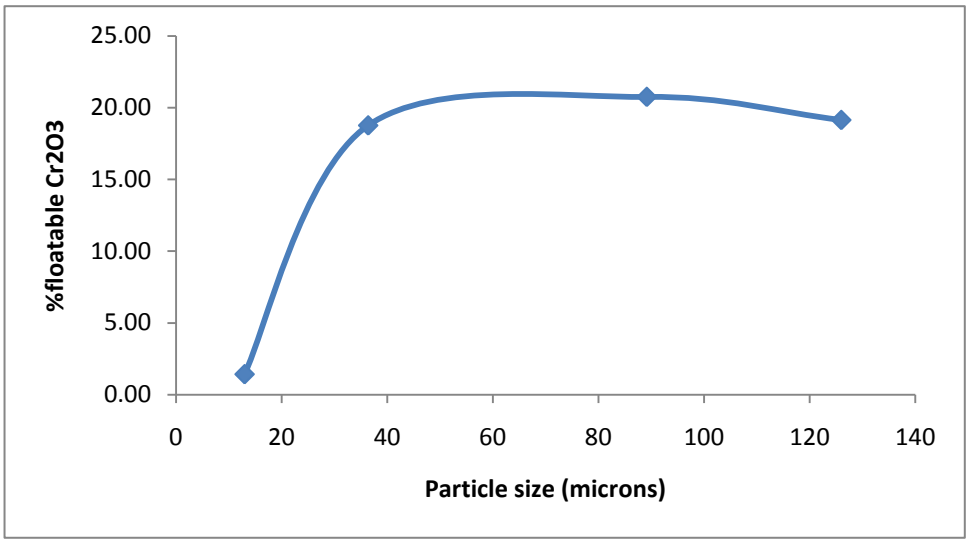

Figure 6.7: Variation of the estimated percentage floatable chromite with particle size

Estimation of non floatable chromite in the feed

From the estimate of floatable chromite, the mass of non floatable chromite can also be calculated; Table 6.9 shows the flowrate of non floatable chromite per each size class, it is noteworthy that 94% (1163.88grams) of the total chromite in the feed is non floatable.

Table 6.9: Flowrates of non floatable chromite per size class in the feed

Size class	**Geo mean particle size**	Mass flowrate Cr2O3 in Size class (g/s) in feed	Mass flowrate floatble Cr2O3 in Size class (g/s) in feed	Mass flowrate non-floatble Cr2O3 in Size class (g/s) in feed
-150 + 106	126	55.47	10.62	44.86
-106 +75	89	67.11	13.92	53.19
-53 + 25	36	189.49	35.55	153.94
-25	**13**	**925.18**	13.28	911.89
Total		**1237.25**	73.36	1163.88

Calculation of the entrainment recovered and true flotation recovered components of the concentrate

From Table 6.6 it appears as if entrainment is negligible for the +25 µm particles, and all the Cr_2O_3 that reports to the concentrate is from true flotation.(*bubble load rate greater than concentrate flowrate per size class*) This may be true for all the +75 µm particles but not for

(+25-53) µm size class. Several researchers (e.g. Yianatos et al., 2009 and Warren and Smith, 1989) have agreed that entrainment is significant for particles sizes less than 50 µm and less so for particles larger than this.

This section presents results of the estimated flowrate of gangue material in concentrate per size class. The calculation of these flowrates is based on the entrainment model presented by Yianatos et al. (2010) equation [3.6]. To use this model a drainage parameter (ϕ) of 0.97 as proposed by Yianatos for industrial scale flotation was used, since the calculated water recovery (R_w) in this primary cleaner cell was 2.15% the corresponding δ parameter of 10 µm, was interpolated from Figure 6.8. Results are shown in Table 6.10. The results confirm that indeed above 53 µm entrainment is negligible i.e. the flowrate of gangue (non floatable chromite) is zero for the +106 and (+75 -106) µm particles sizes. The gangue flowrate is significant in the -25 µm class, it constitute 53.1% (8.57g/s) of the chromite flowrate in concentrate in this size class (16.15g/s) and 21.45% of the total Cr_2O_3 flowrate per second. This entrained chromite in the -25 µm class also represents 0.5% of the total concentrate flow i.e. total concentrate flow is 1703.75g/s. Figure 6.9a also shows the variation of gangue recovery R_G with particle size while Figure 6.9b shows the gangue flowrate per size class in the concentrate

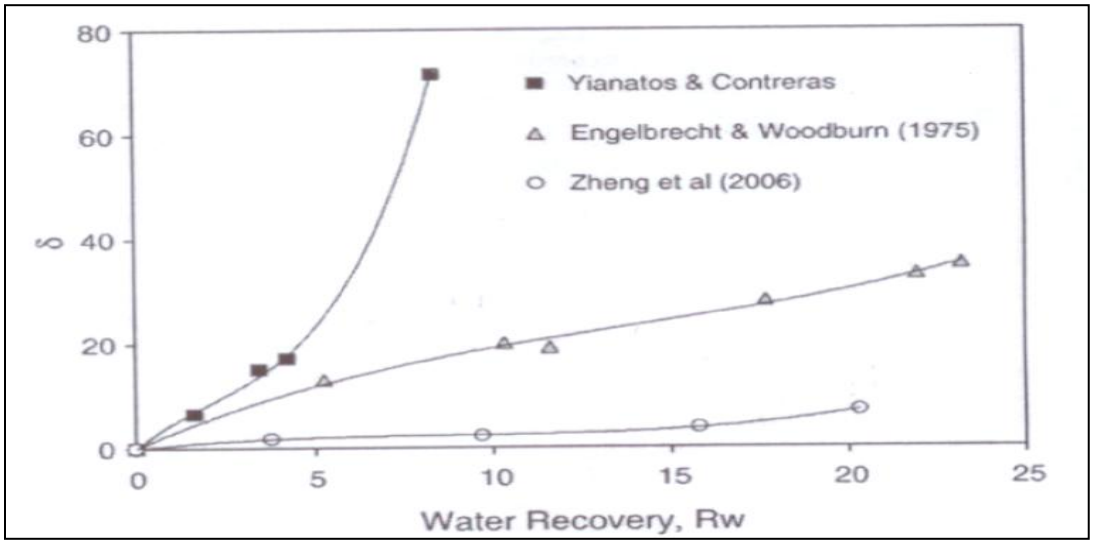

Figure 6.8: Correlation between parameter and water recovery in flotation cells adapted from Yianatos et al. (2010)

Table 6.10a: Model results: Estimation of the floatable and non floatable Cr_2O_3 components of the concentrate

Size class	Geo mean particle size	Entrainment factor EF	Water recovery R_w	%Gangue recovery per size class	Mass flowrate non-floatble Cr2O3 in Size class (g/s) in feed	Mass flowrate non-floatble Cr2O3 in Size class (g/s) in concentrate
-150 + 106	126	0.00	0.0215	0.00	44.86	0.00
-106 +75	89	0.00	0.0215	0.00	53.19	0.00
-53 + 25	36	0.09	0.0215	0.00	153.94	0.29
-25	**13**	0.44	0.0215	0.01	911.89	8.57
Total						8.87

Table 6.10b: Floatable and non floatable Cr_2O_3 components of the concentrate

Size class	Geo mean particle size	Mass flowrate Cr2O3 in Size class (gram/s)	Mass flowrate non-floatble Cr_2O_3 in Size class (gram/s) in concentrate	Mass flowrate floatble Cr_2O_3 in Size class (gram/s) in concentrate
-150 + 106	126	6.53	0.00	6.53
-106 +75	89	8.06	0.00	8.05
-53 + 25	36	10.61	0.29	10.32
-25	**13**	16.15	8.57	7.58
Total		**41.35**	**8.87**	**32.48**

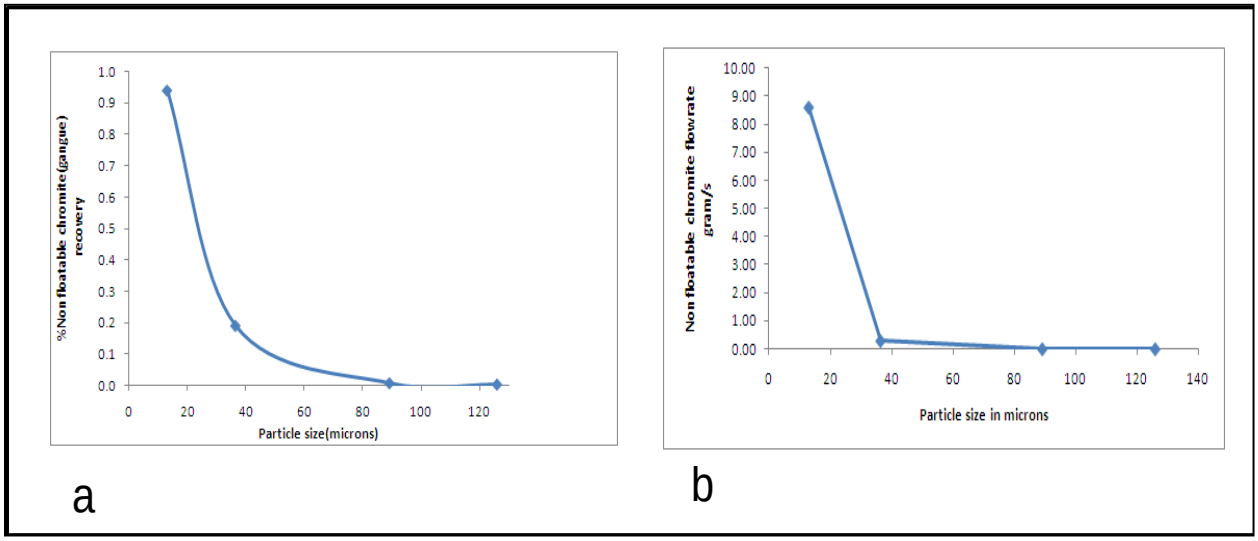

Figure 6.9(a) Gangue (non floatable Cr_2O_3) recovery versus particle size (b) flowrate of the non floatable chromite in the concentrate per size class.

Recalculation of froth recovery per size class using entrainment model results

The froth recovery parameters for chromite per size class that were calculated prior to the use of the Yianatos et al.(2010) entrainment model assumed negligible entrainment. These froth

recovery parameters (Table 6.1) and the froth recovery per size class for the -25 µm (Table 6.7) gave a froth recovery greater than 1. It was proposed that this occurred as a result of high entrainment. This section compares the results of the chromite froth recovery parameter per size class for a situation where

(a) Entrainment is assumed negligible and

(b) Where its contribution to the overall concentrate flow is taken in to account, in this case the Yianatos et al., (2010) entrainment model was applied.

Table 6.11 shows the results. It is interesting to realise that entrainment results in a significant change in the froth recovery parameter of the -25 µm size class i.e. from the unexpected 1.35 to the more sensible 0.63. A small change is observed for the -53+25 µm size class while there is virtually no change for the coarser size classes i.e. +75 µm confirming that entrainment is not significant in coarser size classes. This result is important in that it validates the assumption that where there is a finer grind, entrainment is high such that it cannot be assumed negligible.

Table 6.11: Comparison of froth recovery parameter: negligible entrainment versus non negligible entrainment

Size class	Geo mean particle size	Froth recovery parameter(entrainment negligible)	Froth recovery parameter(entrained particles removed)
-150 + 106	126	0.68	0.68
-106 +75	89	0.64	0.64
-53 + 25	36	0.33	0.32
-25	**13**	1.35	0.63

6.6 Discussion on the use of bubble loads to estimate entrainment

The use of bubble load information to evaluate entrainment in the flotation process is important. Parameters for the existing entrainment models can be obtained without ore liberation data or non-floatable tracer information. Bubble load gives the composition of the mineral that is reporting to the froth phase, by measuring the froth phase particle composition the process that happens to these minerals in the froth phase can be evaluated enhancing froth phase understanding. The amount of non floatable gangue that is locked to the floatable mineral that is

reporting to the concentrate is evaluated from an analysis of the bubble load. Consequently the amount of gangue that is reporting to the concentrate can be calculated since bubble load information provides the true flotation rate. As far as the author can ascertain, Yianatos et al. (2010) were the first researchers to use bubble load information to estimate entrainment. They developed a simple model to estimate entrainment factor, this model was used in this thesis to calculate gangue recovery through its relationship to water recovery and consequently the flowrate of gangue material in the concentrate.

To use bubble load data to calculate entrainment, several measurements are needed. The need for some of these measurements was only realised after the experimental runs. The following section gives some of the information that is required to facilitate a more accurate entrainment estimation procedure using bubble load data. In addition, assumptions that were made to facilitate the calculations and to use the entrainment model in this thesis are also discussed.

6.6.1 Assumptions on grade and floatable mineral recovery

The calculation of gangue recovery requires the knowledge of both the flowrate of gangue in the feed and concentrate. These flowrates per size class are usually obtained from the liberation data of the ore being floated or using non-floatable tracers. With this information gangue recovery and water recovery are calculated and hence the entrainment factor is evaluated. Notwithstanding the importance of these measurements, entrainment can still be estimated by making a set of assumptions on the recovery of floatable minerals then use this recovery to estimate the amount of floatable mineral in feed. The downside of the assumptions that were made in the calculation is that though recoveries of floatable minerals were generally above 90% for Yianatos et.al., (2010) it needs to be ascertained per size class in PGM flotation, especially in this situation where a non floatable mineral is locked to the floatable mineral and there is a high chance of it being liberated with decrease in particle sizes. This may mean a decrease in the hydrophobicity and hence recoveries of less than 90% for finer size classes are possible.

6.6.2 Calculation of the floatable and gangue flowrates of the feed

To use the Yianatos et al. (2010) entrainment model it was essential that the gangue flowrates of both the feed and concentrate be known. This implies that the liberation data of the ore should be known. Where this liberation data was unknown as in this analysis it became imperative that assumptions on grade and recovery of the floatable mineral where chromite is locked be made (*see section 6.5.3: estimation of chromite flowrate in the feed*). These assumptions enabled the calculation of the flowrate of floatable mineral in the feed and hence the flowrate of the gangue was calculated by mass balance. Knowing the gangue recovery and the water recovery plus the flowrate of gangue material in the feed, the entrainment factor EF_i from the entrainment model was calculated. The gangue flowrate per size class in the concentrate was then evaluated.

6.6.3 Model parameters

The Yianatos et al. (2010) model contains two very important parameters viz. The drainage parameter (ϕ) and the parameter δ, which is the particle size that corresponds to an entrainment factor EF_i of 0.5. Instead of using a drainage parameter of 0.97, its measurement and the determination of δ is needed. The use of the values from Yianatos et al. (2010) is questionable since the drainage parameter is a function of the froth properties such as the froth height, froth stability etc. The copper flotation environment where Yianatos et al. (2010) carried out their measurements is different from PGM flotation environment where the measurements in this thesis were done.

The use of bubble loads to estimate entrainment has been demonstrated, the results before and after applying the entrainment model agree that in the larger particles sizes +75 µm entrainment is negligible and its very significant in the -25 µm size class.

Chapter 7

Conclusions and Recommendations

7.1 Conclusions

7.1.2 Bubble load meter: design aspects

The main focus of this study was to develop a bubble load measuring device that is industrially applicable and can give a sample mass in excess of 200grams. The design of the bubble load meter focused much on the optimisation of the sampling part (riser) of the bubble load meter. Experiments to test for particle drop off, rejection of suspended particles, flow regime identification were done.

A bubble load meter based on the positive displacement principle was successfully designed. It was designed with riser diameters 20, 30 and 50mm. It was concluded that the 20 and 30mm riser are adequate as risers for the bubble load meter. For optimum operation the 30mm was chosen as the best riser diameter among the tested riser diameters. The 50mm riser recorded 0.1% of the original NaCl added to flotation cell, implying that under normal operation suspended particles may be recorded as bubble load. Conductivity experiments proved that axial mixing increase with increase in riser diameter. The concentration of NaCl was found to decrease with increase in height for a particular riser diameter. It was proposed that this change in NaCl concentration (inter-bubble liquid) was adequately described by the empirical equation [6.1]. Based on the empirical equation, it was suggested that with an adequate riser height, the 50mm riser could still be used. The axial mixing model output results also show a small difference between the average axial mixing parameter (k) of the 30 and 50mm risers .i.e. 0.83 and 0.84 respectively. It was suggested that the difference in NaCl concentration recorded by the two risers at conductivity probe 3 was amplified by the bubble swarm effect and salt adsorbed on bubble lamella, which seemed to be more intense for the 50mm riser. The big difference between the α -parameter in the axial mixing model for the 30 and 50mm risers (*average of 0.81 and 0.94*

for the 30 and 50mm risers respectively) confirms this assertion. Further work on the 50mm riser is needed. Flexible baffling was tested and because of the thickness of the baffle, results obtained were not satisfactory in fact it worsened the intensity of the axial mixing as circulation due to difference in pressure commenced.

The conductivity results also revealed an increase in NaCl concentration with decrease in frother concentration for all the risers. It was noted that increasing frother concentration (decreasing bubble sizes) resulted in a general increase in the amount of NaCl recorded by each conductivity probe. The number of bubble aggregates sampled per unit time per given cross sectional area was found to influence salt transport i.e. decreasing riser diameter for a given frother concentration resulted in decrease in NaCl concentration recorded by each conductivity probe. This led to the conclusion that salt transport up the column is a combination of axial mixing and NaCl adsorbed on bubble lamella (*decrease in bubble size increase the surface area per given volume of air sampled.*). The output response from the axial mixing modelling also confirmed the bubble swarm and salt adsorbed on bubble lamella theory, comparison of results of a model without the α -parameter, and the response of a model with this parameter have shown that the model without this parameter tend to under predict the salt transport whereas the one with this parameter produced a reasonable fit.

The 30mm bubble load riser was also tested for particle drop-off; no particles were dropping off in this riser.

7.2 Industrial application

Two separate industrial campaigns were done on the first primary rougher and cleaner cell, bubble load masses were lower than the target mass of 200grams. The maximum sample mass obtained was 35.58gramms with a bubble load value of 10.58grams/litre. It was obtained on the first primary cleaner cell with the 20mm ID riser. Froth recovery of 0.69 was obtained on the primary cleaner cell while a froth flow number of 1.55 was obtained for primary rougher cell. The primary rougher cell's froth flow number was attributed to high entrainment gangue. The primary cleaner cell result was more meaningful, though an analysis of the froth recovery on each particle size class revealed that the froth recovery parameter of the -25µm size class was

1.5, which is greater than 1. It was suggested that this was because entrainment was very high in the -25µm size class.

An important aspect that seems to be absent in bubble load measuring literature is the possibility of loss of particles with the recycle water in bubble load measuring devices that use the positive displacement approach. This may be more pronounced when these devices are used to take measurements in flotation environments with a combination of brittle froth and fine particle sizes. Brittle froths allow particles to detach from bubbles in the collection chamber. The detached fine particles have a tendency to follow water stream lines, these fine particles are lost if a means to capture them is not provided. Pictures of loaded filter (*in chapter 6*) show that indeed particles do follow these water streamlines.

It was also demonstrated that bubble load data can be used to evaluate flotation kinetics especially entrainment. Bubble load data was used to estimate entrainment; it was found that in the primary cleaner cell, the entrainment of chromite was very low. The entrained chromite constituted 0.5% of the total concentrate flowrate and is made up of the -25 µm size class. It was 21.45% of the total chromite flowrate in the concentrate. Interestingly, there seemed to be a high degree of chromite floatability in this environment, and the floatability increased with increase in particle sizes. Chromite floatability was attributed to locking to the PGMs and the sulphides.

7.3 Axial mixing model

An axial mixing model to quantify the intensity of axial mixing was developed. The model is based on a tanks-in-series model. Parameter estimation was done using Simulink, a simulation toolbox in Matlab, results show that the developed model fits experimental data reasonably well when an additional parameter α is added. A k-value of 0.83 was obtained for 50mm riser while mean k-values for MIBC concentration range of 5ppm to 20ppm for the 30mm and 20mm riser are 0.83 and 0.76 respectively.

7.4 Recommendations

Measurement of particle loading on bubbles is very important as it helps to understand the processes that take place in the froth phase as well as the sub-processes that take place in the

pulp phase. The primary focus of this study was to develop a bubble load meter that can get in excess of 200grams PGM sample. This could not be achieved within the tenure of the study. A maximum mass of 35.58grams was obtained with the 20mm riser. Increasing the riser diameter of the bubble load meter to 50mm with a corresponding increase in length (*determined by the axial mixing model*) is recommended as one way of increasing the sample mass. The use of a wire coil to reduce axial mixing and mechanical push in the 50mm riser needs to be explored further. Figure 4.17b is a general presentation of this idea.

Though industrial tests were successfully done, there are certain aspects of the bubble load meter that needs further attention, these includes making the equipment less cumbersome by eliminating the water rotameter, peristaltic pump and the surge tank and replacing them with a variable speed centrifugal pump and orifice meter for measuring flowrate. A redesign of the filter to reduce filter paper breakage and to increase sampling time is needed.

The number of measurements on the primary cleaner cell was limited to 1 as a result of difficulties in getting clean water for the bubble load meter. An easy way of loading water and removing the particles, if designed can reduce the loading and unloading times significantly.

Bubble load information can be quite effective in evaluating entrainment in industrial flotation machines without resorting to the use of non-floatable tracer material. A demonstration of how this data is used to estimate entrainment is presented in this thesis (chapter 6). What is notable though is that there are certain measurements that should be done/ should have been done to validate the associated assumptions. These measurements include, mineral liberation information, feed size and grade analysis, the recovery of the floatable mineral per size class and the chromite grade of the floatable mineral that is ‘locking’ the chromite in the feed. A thorough discussion of the measurements that need to be done and the limitations of assumptions made are given in section 6.6 in chapter 6.

References

Arbiter, N. and Harris, C.C., 1962. Flotation Kinetics. In Froth Flotation, ed. D.W. Fuerstenau. 50th Anniversary Volume, AIME., New York, pp. 215-246.

Alvaré, J., Al-Dahhan. M. H., 2006. Liquid phase mixing in trayed bubble column reactors.

Bassett, M. D., Winterbone D. E., and Pearson R. J., 2001. Calculation of steady flow pressure loss coefficients for pipe junctions. *Proc. Instn Mech. Engrs, Part C: J. Mechanical Engineering Science*, **215**, 861-881

Bradshaw, D., and O'Connor, C., 1996. Measurement of the sub-process of bubble loading in flotation. *Minerals Engineering* **9** (4): 443–448.

Cheng, T., Holtham, P., 1995. The particle detachment process in flotation. Minerals Engineering 8 (8), 883–891.

Dyer, C., 1995. An investigation into the properties of the froth phase in flotation process. Msc thesis. University of the Witwatersrand.

Ekmekci. Z., Bradshaw. D.J., Allison S.A., Harris. P.J., 2003. Effects of frother type and froth height on the flotation behaviour of chromite in UG2 ore. *Minerals Engineering.,* **16**: 941–949

Fairhurst. C. P.,1983. Component pressure loss during two-phase flow. *International Conference on the modelling of Multi-phase flow*. pp 1-24

Falutsu and Dobby, 1989. Direct measurement of froth drop back and collection zone recovery in a laboratory flotation column. Minerals Eng, 2(3): 377-386

Falutsu, M., and Dobby, G., 1992. Froth performance in commercial sized flotation columns. *Minerals Engineering.,* **5**: 1207– 1223.

Finch, J.A. and Dobby, G.S., 1990. Column Flotation, Chap. 3, Pergamon Press, Oxford.

Finch. J. A., Nasset. J.E., Accuña. C. 2008. Role of frother on bubble production and behaviour in flotation. *Minerals Engineering* **21:** 949-957

Harris, C.C., 1978. Multiphase models of flotation machines behavior. International Journal of Mineral Processing 5, 107–129.

Harris. T.A., 2000. The development of a Flotation Simulation Methodology Towards an Optimisation Study of UG2 Platinum Flotation Circuits. PhD Thesis. University of Cape Town.

King, R., Hatton, T., Hulbert, D., 1974. Bubble loading during flotation. Transactions of the Institute of Mining and Metallurgy. 83, C112–C115.

King, R.P., 2001. Modelling and Simulation of mineral Processing Systems, Butterworth-Heinemann, pp 290

Kirjavainen, V.M., 1996, Review and analysis of factors controlling the mechanical flotation of gangue minerals. Int. J. Miner. Process., 46: 21-34.

Klassen, V., Mokrousov, V., 1963. An Introduction to the Theory of Flotation. Butterworths, London (Chapter 5).

Laskowski, J.S., Tihone, T.,Williams and K. Ding, 2003. Fundamental properties of the polyoxypropylene alkyl ether flotation frothers, Int. J. Miner Process. **72** (2003), pp. 289–299

Leu. W.,1986. Principles of Compressible Cake Filtration, in Encyclopedia of Fluid Mechanics (N.P. Cheremisinoff, ed), Gulf.

Levenspiel, O., 1972. Chemical Reaction Engineering. second ed. Wiley,New York. pp 253

Maachar, A., Dobby, G.S., 1992. Measurement of feed water recovery and entrainment solids recovery in flotation columns, *Canadian Metallurgical Quarterly,* **31**:167-172

Mathe, Z.T., Harris, M.C. and O'Connor, C.T., 2000. A review of the methods to model the froth phase in non-steady state flotation systems. Minerals Engineering, Vol. 13, No. 2, pp. 127-140

Moys, M.H., 1978, A study of a plug flow model for flotation froth behaviour, *Int. J. Miner.Process.*, 5:221-238.

Moys, M.H., Engelbrecht, J.A., Terblanche, A.N., 1993. Design of baffles to reduce axial mixing in flotation folumns. CIM Bulletin, Vol.86, No.968, pp. 138-143.

Moys, M.H., Engelbrecht, J.A., Terblanche, A.N., 1995. Simulation of the behavior of flexible baffles in flotation columns. The Chemical Engineering journal **59**: 33-38.

Moys, M.H., Yianatos, J.B., Larenas, J., 2010. Measurement of particle loading on bubbles in the flotation process.

Neethling, S.J., Cilliers, J.J., 2002. The entrainment of gangue into a flotation froth. *Int. J. Miner. Process.* **64**: 123–134.

Randall, E.W., Goodall, C.M.,Fairlamb, P.M., Dold, P.L., and O'Connor, C.T., 1989. A method for measuring the sizes of bubbles in two- and three phase systems. *J. Phys. E: Sci. Instrum.*, **22**: 827

Ross, V.E. & Van Deventer, J.S.J.,1988, Mass transport in flotation Column froths, *Column Flotation '88. Proc. Inter. Symp. Column Flotation,* A.I.M.E

Ruzicka, M.C., Drahos, J., Fialova, M., and Thomas, N.H., 2001. Effect of column dimensions on flow regime transition. *Chemical Engineering Science.*, **56**: 6117-6124

Savassi, O., Alexander, D., Johnson, N., Franzidis, J.-P., Manlapig, E.V., 1997. Measurement of froth recovery of attached particles in industrial floatation cells. In: Lauder, D. (Ed.), Sixth Mill Operators' Conference. *Australian Institute of Mining and Metallurgy, Madang– Papua New Guinea,* pp. 149– 156.

Savassi, O.N., Alexander, D.J., Franzidis, J-P., Manlapig, E.V., 1998. An empirical model for entrainment in industrial flotation plants. Miner. Eng. **11** (3), 243–256.

Seaman, D. R , Franzidis, J-P. and Manlapig, E. V., 2004. Bubble load measurement in the pulp zone of industrial flotation machines—a new device for determining the froth recovery of attached particles. *Int J Miner Process.,* **74**(1): pp 1-13

Shaikh, A., Al-Dahhan, M.H., 2007. A review of Flow Regime Transiton in Bubble columns. *International Journal of Chemical Reactor Engineering* **5**, *Review R1*

Smith, P.G and Warren, L.J., 1989, Entrainment of particles into flotation froths, in Frothing in Flotation, *Gordon and Breach, New York,* 123-145

Taitel, Y., Bornea, D., Dukler, A. E., (1980). Modeling flow pattern transitions for steady upward gas-liquid flow in vertical tubes. *AIChE Journal*, **26**(3), 345-54.

Thorne, G. C., 1975. The behavior of lead/zinc ores in industrial flotation circuits with reference to simulation and control, PhD Thesis, University of Queensland.

van Deventer, J.S.J. / Feng, D. / Burger, A.J., 2001. The use of bubble loads to interpret transport phenomena at the pulp-froth interface in a flotation column *Chemical Engineering Science* **56** (1 and 2):6313-6319.

Vassallo. P., Keller. K., 2006. Two-phase frictional pressure drop multipliers for SUVA R-134a flowing in a rectangular duct. *International Journal of Multiphase Flow* **32**: 466-482

Vera, M.A., Franzidis, J.P., Manlapig, E.V., 1999. Simultaneous determination of collection zone rate constant and froth zone recovery in a mechanical flotation environment. *Minerals Engineering.*, **12** (10): 1163–1176.

Wesseldijk. Q.I., Reuter. M.A., Bradshaw. D.J., Harris, P.J.,1999. The flotation behaviour of chromite with respect to the beneficiation of UG2 ore. *Miner. Eng.*, **12** (10), 1177–1184.

Wills. B.A.,1992. Mineral Processing Technology. Fifth ed. pp 491

Yianatos, J.B., Finch, J.A. & Laplante, A.R., 1986,Apparent hindered settling in a gas-liquid-slurry counter-current column, *Int. J. Miner. Process.*, **18**:155-165.

Yianatos, J.B., Moys, M.H., Contreras, F., Villanueva, A., 20, A., 2008. Froth Recovery of industrial flotation cells. *Miner. Eng.*, **21**:817-827

Yianatos,J.B., Contreras. F., Díaz. F., Villanueva. A.,2009. Direct measurement of entrainment in large flotation cells, *Powder Technology* **189**: 42–47

Yianatos,J.B., Contreras. F., 2010. Particle entrainment model for industrial flotation cells, *Powder Technology* **197**: 260–267.

Zheng, X., Johnson, N.W., Franzidis, J.P., 2005. Modelling of entrainment in industrial flotation cells: the effect of solids suspension, *Miner. Eng.*, **18**: 51–58.

Zheng, X., Johnson, N.W., Franzidis, J.P., 2006. Modelling of entrainment in industrial flotation cells: water recovery and degree of entrainment. *Minerals Engineering.*, **19** (11),1191–1203.

Nomenclature

A_c flotation cell cross sectional area at the interface level (cm^2)

A_r Cross sectional area of the riser (cm^2)

B_L Bubble load (g/l)

C concentration of NaCl (mols/litre)

C overall concentrate mass flowrate (tph)

C_{cell} Concentration of NaCl in the flotation cell (mols/litre)

C_i (t) concentration of floatable mineral at time (sec)

C_o initial concentration of NaCl/suspended particles (grams/litre)

EF_i entrainment factor

ENT_i degree of entrainment in size class i

F overall feed mass flowrate (tph)

h height (cm)

H level below the pulp-froth interface (cm)

HHG high high grade concentrate

H_j height of the riser from the entry point to conductivity probe *j* .

J_{dwn} downward water velocity (cm/s)

J_G Superficial gas velocity (cm/s)

J_L superficial liquid velocity

J_{up} upward water velocity (cm/s)

k a constant

k_i is the first order rate constant for size class *i*

M_B mass flowrate of minerals entering the froth, as particle-bubble aggregate (true flotation), across the pulp/froth interface (tph)

M_C is the mass flowrate of floatable minerals recovered into the concentrate by true flotation (tph),

P_{abb} absolute pressure at which the measure volume was taken (kpa)

P_{atm} atmospheric pressure (kpa)

Q_m element of fluid

R_C is the collection zone recovery

R_f is the froth zone recovery.

R_G the overall flotation recovery.

R_W Water recovery

V flotation cell volume (cm^3)

V_g the measured volume of air (cm^3)

X_B bubble load grade

X_C mineral (or valuable species) grade in the concentrate

Subscripts

B bubble load

C concentrate

dwn flow downwards

F feed

G gangue

g gas

i size class

j conductivity probe number

L liquid

sl slurry

up flow upwards

W water

Greek letters

λ_B bubble load;

ΔL height difference between manometer inlets

Δh height difference between manometer levels

Δz height difference between two points in this section(cm)

ε_g gas hold up

ρ_w density of water.

ρ_{sl} density of slurry

ρ_f density of the froth.

Appendices

Appendix A Calibration curves

1. **50mm riser**

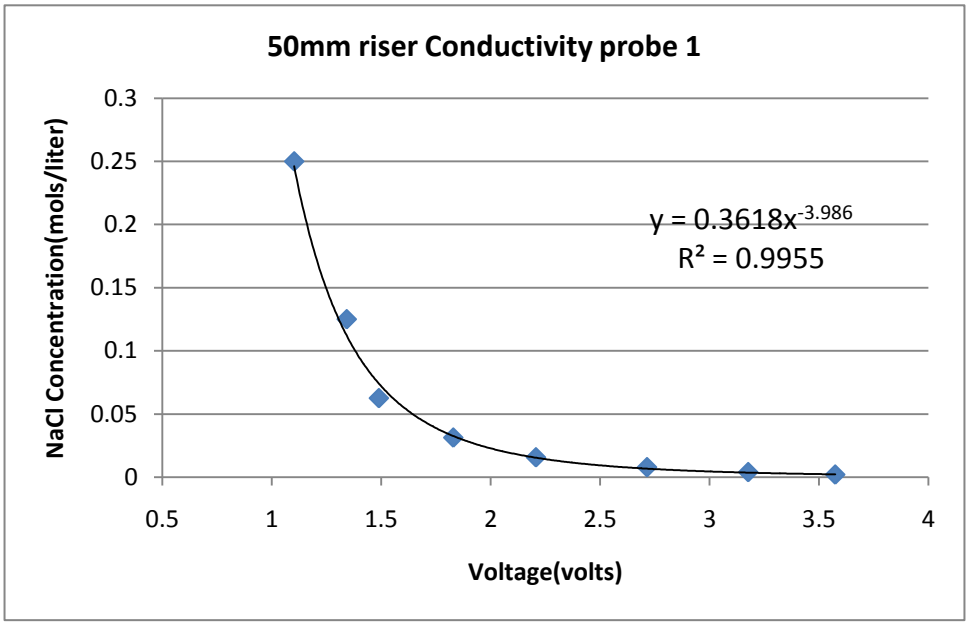

Figure A.1: 50mm riser calibration curve conductivity probe 1

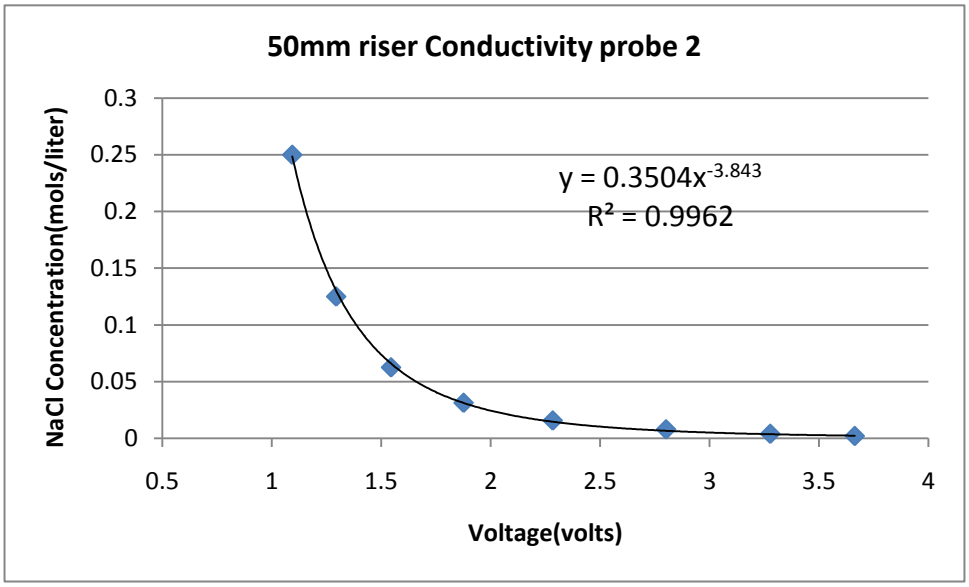

Figure A.2: 50mm riser calibration curve conductivity probe 2

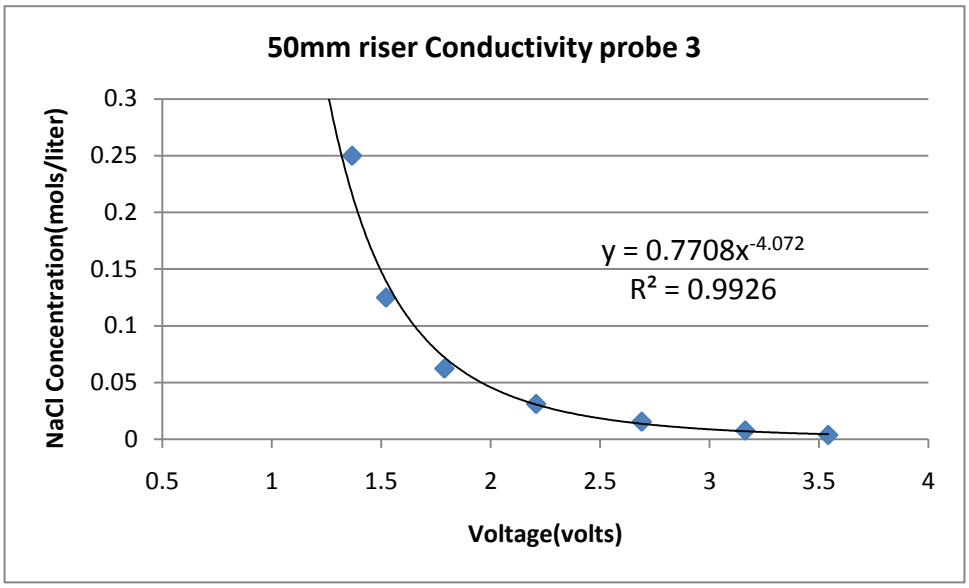

Figure A.3: 50mm riser calibration curve conductivity probe 3

2. 20mm riser

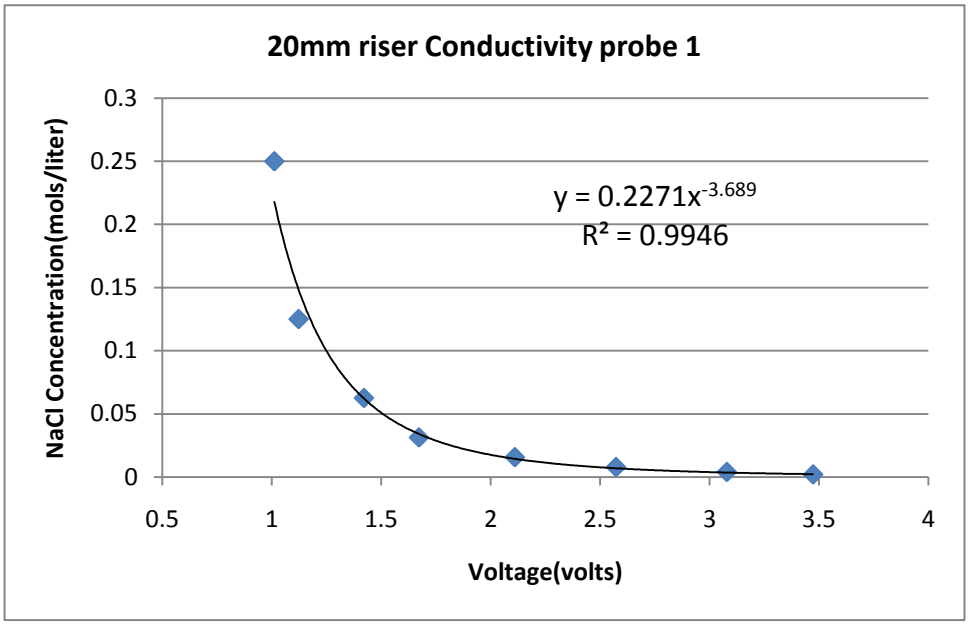

Figure A.4: 20mm riser calibration curve conductivity probe 1

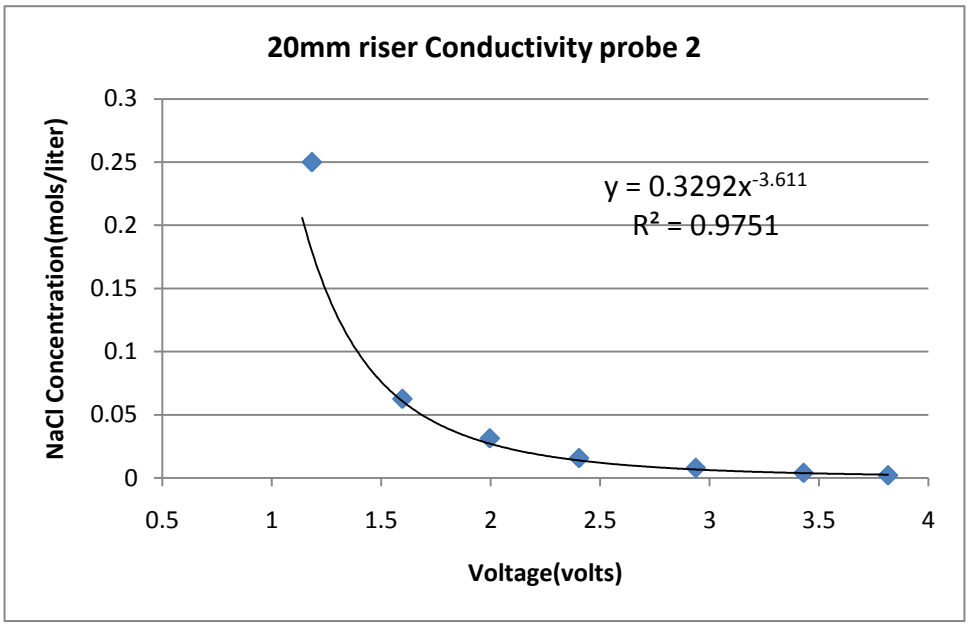

Figure A.5: 20mm riser calibration curve conductivity probe 2

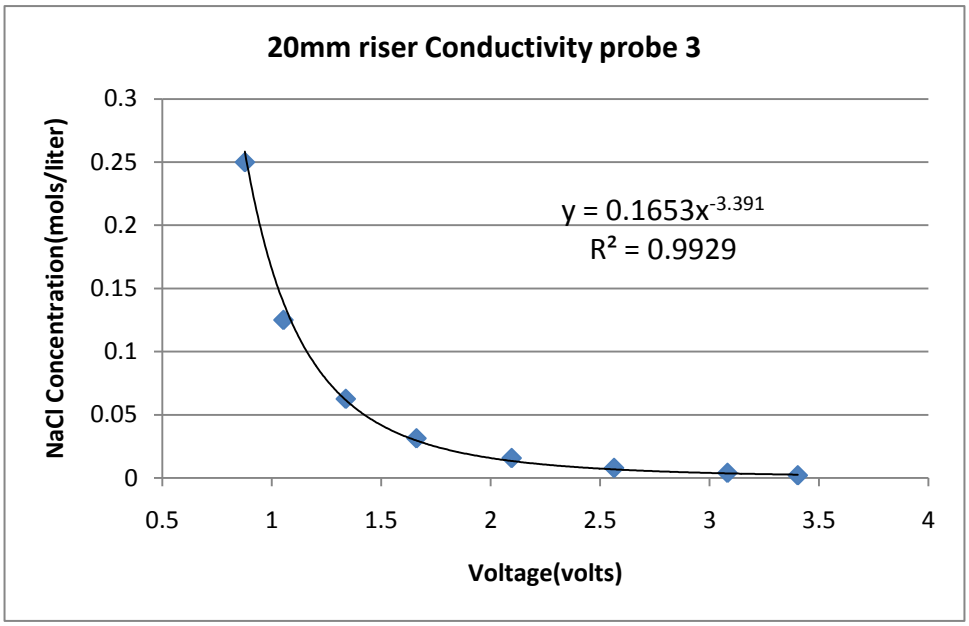

Figure A.6: 20mm riser calibration curve conductivity probe 3

3. 30mm riser

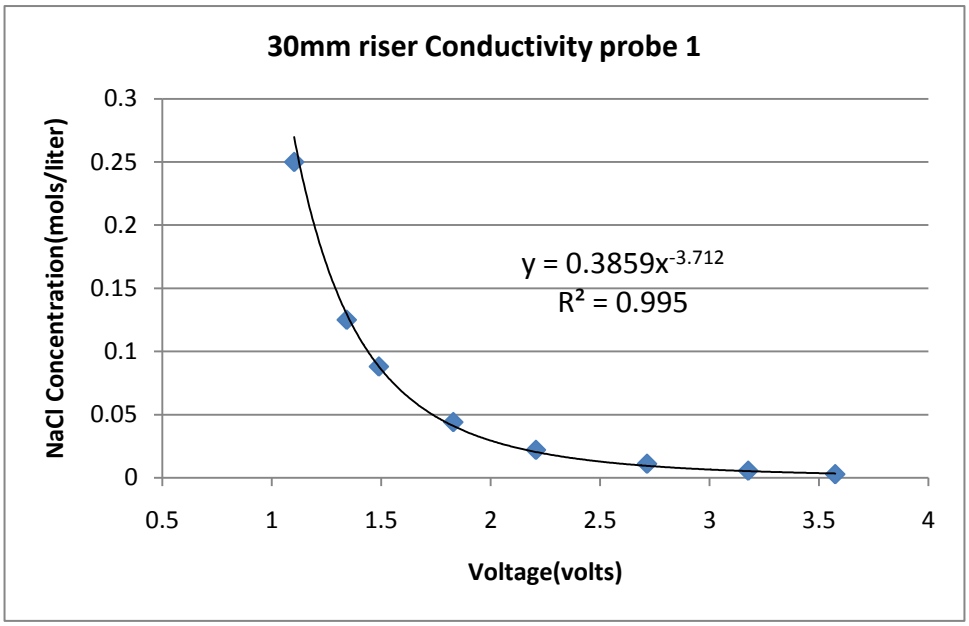

Figure A.7: 30mm riser calibration curve conductivity probe 1

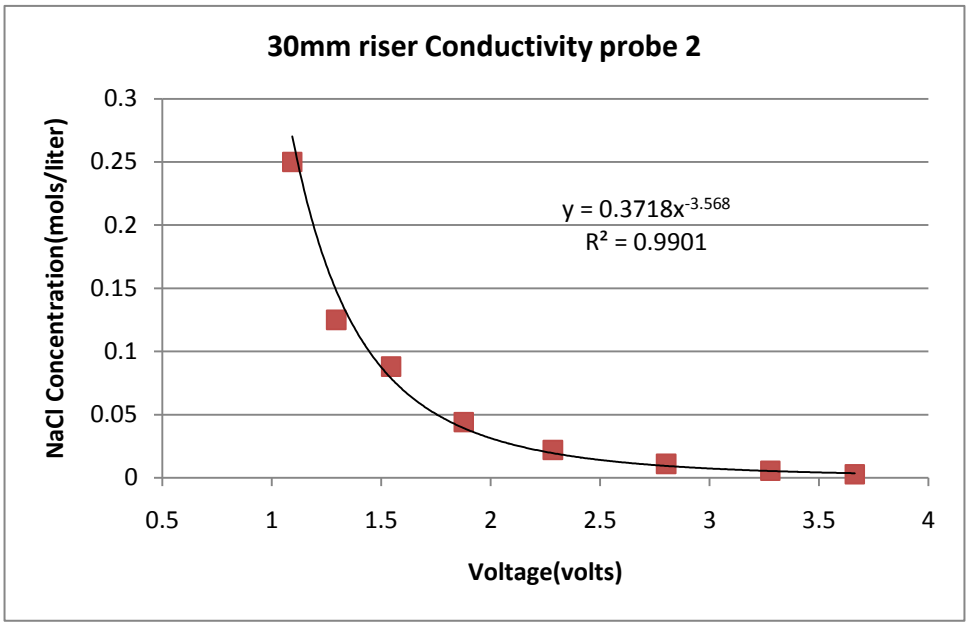

Figure A.8: 30mm riser calibration curve conductivity probe 2

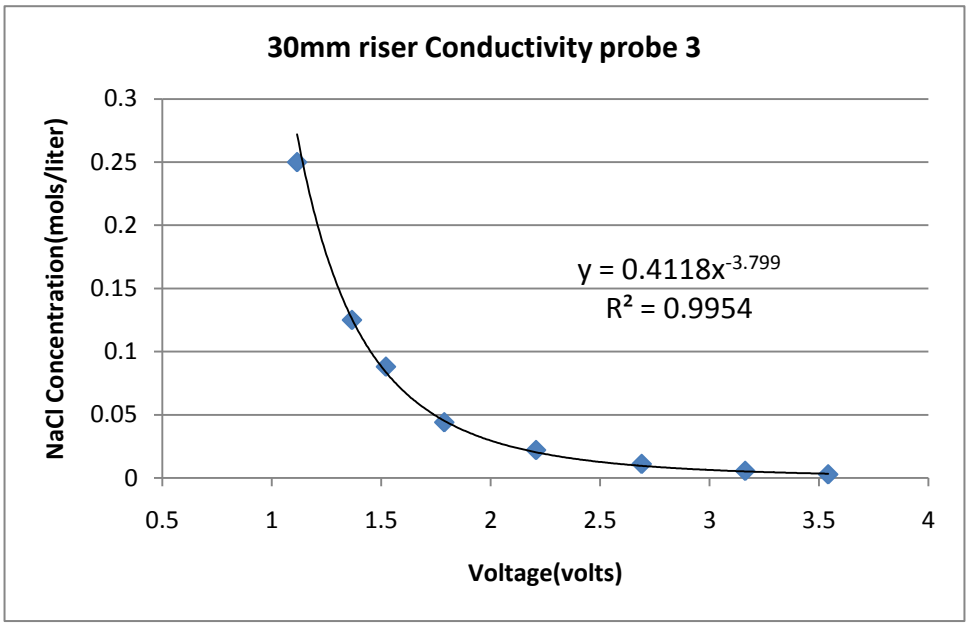

Figure A.9: 30mm riser calibration curve conductivity probe 3

Calibration equations

In order to convert the voltage signals into corresponding concentration output, the following equations were used.

Table A1. Calibration equations

50mm riser	**Equation**
Conductivity probe 1	$Conc = 0.3618 \times v^{-3.986}$
Conductivity probe 2	$Conc = 0.3504 \times v^{-3.843}$
Conductivity probe 3	$Conc = 0.7708 \times v^{-4.072}$
30mm riser	
Conductivity probe 1	$Conc = 0.3859 \times v^{-3.712}$
Conductivity probe 2	$Conc = 0.3718 \times v^{-3.568}$
Conductivity probe 3	$Conc = 0.4118 \times v^{-3.799}$
20mm riser	
Conductivity probe 1	$Conc = 0.2271 \times v^{-3.689}$
Conductivity probe 2	$Conc = 0.3292 \times v^{-3.611}$
Conductivity probe 3	$Conc = 0.1653 \times v^{-3.391}$

Appendix B – Analysis of the 20mm and 50mm conductivity data

This appendix contains the comprehensive analysis of the 20 and 50mm riser.

B.1 Conductivity probes results for the 50mm riser

This section presents the filtered output signal response from the conductivity probes on the 50mm riser. A brief description of the results is also given. The voltage output signal was converted into the corresponding concentration-time output using equations in table A 1. A moving average of 22 steps was used to remove noise from the voltage output signal. Salt tracer was added 60 seconds after starting a run.

50mm results: No frother

The maximum change in concentration recorded when no frother was introduced is 0.013mols/litre, constituting 1.3% of the original NaCl added to the flotation cell. Conductivity probe 2 and 3, recorded no salt. Figure B.1a to Figure B.1c shows the responses of each conductivity probe while Figure B.1d shows the three probes when plotted on the same scale.

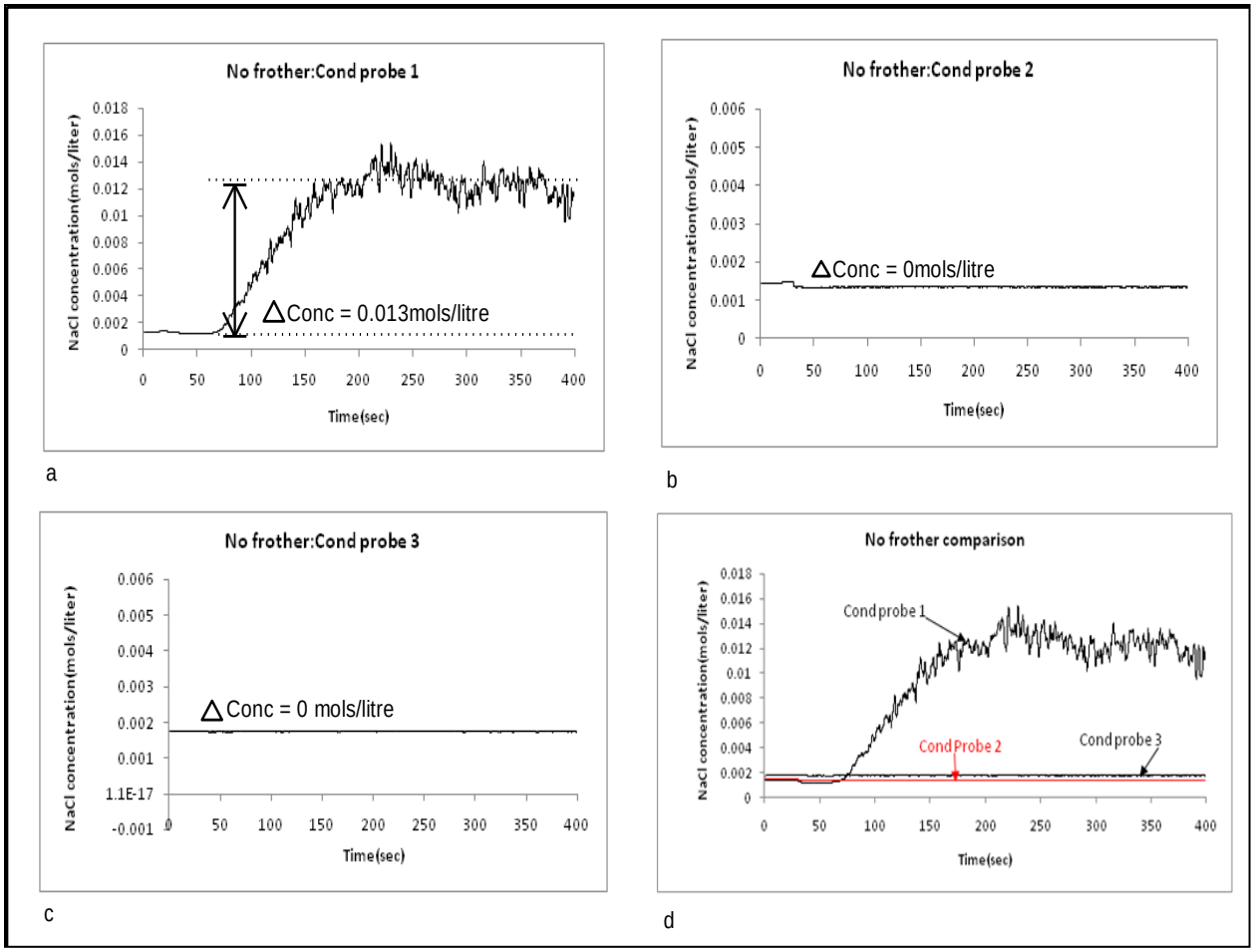

Figure B.1 Conductivity responses for the 50mm riser when no frother is added to the flotation cell

50mm riser conductivity test results: 4ml of 1% v/v MIBC

Addition of 5ppm MIBC to the flotation cell resulted in the change in concentration shown by Figure B.2. The maximum change in concentration recorded was recorded by conductivity probe 1(Figure B.2a). This change represented 3.28% of the original NaCl added to the flotation cell. Conductivity probes 2 and 3 recorded 0.37 and 0.016% respectively

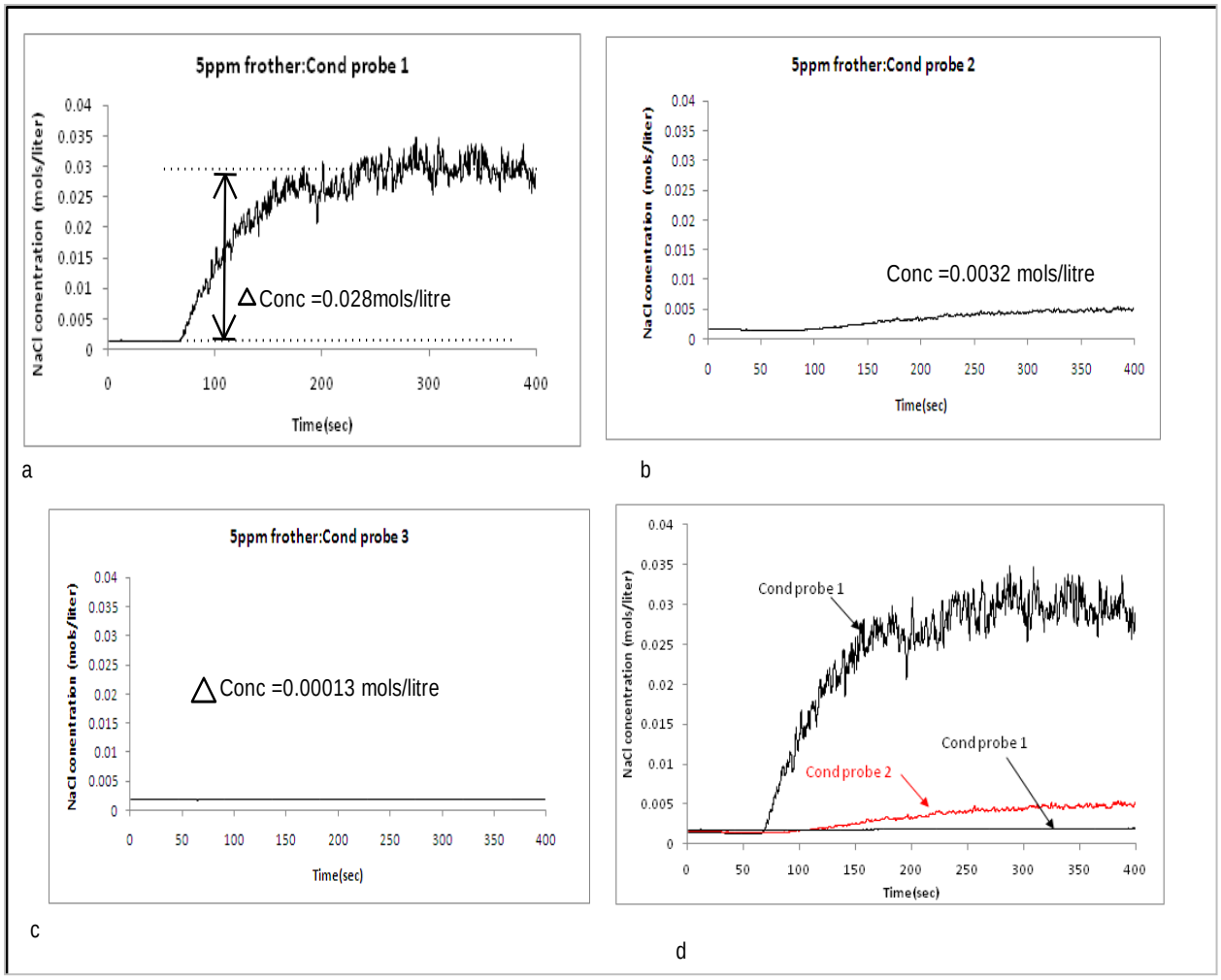

Figure B.2 Conductivity responses for the 50mm riser when 5ppm MIBC is added to the flotation cell

50mm riser conductivity test results: 8ml of 1% v/v MIBC (10ppm)

Increasing the concentration of MIBC to 10ppm resulted in the responses shown in Figure B.3. Figure B.3a, shows a change in NaCl concentration of 0.027mols/litre which is 3.16% of the original 0.5mols NaCl added to the flotation cell. Conductivity probes 2 and 3 recorded 0.00156mols/litre and 0.00018mols/litre representing 0.47 and 0.09% of the initial NaCl respectively.

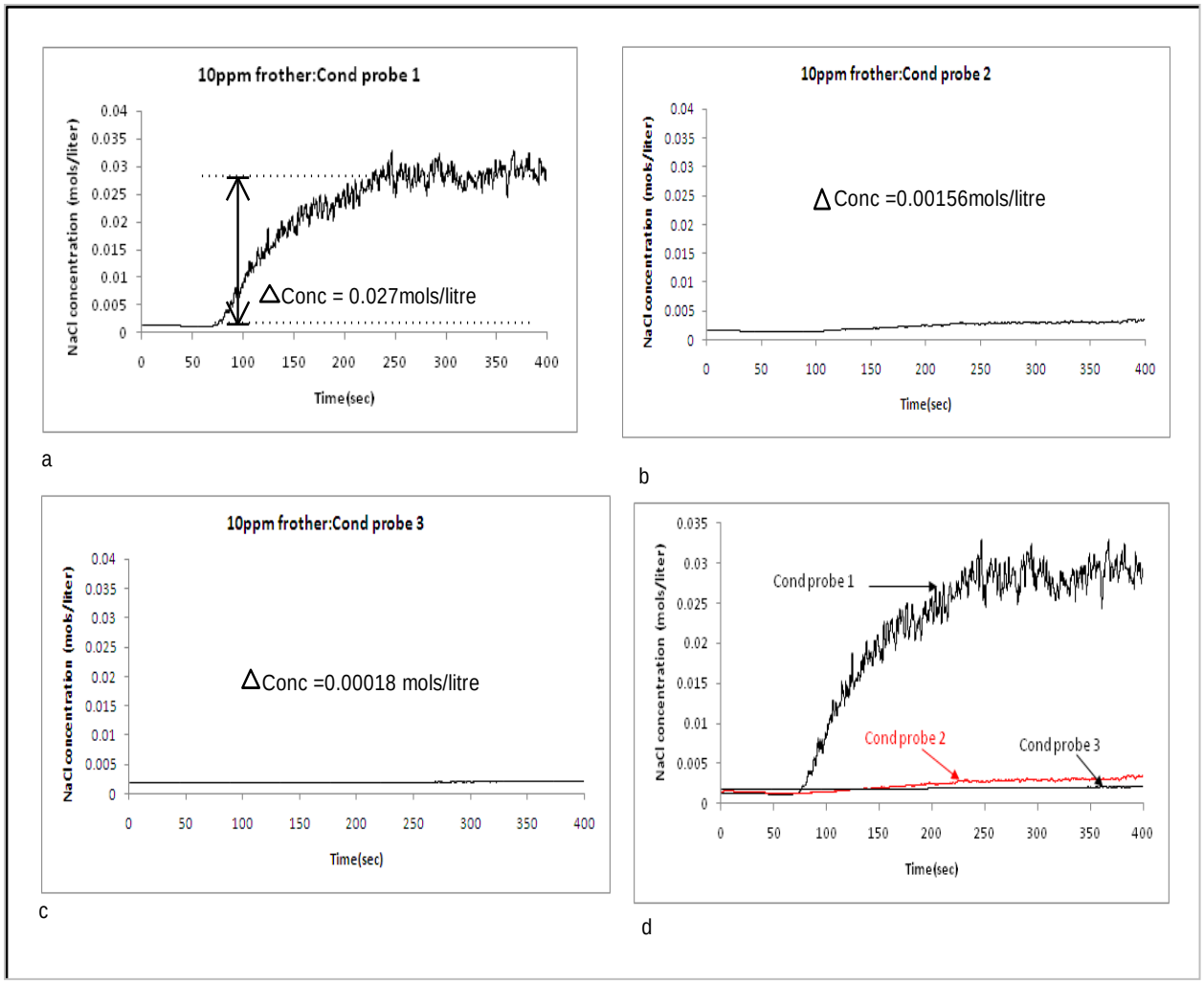

Figure B.3 Conductivity responses for the 50mm riser when 10ppm MIBC is added to the flotation cell

50mm riser conductivity test results: 16ml of 1% v/v MIBC (20ppm)

Figure B.4a to B.4c shows how concentration of the NaCl transport up the 50mm riser varies with height when 20ppm MIBC is added. 0.031mols/litre which is 3.70% of the original NaCl was is the average of the steady state concentration recorded by conductivity probe 1. Conductivity probe 2 recorded 0.75% while conductivity probe 3 recorded 0.038% of the original NaCl added to the flotation cell. The response of the three conductivity probes is shown in Figure B.4d.

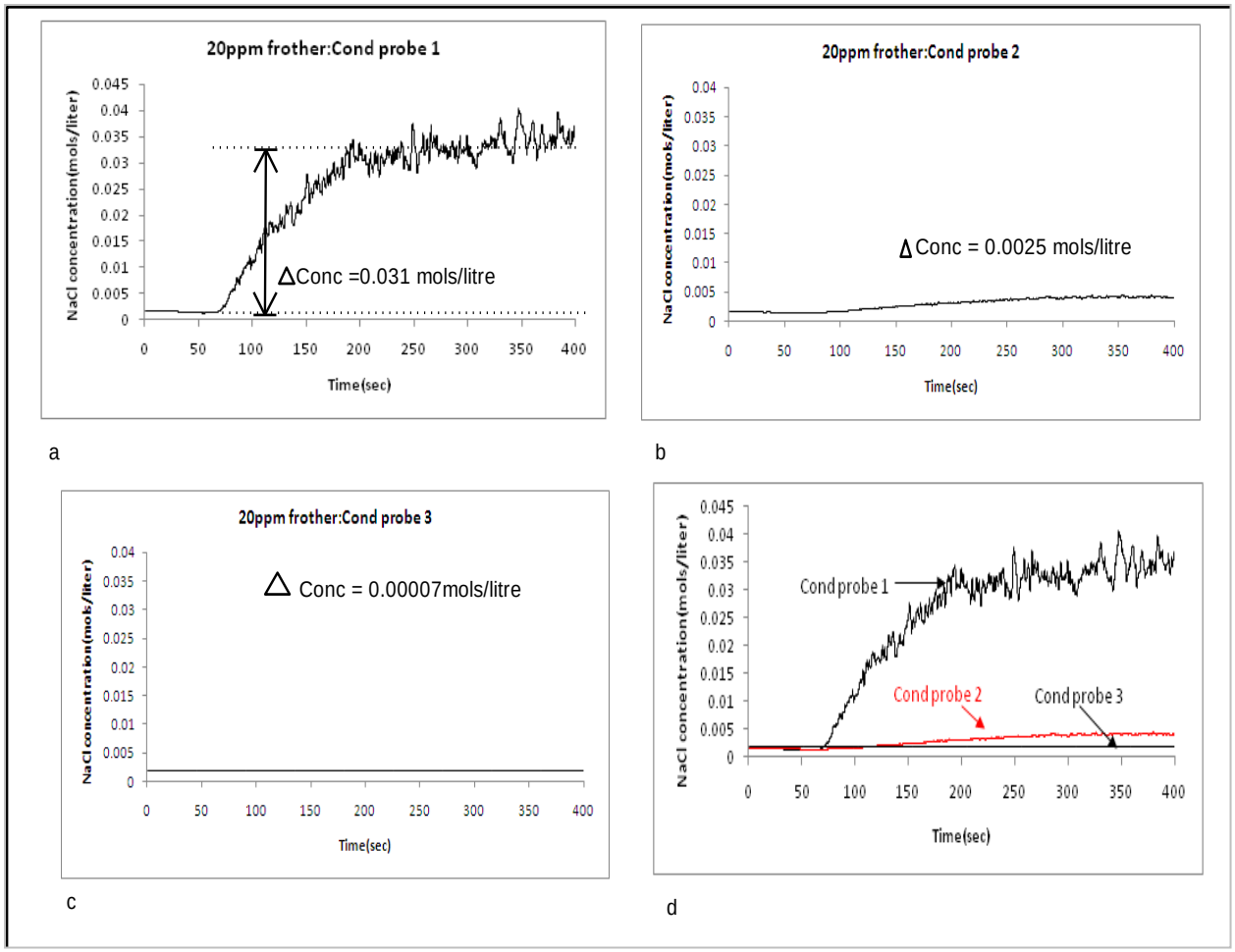

Figure B.4 Conductivity responses for the 50mm riser when 20ppm MIBC is added to the flotation cell

B.2. 20mm riser conductivity test results

This section presents the response of 20mm riser to stimulus response experiments.

20mm riser No frother results

When no frother is added, Figure B.5a to Figure B.5c shows the changes in concentration at each conductivity probe. Conductivity probes 2 and 3 recorded no salt in fact the recorded conductivity is less than that of water as result of the air bubbles. It is important to note that the effect of bubbles in this riser is much more pronounced as compared to the 30 and 50mm riser. This because the brass conductivity probes are fairly close to each other, thus any slight change in voltage is recorded. 0.0015% of the added NaCl is recorded by conductivity probe 1

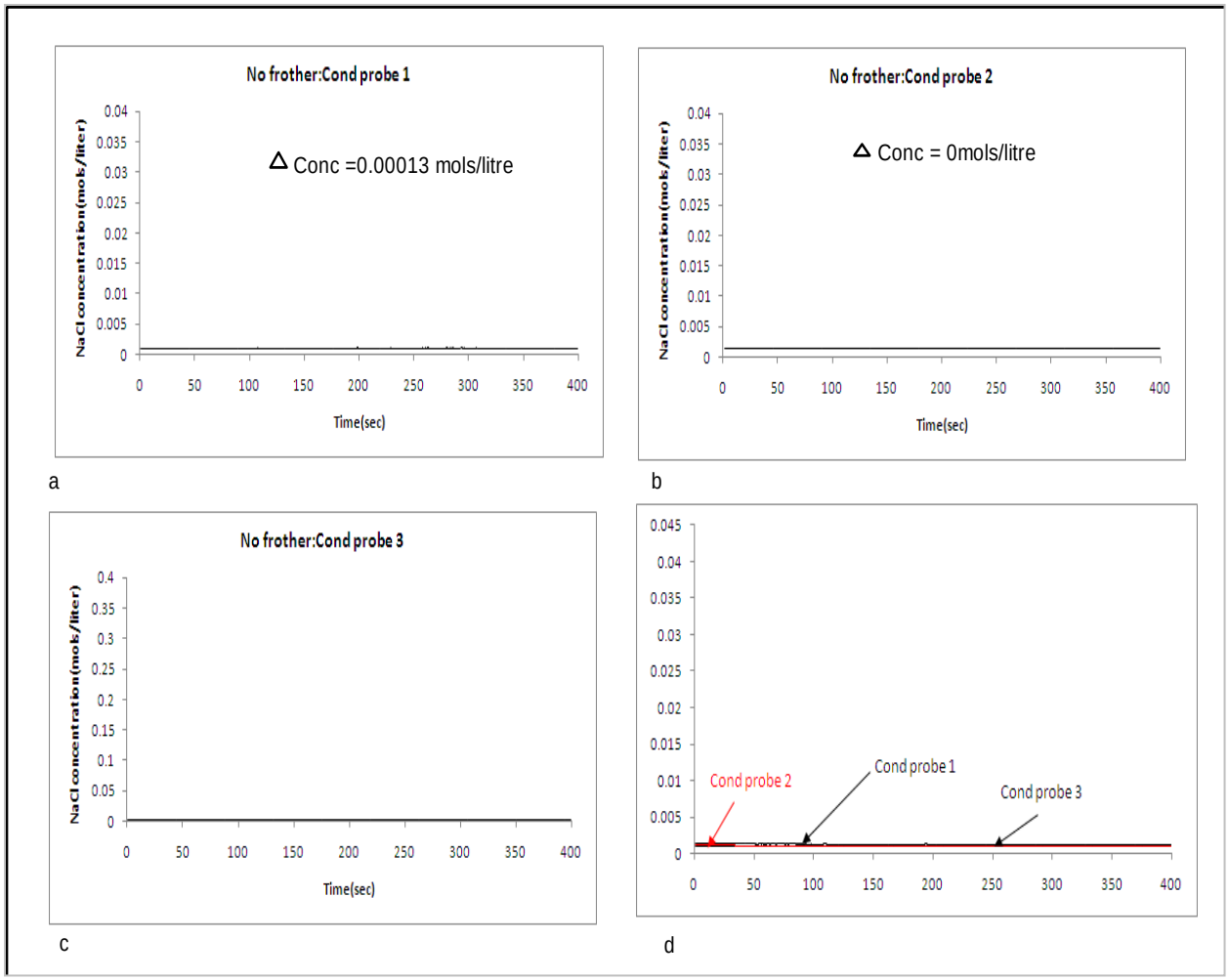

Figure B.5 Conductivity responses for the 20mm riser when No frother MIBC is added to the flotation cell

20mm riser conductivity test results: 4ml of 1% v/v MIBC (5ppm)

The average of the peak concentration recorded by conductivity probe 1 is shown in Figure B.6a, this is 0.80% of the original amount of NaCl added to the flotation cell. While conductivity probe 2 recorded 0.0049mols/litre (Figure B.6b) which is 0.18% of the original amount of salt tracer, conductivity probe 3 recorded no salt (Figure B.6c). Figure B.6 d shows the responses when the three probes are plotted on the same scale.

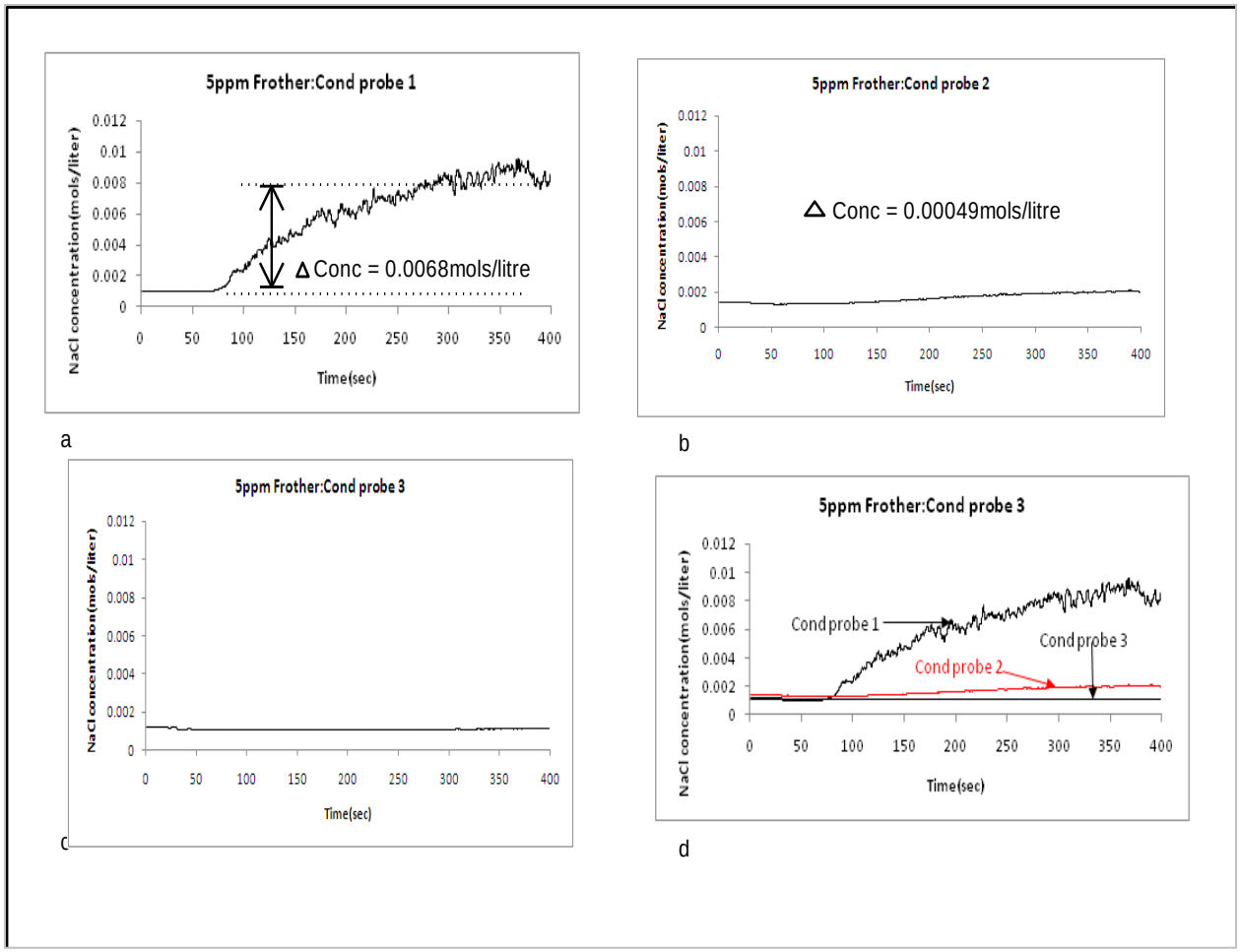

Figure B.6 Conductivity responses for the 20mm riser when 5ppm MIBC is added to the flotation cell

20mm riser conductivity test results: 8ml of 1%MIBC (10ppm)

The response when 10ppm of MIBC was added to the flotation cell is shown in Figures B.7a to B.7d. While conductivity probe 3 recorded no salt at all, conductivity probes 1 and 2 recorded 0.68 and 0.12% of the 0.5mols added to the flotation cell respectively.

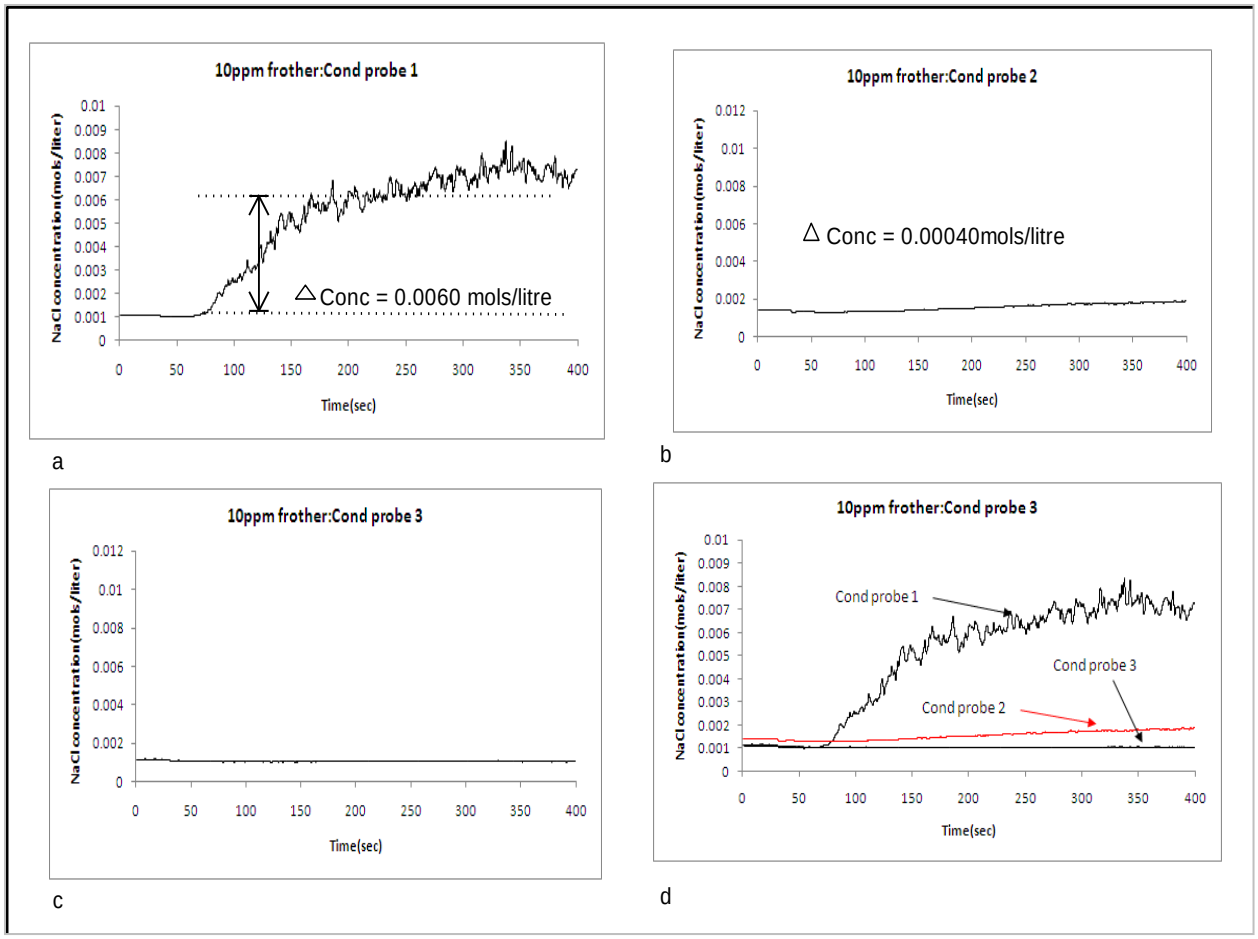

Figure B.7 Conductivity responses for the 20mm riser when 10ppm MIBC is added to the flotation cell

20mm riser conductivity test results: 16ml of 1%MIBC (20ppm)

When 20ppm frother is added to the flotation cell, 0.77 and 0.074% of NaCl added to the flotation cell reaches conductivity probes 1 and 2 respectively. Conductivity probe 3 records no salt at all. Figure 4.18a to Figure 4.18c shows each conductivity probe's response. Figure 4.19d then shows the responses of the three probes when plotted together.

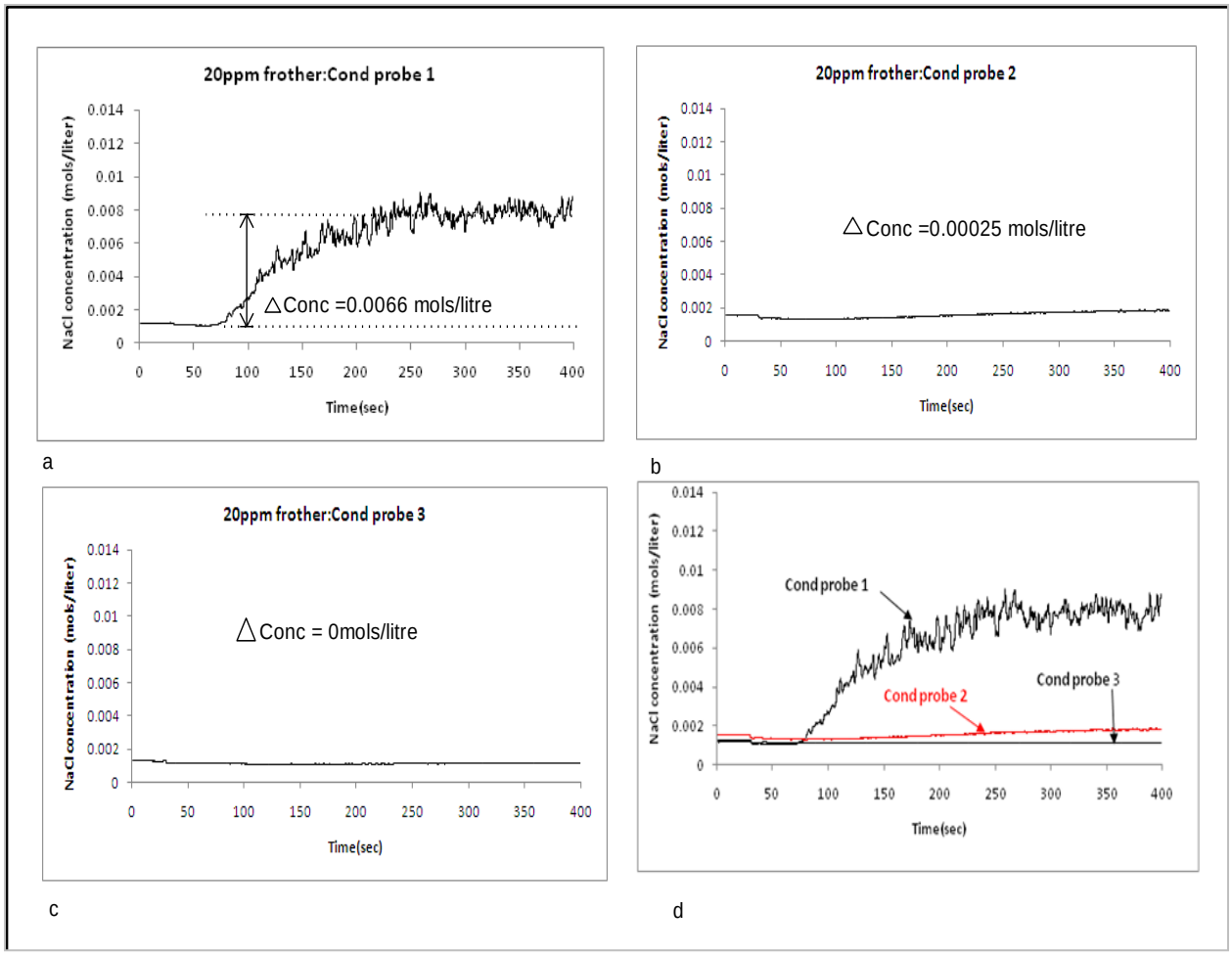

Figure B.8 Conductivity responses for the 20mm riser when 10ppm MIBC is added to the flotation cell

Appendix C –Bubble load meter operating tables

This appendix contains tables for operating the bubble load meter for all risers. The tables are used when the superficial gas velocity in the flotation cell is known.

Table C1: 20mm riser recirculation water estimation

pipe ID	2.00		
j_g (cm/s)	Water flowrate (ml/s)	Recirculation Flowrate(ml/s)	Rotameter reading
0.00	0.00	0.00	6.47
0.10	0.31	0.63	6.74
0.20	0.63	1.26	7.01
0.30	0.94	1.88	7.29
0.40	1.26	2.51	7.56
0.50	1.57	3.14	7.83
0.60	1.88	3.77	8.11
0.70	2.20	4.40	8.38
0.80	2.51	5.03	8.66
0.90	2.83	5.65	8.93
1.00	3.14	6.28	9.20
1.10	3.46	6.91	9.48
1.20	3.77	7.54	9.75
1.30	4.08	8.17	10.02
1.40	4.40	8.80	10.30
1.50	4.71	9.42	10.57
1.60	5.03	10.05	10.85
1.70	5.34	10.68	11.12
1.80	5.65	11.31	11.39
1.90	5.97	11.94	11.67
2.00	6.28	12.57	11.94

Table C2: 30mm riser recirculation water estimation

pipe ID	3.00		
j_g (cm/s)	Water flowrate (ml/s)	Recirculation Flowrate(ml/s)	Rotameter reading
0.00	0.00	0.00	6.47
0.10	0.71	1.41	7.08
0.20	1.41	2.83	7.70
0.30	2.12	4.24	8.31
0.40	2.83	5.65	8.93
0.50	3.53	7.07	9.55
0.60	4.24	8.48	10.16
0.70	4.95	9.90	10.78
0.80	5.65	11.31	11.39
0.90	6.36	12.72	12.01
1.00	7.07	14.14	12.62
1.10	7.78	15.55	13.24
1.20	8.48	16.96	13.86
1.30	9.19	18.38	14.47
1.40	9.90	19.79	15.09
1.50	10.60	21.21	15.70
1.60	11.31	22.62	16.32
1.70	12.02	24.03	16.94
1.80	12.72	25.45	17.55
1.90	13.43	26.86	18.17
2.00	14.14	28.27	18.78

Table C3: 50mm riser recirculation water estimation

pipe ID	5.00		
j_g (cm/s)	Water flowrate (ml/s)	Recirculation Flowrate(ml/s)	Rotameter reading
0.00	0.00	0.00	6.47
0.10	1.96	3.93	8.18
0.20	3.93	7.85	9.89
0.30	5.89	11.78	11.60
0.40	7.85	15.71	13.31
0.50	9.82	19.63	15.02
0.60	11.78	23.56	16.73
0.70	13.74	27.49	18.44
0.80	15.71	31.42	20.15
0.90	17.67	35.34	21.86
1.00	19.63	39.27	23.58
1.10	21.60	43.20	25.29
1.20	23.56	47.12	27.00
1.30	25.53	51.05	28.71
1.40	27.49	54.98	30.42
1.50	29.45	58.90	32.13
1.60	31.42	62.83	33.84
1.70	33.38	66.76	35.55
1.80	35.34	70.69	37.26
1.90	37.31	74.61	38.97
2.00	39.27	78.54	40.69

Appendix C2: Bubble load meter control tables

Riser diameter(cm)	3	Velocity at T			Velocity at T
Rotameter reading	Flowrate ml/s	3cm ID	Rotameter reading	Flowrate ml/s	3cm ID
7.00	1.23	0.17	41.00	79.26	11.21
8.00	3.52	0.50	42.00	81.56	11.54
9.00	5.82	0.82	43.00	83.85	11.86
10.00	8.11	1.15	44.00	86.15	12.19
11.00	10.41	1.47	45.00	88.44	12.51
12.00	12.70	1.80	46.00	90.74	12.84
13.00	15.00	2.12	47.00	93.03	13.16
14.00	17.29	2.45	48.00	95.33	13.49
15.00	19.59	2.77	49.00	97.62	13.81
16.00	21.88	3.10	50.00	99.92	14.14
17.00	24.18	3.42	51.00	102.21	14.46
18.00	26.47	3.75	52.00	104.51	14.79
19.00	28.77	4.07	53.00	106.80	15.11
20.00	31.06	4.39	54.00	109.10	15.43
21.00	33.36	4.72	55.00	111.39	15.76
22.00	35.65	5.04	56.00	113.69	16.08
23.00	37.95	5.37	57.00	115.98	16.41
24.00	40.24	5.69	58.00	118.28	16.73
25.00	42.54	6.02	59.00	120.58	17.06
26.00	44.83	6.34	60.00	122.87	17.38
27.00	47.13	6.67	61.00	125.17	17.71
28.00	49.43	6.99	62.00	127.46	18.03
29.00	51.72	7.32	63.00	129.76	18.36
30.00	54.02	7.64	64.00	132.05	18.68
31.00	56.31	7.97	65.00	134.35	19.01
32.00	58.61	8.29	66.00	136.64	19.33
33.00	60.90	8.62	67.00	138.94	19.66
34.00	63.20	8.94	68.00	141.23	19.98
35.00	65.49	9.27	69.00	143.53	20.30
36.00	67.79	9.59	70.00	145.82	20.63
37.00	70.08	9.91	71.00	148.12	20.95
38.00	72.38	10.24	72.00	150.41	21.28
39.00	74.67	10.56	73.00	152.71	21.60
40.00	76.97	10.89	74.00	155.00	21.93
			75.00	157.30	22.25
			76.00	159.59	22.58

Riser diameter(cm)	5	Velocity at T			Velocity at T
Rotameter reading	Flowrate ml/s	5cm ID	Rotameter reading	Flowrate ml/s	5cm ID
7.00	1.23	0.06	41.00	79.26	4.04
8.00	3.52	0.18	42.00	81.56	4.15
9.00	5.82	0.30	43.00	83.85	4.27
10.00	8.11	0.41	44.00	86.15	4.39
11.00	10.41	0.53	45.00	88.44	4.50
12.00	12.70	0.65	46.00	90.74	4.62
13.00	15.00	0.76	47.00	93.03	4.74
14.00	17.29	0.88	48.00	95.33	4.86
15.00	19.59	1.00	49.00	97.62	4.97
16.00	21.88	1.11	50.00	99.92	5.09
17.00	24.18	1.23	51.00	102.21	5.21
18.00	26.47	1.35	52.00	104.51	5.32
19.00	28.77	1.47	53.00	106.80	5.44
20.00	31.06	1.58	54.00	109.10	5.56
21.00	33.36	1.70	55.00	111.39	5.67
22.00	35.65	1.82	56.00	113.69	5.79
23.00	37.95	1.93	57.00	115.98	5.91
24.00	40.24	2.05	58.00	118.28	6.02
25.00	42.54	2.17	59.00	120.58	6.14
26.00	44.83	2.28	60.00	122.87	6.26
27.00	47.13	2.40	61.00	125.17	6.37
28.00	49.43	2.52	62.00	127.46	6.49
29.00	51.72	2.63	63.00	129.76	6.61
30.00	54.02	2.75	64.00	132.05	6.73
31.00	56.31	2.87	65.00	134.35	6.84
32.00	58.61	2.98	66.00	136.64	6.96
33.00	60.90	3.10	67.00	138.94	7.08
34.00	63.20	3.22	68.00	141.23	7.19
35.00	65.49	3.34	69.00	143.53	7.31
36.00	67.79	3.45	70.00	145.82	7.43
37.00	70.08	3.57	71.00	148.12	7.54
38.00	72.38	3.69	72.00	150.41	7.66
39.00	74.67	3.80	73.00	152.71	7.78
40.00	76.97	3.92	74.00	155.00	7.89
			75.00	157.30	8.01
			76.00	159.59	22.58

Riser diameter(cm)	2.00	Velocity at T			Velocity at T
Rotameter reading	Flowrate ml/s	2cm ID	Rotameter reading	Flowrate ml/s	2cm ID
7.00	1.23	0.39	41.00	79.26	25.23
8.00	3.52	1.12	42.00	81.56	25.96
9.00	5.82	1.85	43.00	83.85	26.69
10.00	8.11	2.58	44.00	86.15	27.42
11.00	10.41	3.31	45.00	88.44	28.15
12.00	12.70	4.04	46.00	90.74	28.88
13.00	15.00	4.77	47.00	93.03	29.61
14.00	17.29	5.50	48.00	95.33	30.34
15.00	19.59	6.24	49.00	97.62	31.07
16.00	21.88	6.97	50.00	99.92	31.81
17.00	24.18	7.70	51.00	102.21	32.54
18.00	26.47	8.43	52.00	104.51	33.27
19.00	28.77	9.16	53.00	106.80	34.00
20.00	31.06	9.89	54.00	109.10	34.73
21.00	33.36	10.62	55.00	111.39	35.46
22.00	35.65	11.35	56.00	113.69	36.19
23.00	37.95	12.08	57.00	115.98	36.92
24.00	40.24	12.81	58.00	118.28	37.65
25.00	42.54	13.54	59.00	120.58	38.38
26.00	44.83	14.27	60.00	122.87	39.11
27.00	47.13	15.00	61.00	125.17	39.84
28.00	49.43	15.73	62.00	127.46	40.57
29.00	51.72	16.46	63.00	129.76	41.30
30.00	54.02	17.19	64.00	132.05	42.03
31.00	56.31	17.92	65.00	134.35	42.76
32.00	58.61	18.65	66.00	136.64	43.49
33.00	60.90	19.39	67.00	138.94	44.22
34.00	63.20	20.12	68.00	141.23	44.96
35.00	65.49	20.85	69.00	143.53	45.69
36.00	67.79	21.58	70.00	145.82	46.42
37.00	70.08	22.31	71.00	148.12	47.15
38.00	72.38	23.04	72.00	150.41	47.88
39.00	74.67	23.77	73.00	152.71	48.61
40.00	76.97	24.50	74.00	155.00	49.34
			75.00	157.30	50.07
			76.00	159.59	50.80

Appendix D –UG2 ore composition

Typical UG2 ore composition

Mineral		%Composition	Density (kg/m^3)
Pyroxine	Clinopyroxine ($CaAl_2SiO_6$)	38.4	3200-3380
	Orthopyroxene ($MgSiO_3$)		
Chromite	$FeCr_2O_4$	36.8	4320-4570
Feldspar	Anorthite	17.5	2560-2760
	Albite		
	Potash Spar		
Olivine	Mg_2SiO_4	0.6	3300
	Ca_2SiO_4		
	Mn_2SiO_4		
	$FeSiO_4$		
	Co_2SiO_4		
	$NiSiO_4$		
Alteration silicates		3.9	
Other Silicates		1.7	
Base Metal Sulphides		0.3	
Other		0.8	
Total		**100**	